UNIVERSITY OF CALIFORNIA

Santa Barbara

High Active Nitrogen Flux Growth of (Indium) Gallium Nitride by Plasma Assisted Molecular Beam Epitaxy

A dissertation submitted in partial satisfaction of the

requirements for the degree of

Doctor of Philosophy

in

Materials

by

Brian Matthew McSkimming

Committee in charge:

Professor James S. Speck, Chair

Professor Steven P. Denbaars

Professor Arthur C. Gossard

Professor Umesh K. Mishra

December 2015

The dissertation of Brian Matthew McSkimming is approved.

Steven P. Denbaars

Arthur C. Gossard

Umesh K. Mishra

James S. Speck, Chair

October 2015

High Active Nitrogen Flux Growth of (Indium) Gallium Nitride by

Plasma Assisted Molecular Beam Epitaxy

Copyright © 2015

by

Brian Matthew McSkimming

Acknowledgements

First and foremost, I would like to thank my committee and particularly Prof. Jim Speck for his acceptance of me into his group, his guidance along the way, his cheerleading when things were challenging and his constant drive towards performing the best science possible. It was his passion for the III-Nitrides which made me want to work with him at UCSB, and his constant drive to do the best work possible that made working with him so rewarding. From constant edits of papers with Strunk and White at hand to our debates over N vs N_2^* (which aren't over yet), I couldn't imagine my Ph.D. being what it was without him. I am very much indebted to Prof. Art Gossard for agreeing to be on my committee. The many fruitful discussions in both private and in MBE meetings brought a depth to my work that would have been missing without his input. Prof. Gossard's constant questioning of how things could be done differently always brought new insight to my work, and I most graciously thank him for each and every one of his insights. I also very much appreciated having Prof. Steve Denbaars on my committee. He brought a vast knowledge of growth and devices to my committee and always gave great suggestions on how to improve the basic devices used throughout my work. Further, I believe I took nearly every class offered which he taught, from basic solid state physics to MOCVD; Prof. Denbaars is an amazing educator and there wasn't a single class that didn't expand my knowledge in some way. Finally, last and most certainly not least I would like to thank Prof. Umesh Mishra. Prof. Mishra has a rare combination of charisma and knowledge that leaves you always wanting to spend as

much time with him as possible because you never know when you might soak in some tidbit about electron transport through a semiconductor that solves all your questions.

Throughout my Ph.D., I had the great privilege to work and interact with what feels like hundreds of people, each amazing in their own right, each and every one enriching my time at UCSB. To try to name them all would be a fool's errand which I'm not going to even try. However there are some people who deserve a special thank you. First, my officemates over my time here have been integral to the maintenance of my sanity. Far beyond that though was the constant conversations and dialogue about our work, everyone helping each other in every way possible. For this and so much more, thank you Tammy, Jordan, Erin and Stacy. Maybe someday someone will be successful in keeping a plant alive in our office. Second I'd like to thank all the suitemates that I've had the pleasure of sharing space with over the years, from Samantha, Liz and Siddha to Chris, Justin and Ben and all the rest of my suitemates. From working through classwork together to letting me ask all kinds of questions, you all have made my time at UCSB better in so many ways. Third I wish to thank all of the fellow graduate students, postdocs and research scientists in the MBE lab that I have had the pleasure to work with over the years. You have all been my family away from home and hold a special place in my heart. I need to specially thank Chad Gallinet and Erin Young for being the amazing people you are. Chad made my first year at UCSB most welcoming, and Erin has been a sounding board and friend throughout. Finally, I would also like to acknowledge the staff members in the x-ray facility, microscopy facility,

cleanroom, Materials office, and SLEEC office for keeping the equipment running and for helping with everything necessary to keep my graduate work moving forward.

Alexander Fang deserves a special thank you for taking under his wing an undergraduate student who was "a loser like him". That summer we spent together put me on the path which has culminated in this degree, and for that I am indebted to him forever.

Very special thanks are necessary for John English, Andy Jackson and Kurt Olsson. The MBE lab is an amazing place, with students from many departments and advisors, and somehow you three keep it running. From searching for the tiniest leak to helping me retrofit the Gen II electronics, I owe all the equipment knowledge I have to you. Even more than that, John has been that special grandfather figure that we all search for and I'm a better person just for having the opportunity to work with him.

I would be nothing, literally, if it weren't for my family. Words cannot express the undying gratitude I have for the years of support and love. Special thanks to my mother, Sandy, for 35+ years of teaching me how to be the best man I can be, and to never losing faith in my endeavors. You've always been there for me no matter what, and my completion of this Ph.D. is as much your success as it is mine. Thanks to my brother Dan for letting me finish my degree before you. More importantly you've been a partner through some of the toughest times and have always given your ear when I need it most. We've struggled through so many of the same battles, and to have you as a brother has always

made me proud. Thanks to my sister Megan for being the successful one of us three, moving forward in your life and giving both Dan and I something to strive for.

Last and most certainly not least I need to thank my fiancée Lili. Through my toughest times you have been the rock that has kept me going. Through the late nights you stayed up waiting for me. All the meals you brought to me in the lab, all the notes and all the love you have shown me has given me the strength to push through and finish my degree. From the deepest cockles of my heart thank you, thank you, thank you.

Curriculum Vitae

Brian Matthew McSkimming

EDUCATION

Ph.D. in Materials Science **Fall 2015**
University of California, Santa Barbara

> *Dissertation title:* "High Active Nitrogen Flux Growth of (Indium) Gallium Nitride by Plasma Assisted Molecular Beam Epitaxy"
> *Committee:* Steven Denbaars, Art Gossard, Umesh Mishra, James S. Speck (Chair)

B.S. in Electrical Engineering, *summa cum laude* **2009**
State University of New York, University at Buffalo

B.A. in Mathematics, *summa cum laude* **2009**
State University of New York, University at Buffalo

RESEARCH EXPERIENCE

Graduate Researcher **2009-Present**
Materials Science and Engineering, University of California, Santa Barbara

- Performed plasma assisted MBE growth of GaN and InGaN utilizing a modified plasma source resulting in record active nitrogen fluxes
- Responsible for all maintenance and upgrading of MBE equipment (Varian Mod Gen II and Veeco 930)
- Performed complete processing of select samples for Hall Effect measurements on mesa-isolated lithographically defined Van der Pauw structures
- Characterized samples using AFM, XRD, SEM, PL and Hall Effect measurements

Undergraduate Research Assistant **2008-2009**
Electrical Engineering, State University of New York, University at Buffalo

- Created new lab experiments and activities for Introduction to Nanotechnology class
- Edited and reviewed textbook on introductory quantum mechanics

Undergraduate Research Assistant **2006-2009**
Computer Science and Engineering, State University of New York, University at Buffalo

- Led team of 3-5 students creating software application for use in Introduction to Computer Programming class

NNIN i-REU Intern **Summer 2008**

National Institute of Material Science (NIMS), Tsukuba, Japan

- Performed MBE growth of GaAs quantum dots using droplet epitaxy
- Characterized quantum dots through AFM and PL experiments

NNIN REU Intern **Summer 2007**

Electrical and Computer Engineering, University of California, Santa Barbara

- Characterized lasers to optimize current aperture
- Assisted in the processing of lasers and optimized thermal annealing of contacts

TEACHING/MENTORING EXPERIENCE

NNIN Chip Camp Lead Instructor **2012-2015**

Electrical and Computer Engineering, University of California, Santa Barbara

- Guided ~20-30 middle/high school students through a basic cleanroom processing exercise
- Led discussions about nanotechnology and its impact on ethics and society

NNIN REU Mentor **Summer 2014**

Materials Science and Engineering, University of California, Santa Barbara

- Responsible for education and management of 2 summer interns
  - Project: "Optimization of High Growth Rate GaN Thin Film Mobility"
  - Project: "Characterization and Modeling of Carrier Transport in GaN Thin Films"

CISEI Research Mentor **Summer 2013**

Materials Science and Engineering, University of California, Santa Barbara

- Responsible for education and management of an international intern
  - Project: "Optimization of High Temperature GaN Thin Film Mobility"

NNIN REU Mentor **Summer 2012**

Materials Science and Engineering, University of California, Santa Barbara

- Responsible for education and management of an undergraduate intern
  - Project: "Carbon doping of $(10\bar{1}1)$ GaN for p-type Conductivity"

Lead Teaching Assistant, Introduction to Materials **Winter 2011**
Materials Science and Engineering, University of California, Santa Barbara

- Managed team of 6 teaching assistants responsible for ~150 students
- Created all exams and homework assignments

Reader/Grader, Introduction to Materials **Summer 2009**
Materials Science and Engineering, University of California, Santa Barbara

- Graded all exams and homework assignments for ~35 students

Lab/Teaching Assistant, Introduction to Nanotechnology **Fall 2008**
Electrical Engineering, State University of New York, University at Buffalo

- Created and graded all exams, homework and laboratory assignments for ~25 students

PUBLICATIONS

Z. Zhang, E. Farzana, W. Sun, J. Chen, E. X. Zhang, D. M. Fleetwood, R. D. Schrimpf, **B. M. McSkimming**, E. C. H. Kyle, J. S. Speck, A. R. Arehart, S. A. Ringel, "Thermal Stability of Deep Level Defects Induced by High Energy Proton Irradiation in n-type GaN", J. Appl. Phys., **118**, 155701 (2015)

B. M. McSkimming, C. Chaix, J. S. Speck, "High Nitrogen Flux Growth of GaN by Plasma Assisted Molecular Beam Epitaxy", J. Vac. Sci. Technol. A **33**, 05E128, (2015)

X. S. Nguyen, K. Lin, Z. Zhang, **B. McSkimming**, A. R. Arehart, J. S. Speck, S. A. Ringel, E. A. Fitzgerald, S. J. Chua, "Correlation of a generation-recombination center with a deep level trap in GaN", Appl Phys Lett, **106**, 102101, (2015)

J. Son, V. Chobpattana, **B. M. McSkimming**, S. Stemmer, "In-situ nitrogen plasma passivation of Al_2O_3/GaN interface states", J Vac Sci Technol A, **33**, 020602, (2015)

Z. Zhang, C. M. Jackson, A. R. Arehart, **B. McSkimming**, J. S. Speck, S. A. Ringel, "Direct Determination of Energy Band Alignments of Ni/Al_2O_3/GaN MOS Structures using Internal Photoemission Spectroscopy", J Electron Mater, **33**, 828-832, (2014)

B. M. McSkimming, F. Wu, T. Huault, C. Chaix, J. S. Speck, "Plasma assisted molecular beam epitaxy of GaN with growth rates > 2.6 μm/h", J Crys Growth, **386**, 168-174, (2014)

H. Okumura, **B. M. McSkimming**, T. Huault, C. Chaix, J. S. Speck, "Growth diagram of N-face GaN ($000\bar{1}$) grown at high rate by plasma-assisted molecular beam epitaxy", Appl Phys Lett, **104**, 012111, (2014)

Z. Zhang, A.R. Arehart, E. Cinkilic, J. Chen, E.X. Zhang, D.M. Fleetwood, R.D. Schrimpf, **B. McSkimming**, J.S. Speck, S.A. Ringel, "Impact of proton irradiation on deep level states in n-GaN", Appl Phys Lett, **103**, 042102, (2013)

C.M. Jackson, A.R. Arehart, E. Cinkilic, **B. McSkimming**, J.S. Speck, S.A. Ringel, "Interface trap characterization of atomic layer deposition Al_2O_3/GaN metal-insulator-semiconductor capacitors using optically and thermally based deep level spectroscopies", J Appl Phys, **113**, 204505, (2013)

J. Son, V. Chobpattana, **B. M. McSkimming**, S. Stemmer, "Fixed charge in high-k/GaN metal-oxide semiconductor capacitor structures", Appl Phys Lett, **101**, 102905, (2012)

C. A. Hurni, O. Bierwagen, J. R. Lang, **B. M. McSkimming**, C. S. Gallinat, E. C. Young, D. A. Browne, U. K. Mishra, J. S. Speck, "pn junctions on Ga-face GaN grown by NH_3 molecular beam epitaxy with low ideality factors and low reverse currents", Appl Phys Lett, **97**, 222113, (2010)

T. Mano, M. Abbarachi, T. Kuroda, **B. McSkimming**, A. Ohtake, K. Mitsuishi, K. Sakoda, "Self-assembly of symmetric GaAs quantum dots on (111)A substrates: suppression of fine-structure splitting", Appl Phys Express, **3**, 065203, (2010)

CONFERENCE PRESENTATIONS

B.M. McSkimming, C. Chaix, J.S. Speck, "PAMBE Growth of GaN in Extreme Decomposition Regime", 42nd International Symposium on Compound Semiconductors, June 28-July 2, 2015, Santa Barbara, CA, USA

B.M. McSkimming, C. Chaix, J.S. Speck, "PAMBE Growth of GaN with Extreme Active Nitrogen Flux", 42nd International Symposium on Compound Semiconductors, June 28-July 2, 2015, Santa Barbara, CA, USA

D. Fleetwood, J. Chen, T. Roy, E. Zhang, Y. Puzyrev, S. Pantelides, R. Schrimpf, E. Kyle, **B. McSkimming**, S. Kaun, J. Speck, "1/f Noise and Defects in GaN/AlGaN HEMTs", Microelectronics Reliability and Qualification Working Meeting, Jan. 27-28, 2015, El Segundo, CA, USA

B.M. McSkimming, T. Huault, C. Chaix, J.S. Speck, "PAMBE Growth of GaN with Extreme Active Nitrogen Flux", 18th International Conference on Molecular Beam Epitaxy, Sept. 7-12, 2014, Flagstaff, AZ, USA

B.M. McSkimming, T. Huault, C. Chaix, J.S. Speck "Ultra High Active Nitrogen Flux Growth of GaN by PAMBE", 30th North American Molecular Beam Epitaxy Conference, Oct. 5-11, 2013, Banff, Alberta, Canada

C. Hurni, P. Burke, J. Lang, **B. McSkimming**, E. Young, U. Mishra, J. Speck, "Low Temperature p-GaN Grown by NH_3 MBE", 2011 Electronic Materials Conference, June 22-24, 2011, Santa Barbara, CA, USA

G. Wang, **B. McSkimming**, Z. Marzec, J. Gardner, A. Decker, C. Alphonce, "Green: a flexible UML class diagramming tool for Eclipse", 22nd Conference on Object-Oriented Programming Systems and Applications, Oct. 21-25, 2007, Montreal, Quebec, Canada

ABSTRACT

High Active Nitrogen Flux Growth of (Indium) Gallium Nitride by

Plasma Assisted Molecular Beam Epitaxy

by

Brian Matthew McSkimming

Plasma-assisted molecular beam epitaxy (PAMBE) growth of gallium nitride (GaN) has evolved over the past two decades due to progress in growth science and in the active nitrogen plasma source hardware. The transition from electron cyclotron resonance (ECR) microwave plasma sources to radio frequency (RF) plasma sources has enabled higher growth rates, reduced ion damage and improved operation at higher growth chamber pressures. Even with further improvements in RF plasma sources, PAMBE has remained primarily a research tool partially due to limitations in material growth rates.

This dissertation presents results based upon two modifications of a commercially available nitrogen plasma source. These modifications have resulted in record active nitrogen fluxes, and therefore record growth rates of more than 7.6 μm/h. For optimized growth conditions in

the standard metal-rich growth regime, the surfaces displayed a clear step-terrace structure with an average RMS roughness (3 μm×3 μm) on the order of 1 nm. Secondary ion mass spectroscopy (SIMS) impurity analysis demonstrates unintentional oxygen incorporation of ~1×1016, comparable to the metal organic chemical vapor deposition (MOCVD) grown template layer. Additionally, a revised universal growth diagram is proposed allowing the rapid determination of the metal flux needed to grow in a specific growth regime for any and all active nitrogen fluxes available.

High temperature nitrogen rich PAMBE growth of GaN has been previously demonstrated as a viable alternative to the challenges presented in maintaining the Ga bilayer required by metal rich growth of GaN. This dissertation also present results demonstrating PAMBE growth of GaN at a substrate temperature more than 150 °C greater than our standard Ga rich GaN growth regime and ~100 °C greater than any previously reported PAMBE growth of GaN. Finally, a revised growth diagram is proposed highlighting a large growth window available at high temperatures.

Table of Contents

Chapter 1: Introduction and Background 1

1.1 Basic Properties of III-Nitrides...2

1.2 Growth of III-Nitrides...5

1.2.1 Metal Organic Chemical Vapor Deposition (MOCVD)..............5

1.2.2 Molecular Beam Epitaxy (MBE)...6

1.3 Why Molecular Beam Epitaxy of III-Nitrides?....................................7

1.4 Overview of the Thesis..8

1.5 References..9

Chapter 2: Experimental Details and Equipment Description....................................12

2.1 Growth System 13

2.1.1 Entry Exit Chamber 15

2.1.2 Buffer Chamber 16

2.1.3 MBE Growth Chamber..17

2.1.4 System Manifold..23

2.1.5 Electronics Cabinet..24

2.1.6 Growth Software..25

2.2 In-Situ Characterization..26

2.2.1 Reflection High Energy Electron Diffraction (RHEED)...........27

2.2.2 Optical Pyrometry..28

2.2.3 Residual Gas Analyzer 28

2.3 Substrates..29

2.4 Plasma Assisted Molecular Beam Epitaxy of GaN 30

2.5 Conclusions...34

2.6 References...35

Chapter 3: Low Temperature PAMBE Growth of GaN 37

3.1 First Generation Riber Plasma Source Results...................................38

3.1.1 Growth Rate..38

3.1.2 Surface Morphology 42

3.1.3 Unintentional Impurity Incorporation.......................................45

3.1.4 Electron Mobility......48

3.1.5 Growth Diagram Modification for High Flux Nitrogen......50

3.2 Second Generation Riber Plasma Source......55

3.2.1 Growth Rate......55

3.2.3 SIMS Doping/Impurity Analysis......61

3.2.4 Thick Buffer Growth......65

3.2.5 Electron Mobility......67

3.2.6 Detrimental Ion Flux......69

3.3 Conclusions......69

3.4 References......71

Chapter 4: High Temperature PAMBE Growth of GaN......74

4.1 Decomposition Analysis......75

4.2 Surface Morphology......79

4.3 Growth Diagram......84

4.4 Electron Mobility......85

4.5 Conclusions......87

4.6 References..88

Chapter 5: High Nitrogen Flux Growth of InGaN..89

5.1 Initial InGaN Growth..90

5.2 Growth of a PAMBE LED 99

5.3 Conclusions...104

5.4 References...105

Chapter 6: Conclusions and Future Work 106

Appendix A: Processing Methods 110

A.1 n-type Hall Effect Samples 110

Appendix B: Active Nitrogen – N vs. N_2^* 113

B.1 Active Nitrogen..113

B.2 Measurement Techniques 118

B.2.1 Optical Emission Spectroscopy (OES) 119

B.2.2 Line of Sight Quadrupole Mass Spectroscopy (LOS-QMS) ...121

B.2.3 Line of Sight Threshold Ionization Mass Spectroscopy (LOS-TIMS) 122

B.3 Literature Results from OES 122

B.4 Literature Results from LOS-QMS & LOS-TIMS 128

B.5 Conclusions 131

B.6 References 132

Appendix C: Ion Measurement Technique 136

C.1 Ion Measurement Technique – Langmuir-like Probe 137

C.2 References 140

Chapter 1: Introduction and Background

Plasma-assisted molecular beam epitaxy (PAMBE) growth of gallium nitride (GaN) has evolved over the past two decades due to progress in growth science and in the active nitrogen plasma source hardware. The transition from electron cyclotron resonance (ECR) microwave plasma sources to radio frequency (RF) plasma sources has enabled higher growth rates, reduced ion damage [1] and improved operation at higher growth chamber pressures [2], [3]. Even with further improvements in RF plasma sources, PAMBE has remained primarily a research tool which is in part due to limitations in material growth rates and techniques.

This thesis explores the growth of GaN and indium gallium nitride (InGaN) thin films by PAMBE utilizing a novel modification of a commercially available nitrogen plasma source. This modified plasma source allows for exceptionally high amounts of active

nitrogen to be present at the growth surface resulting in record growth rates and growth regimes previously unattainable by PAMBE.

To begin, a brief discussion of the basic properties of group III-Nitrides will be presented to provide an overview of this remarkable material system. A historical look at how GaN has been grown and is grown today then leads into why PAMBE was chosen to be the focus of this work. Finally, a summary of the remaining chapters is presented.

1.1 Basic Properties of III-Nitrides

The group III-Nitride system has at its disposal perhaps the largest bandgap range of any material system, from ~0.7 eV for InN to more than 6.2 eV for AlN [4]. Figure 1 demonstrates this wide bandgap range as compared to the in-plane lattice constant for each binary compound. This wide variation in available bandgaps provides the basis for a multitude of GaN based devices, from lasers and LEDs to many flavors of transistors.

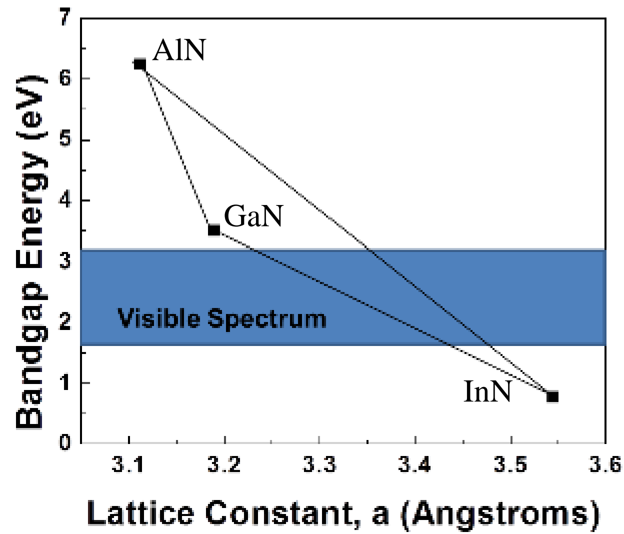

Figure 1 -- Bandgap energy vs in plane lattice constant a, for the binary III-Nitrides. Note that bowing parameters have been neglected.

The most stable crystal structure of GaN and its alloys is the wurtzite crystal structure, as shown in Fig. 2. GaN also exists in other polytypes, for example there have been reports of cubic phase (β-GaN) [5] and mixed wurtzite/cubic phase [6]. For this work we focused only on wurtzite GaN (α-GaN).

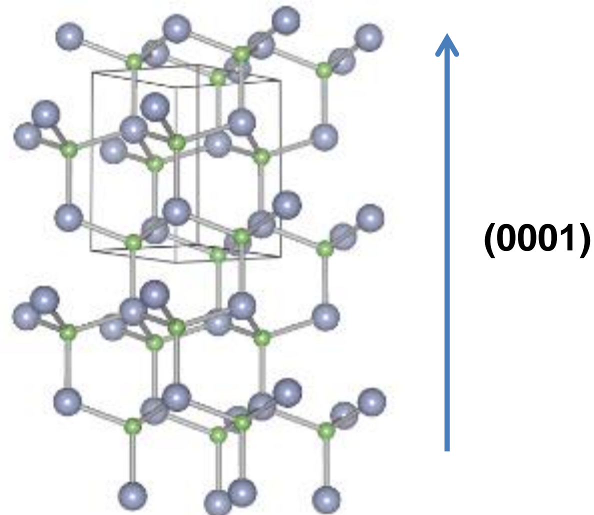

Figure 2 -- Image of the wurtzite structure of GaN. The rectangular solid denotes the wurtzite crystal structure primitive cell. The large blue spheres represent gallium atoms, while the small green spheres represent nitrogen atoms.

One of the key features of wurtzite GaN is the lack of centro-symmetry of the crystal. This results in a large spontaneous and pietzoelectric polarization which can be manipulated, forming the basis for many electronic and optoelectronic devices. Traditionally, most growth has been performed on the c-plane or in the (0001) growth direction which is the most polar and thus exhibits the strongest polarization.

Recently there has been a large amount of interest in growing on semi-polar and non-polar planes, especially for optoelectronic devices. Growth of optoelectronic devices on

these planes mitigates the quantum confined stark effect (QCSE) which separates the electron and hole wavefunctions and results in poor efficiency of optoelectronic devices.

1.2 Growth of III-Nitrides

1.2.1 Metal Organic Chemical Vapor Deposition (MOCVD)

Metal organic chemical vapor deposition (MOCVD) is the industry standard growth technique for GaN and GaN devices. In general, highly pure metal organic precursors are flowed over a heated substrate at near atmospheric pressures. Upon coming into contact with a gaseous boundary layer, the metal organic molecules begin to decompose leaving behind the metal atoms desired for growth.

Early work on MOCVD growth of GaN performed by Profs. Akasaki and Amano [7], [8] was hindered by non-uniformities in crystal quality and the lack of observable p-type doping. Through the use of low energy electron beam irradiation [9] p-type conduction was observed via Mg doping, although the nature of the technique prevented industrial adoption.

Interest in MOCVD of GaN improved dramatically in the early 1990’s with the discovery by Nakamura et al. [10], that Mg doping of GaN was compensated by hydrogen and this hydrogen could be thermally annealed out of the material providing for high p-type

conductivity. Shortly thereafter Nakamura et al. demonstrated the first candela-class high brightness LED [11] and quantum well laser diodes [12].

1.2.2 Molecular Beam Epitaxy (MBE)

Molecular beam epitaxy (MBE) is the growth technique chosen for this work. In principal, MBE is a relatively simple yet incredibly powerful growth technique. Elemental sources are evaporated in an ultra-high vacuum environment and this evaporated material is directed towards a heated substrate. Upon impinging on the substrate the adsorbed atoms, or adatoms, aided with the thermal energy of the substrate diffuse to a native bonding site. In this way, crystal layers are epitaxially grown on the substrate.

In practice however, crystal growth by MBE can be a challenging endeavor. This can be especially true for GaN. The challenge in MBE growth of GaN lies in the group V component, specifically nitrogen. There are two methods of achieving nitrogen: either using a nitrogen plasma to provide active nitrogen, or using ammonia (NH_3) which pyrolitcally decomposes on the substrate surface thus providing the necessary nitrogen for growth.

MBE of most compound semiconductors (GaAs, InP, etc.) is performed in a group V rich environment at temperatures near half of the melting point of the semiconductor [13]. Contrary to this, PAMBE of GaN is commonly performed at temperatures far lower than half of the GaN melting point due to the low decomposition temperature of GaN in vacuum

[14]. N-rich growth at these low temperatures suffers from a faceted rough surface morphology [15] which is due to the large kinetic barriers to adatom surface migration [16], [17]. To provide sufficient adatom mobility to facilitate high quality material it has been demonstrated that Ga-rich growth with a ~2.4 ML laterally contracted bilayer is necessary [15], [18], [19]. More specific details regarding PAMBE growth of GaN will be provided in the next chapter.

NH_3-MBE traditionally has higher growth temperatures, due to the large overpressure of NH_3 in the system providing significantly more nitrogen to the sample surface. This overpressure mitigates the crystal decomposition thus allowing for growth similar to traditional MBE of III-V compounds.

1.3 Why Molecular Beam Epitaxy of III-Nitrides?

Given the fact that MOCVD is the industry standard modern growth technique for GaN, then why should we even consider growing III-Nitrides by MBE? There is no single answer to this question, but instead a long list of reasons.

First, the ultra-high vacuum environment of MBE minimizes the unintentional dopants within the material. Primarily these include carbon and oxygen, where carbon is a known amphoteric dopant and oxygen is the leading culprit of unintentional n-type material. Second, MBE throughout multiple material systems has abrupt turn-on/turn-off of

intentional dopants. Most notably in the nitrides is Mg, which has a known memory effect in MOCVD reactors. Combining this abrupt doping ability with the fact that MBE p-type material is activated as-grown alone provides a powerful reason for interest in this growth technique. Finally, there have been numerous achievements in MBE grown material including record electron mobilities in GaN [20], demonstration of pure AlN interlayers [21], [22] and homogeneous InAlN [23].

1.4 Overview of the Thesis

Chapter 2 is devoted to descriptions of the MBE system used throughout our research and the experimental techniques involved. Chapter 3 presents low temperature Ga-rich growth results across various modifications of the high flux plasma source. Growth rates in excess of 7 μm/h were achieved with smooth surfaces and high crystal quality. Chapter 4 describes the exploration of a high temperature growth regime. GaN was grown at temperatures in excess of 850 °C with high crystal quality. Additionally, a high temperature growth window was found and the implications of Ga/N ratio explored. Chapter 5 presents work on high nitrogen flux growth of InGaN including the growth of a MBE LED. Finally, in chapter 6 conclusions and future work are presented for the reader.

1.5 References

[1] V. Kirchner, H. Heinke, U. Birkle, S. Einfeldt, D. Hommel, H. Selke, and P. L. Ryder, "Ion-induced crystal damage during plasma-assisted MBE growth of GaN layers," *Phys. Rev. BCondensed Matter*, vol. 58, no. 23, pp. 15749–15755, 1998.

[2] A. V. Blant, O. H. Hughes, T. S. Cheng, S. V. Novikov, and C. T. Foxon, "Nitrogen species from radio frequency plasma sources used for molecular beam epitaxy growth of GaN," *Plasma Sources Sci. Technol.*, vol. 9, no. 1, pp. 12–17, 2000.

[3] A. Georgakilas, H. M. I. N. Ng, and P. Komninou, "Plasma-Assisted Molecular Beam Epitaxy of III-V Nitrides," in *Nitride Semiconductors: Handbook on Materials and Devices*, P. Ruterana, M. Albrecht, and J. Neugebauer, Eds. Weinheim: Wiley-VCH, 2003, pp. 109–111.

[4] I. Vurgaftman and J. R. Meyer, "Band parameters for nitrogen-containing semiconductors," *J. Appl. Phys.*, vol. 94, no. 6, pp. 3675–3696, 2003.

[5] J. I. Pankove, "Luminescence in GaN," *J. Lumin.*, vol. 7, pp. 114–126, 1973.

[6] M. Katsikini, E. C. Paloura, and T. D. Moustakas, "Experimental determination of the N-p-partial density of states in the conduction band of GaN: Determination of the polytype fractions in mixed phase samples," *J. Appl. Phys.*, vol. 83, no. 3, p. 1437, 1998.

[7] M. Hashimoto, H. Amano, N. Sawaki, and I. Akasaki, "Effects of hydrogen in an ambient on the crystal growth of GaN using Ga(CH3)3 and NH3," *J. Cryst. Growth*, vol. 68, no. 1, pp. 163–168, Sep. 1984.

[8] H. Amano, N. Sawaki, I. Akasaki, and Y. Toyoda, "Metalorganic vapor phase epitaxial growth of a high quality GaN film using an AlN buffer layer," *Appl. Phys. Lett.*, vol. 48, no. 5, p. 353, 1986.

[9] H. Amano, M. Kito, K. Hiramatsu, and I. Akasaki, “P-Type Conduction in Mg-Doped GaN Treated with Low-Energy Electron Beam Irradiation (LEEBI),” *Jpn. J. Appl. Phys.*, vol. 28, no. Part 2, No. 12, pp. L2112–L2114, Dec. 1989.

[10] S. Nakamura, N. Iwasa, M. Senoh, and T. Mukai, “Hole Compensation Mechanism of P-Type GaN Films,” *Jpn. J. Appl. Phys.*, vol. 31, no. Part 1, No. 5A, pp. 1258–1266, May 1992.

[11] S. Nakamura, T. Mukai, and M. Senoh, “Candela-class high-brightness InGaN/AlGaN double-heterostructure blue-light-emitting diodes,” *Appl. Phys. Lett.*, vol. 64, no. 13, p. 1687, 1994.

[12] S. Nakamura, M. Senoh, S. Nagahama, N. Iwasa, T. Yamada, T. Matsushita, H. Kiyoku, and Y. Sugimoto, “InGaN-Based Multi-Quantum-Well-Structure Laser Diodes,” *Jpn. J. Appl. Phys.*, vol. 35, no. Part 2, No. 1B, pp. L74–L76, Jan. 1996.

[13] J. Tsao, *Materials Fundamentals of Molecular Beam Epitaxy*. London, UK: Academic Press, 1993.

[14] S. Fernández-Garrido, G. Koblmüller, E. Calleja, and J. S. Speck, “In situ GaN decomposition analysis by quadrupole mass spectrometry and reflection high-energy electron diffraction,” *J. Appl. Phys.*, vol. 104, no. 3, pp. 1–6, 2008.

[15] E. Tarsa, B. Heying, X. Wu, P. Fini, S. DenBaars, and J. Speck, “Homoepitaxial growth of GaN under Ga-stable and N-stable conditions by plasma-assisted molecular beam epitaxy,” *J. Appl. Phys.*, vol. 82, no. June, p. 5472, 1997.

[16] N. Newman, “The energetics of the GaN MBE reaction: a case study of meta-stable growth,” *J. Cryst. Growth*, vol. 178, no. 1–2, pp. 102–112, 1997.

[17] T. Zywietz, J. Neugebauer, and M. Scheffler, “Adatom diffusion at GaN (0001) and $(000\bar{1})$ surfaces,” *Appl. Phys. Lett.*, vol. 73, no. 4, pp. 487–489, 1998.

[18] B. Heying, I. Smorchkova, C. Poblenz, C. Elsass, P. Fini, S. Den Baars, U. Mishra,

and J. S. Speck, "Optimization of the surface morphologies and electron mobilities in GaN grown by plasma-assisted molecular beam epitaxy," *Appl. Phys. Lett.*, vol. 77, no. 18, p. 2885, 2000.

[19] J. Northrup, J. Neugebauer, R. Feenstra, and a. Smith, "Structure of GaN(0001): The laterally contracted Ga bilayer model," *Phys. Rev. B*, vol. 61, no. 15, pp. 9932–9935, 2000.

[20] E. C. H. Kyle, S. W. Kaun, P. G. Burke, F. Wu, Y.-R. Wu, and J. S. Speck, "High-electron-mobility GaN grown on free-standing GaN templates by ammonia-based molecular beam epitaxy," *J. Appl. Phys.*, vol. 115, no. 19, p. 193702, May 2014.

[21] S. W. Kaun, B. Mazumder, M. N. Fireman, E. C. H. Kyle, U. K. Mishra, and J. S. Speck, "Pure AlN layers in metal-polar AlGaN/AlN/GaN and AlN/GaN heterostructures grown by low-temperature ammonia-based molecular beam epitaxy," *Semicond. Sci. Technol.*, vol. 30, no. 5, p. 055010, May 2015.

[22] B. Mazumder, S. W. Kaun, J. Lu, S. Keller, U. K. Mishra, and J. S. Speck, "Atom probe analysis of AlN interlayers in AlGaN/AlN/GaN heterostructures," *Appl. Phys. Lett.*, vol. 102, no. 11, p. 111603, 2013.

[23] S. W. Kaun, E. Ahmadi, B. Mazumder, F. Wu, E. C. H. Kyle, P. G. Burke, U. K. Mishra, and J. S. Speck, "GaN-based high-electron-mobility transistor structures with homogeneous lattice-matched InAlN barriers grown by plasma-assisted molecular beam epitaxy," *Semicond. Sci. Technol.*, vol. 29, no. 4, p. 045011, Apr. 2014.

Chapter 2: Experimental Details and Equipment Description

The foundation of any research lies both in a strong scientific base and in the equipment used. This chapter describes the growth equipment used throughout our research. In addition, some basic experimental details are explained and detailed.

Chapter 2: Experimental Details and Equipment Description

2.1 Growth System

The molecular beam epitaxy (MBE) system used throughout this work was a modified Varian Gen II (referred to as the Nitride Gen II at UCSB and throughout this chapter). The Gen II is traditionally a research and development system, capable of growth on a single substrate up to 3" in diameter. This is in stark contrast to production level MBE systems capable of growing on wafers up to 300 mm in diameter, or platens of substrates containing 7 x 6" wafers, 14 x 4" wafers, or 23 x 3" wafers [1].

The Nitride Gen II contains 3 distinct vacuum chambers as can be seen in Fig. 1: an (a) entry/exit transfer chamber, a (b) buffer chamber and (c) the main growth chamber.

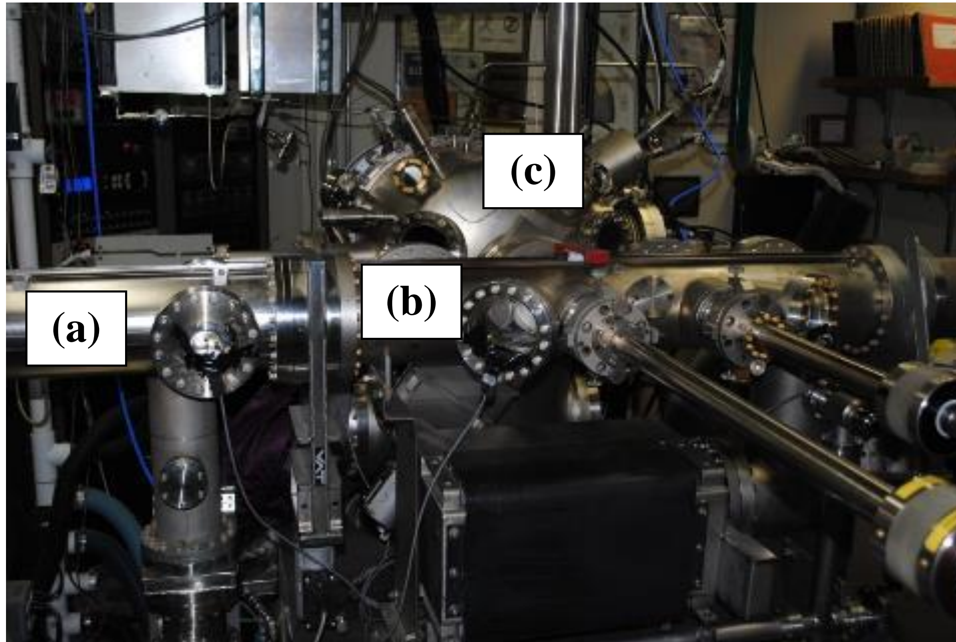

Figure 3 – Image of the Nitride Gen II denoting (a) Entry/Exit chamber, (b) Buffer chamber and (c) the Growth chamber.

Each chamber is isolated from the other via a VAT gate valve which is rated to leak at less than 3 x 10^{-10} Torr l/s [2].

Samples are transferred between the entry/exit chamber and the buffer chamber via a magnetically coupled trolley system. Currently the system has blocks allowing for sample sizes of 1 cm^2 x 1 cm^2, ¼ of a 2" wafer, a full 2" wafer, and blocks allowing for samples to be indium bonded to a Si substrate.

2.1.1 Entry Exit Chamber

Ideally, the entry/exit (E/E) transfer chamber, Fig. 2, is the only chamber of the system which regularly sees the outside environment. The E/E chamber is vented to atmosphere approximately once per day using house nitrogen gas to allow for loading and unloading of samples.

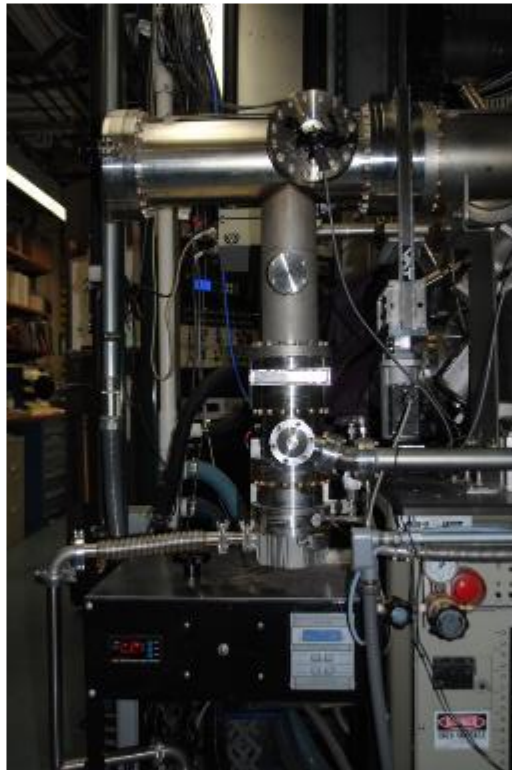

Figure 4 -- Entry exit chamber of the Nitride Gen II

Pumping on this chamber is accomplished with a Agilant TV301 NAV turbomolecular (turbo) pump that is roughed by an Edwards XDS 10 scroll pump. This turbo pump has a pumping capability of 250 l/s for nitrogen, 220 l/s for helium and 200 l/s

for hydrogen [3]. The E/E turbo pump is also capable of being opened to the system manifold (to be discussed later), allowing for pumping of any chamber by the E/E turbo pump. When the E/E turbo pump is being used for this, it can be isolated from the E/E chamber itself via a VAT gate valve.

Venting of the E/E chamber is accomplished through an in-house developed system, containing a baratron pressure gauge, the controller until for the E/E turbo pump and a push button to initiate venting of the system. This in-house system controls the spin-up/spin-down of the turbo pump as well as has a built-in delay switch for the nitrogen purge to start.

2.1.2 Buffer Chamber

The buffer chamber serves as an isolated chamber between the E/E chamber and the main growth chamber itself. It contains a heater station to allow for baking of samples and sample holders, capable of temperatures in excess of 800 °C. Pumping of the buffer chamber is accomplished with a 220 l/s ion pump. In addition, there is a Ti-sublimation pump available on the chamber, allowing for rapid pump-down as necessary. An image of the buffer chamber is presented in Fig. 3.

This chamber also houses the transfer arms used to load samples into the growth chamber and onto the buffer chamber's heater station.

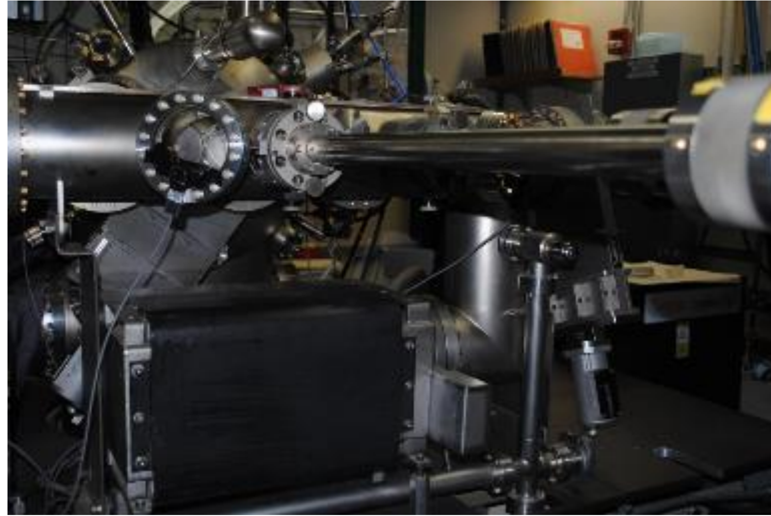

Figure 5 -- The Buffer Chamber on the Nitride Gen II.

2.1.3 MBE Growth Chamber

The heart and soul of the Nitride Gen II is its growth chamber which can be seen in Fig. 4.

Figure 6 -- The Nitride Gen II growth chamber as seen from the front right of the source flanges.

The growth chamber has 8 source ports, 4 upward facing and 4 downward facing, and the way they are used are described below. There are also numerous in-situ characterization tools attached to the growth chamber which will also be described later in this chapter.

Substrate heating is done with a water-cooled graphite-composite substrate heater, capable of temperatures in excess of 1100 °C. The substrate heater assembly is capable of rotation along two azimuths, one for moving the sample from the loading position to the growth position and the other for rotation of the sample during growth.

On the back of the substrate heater is one of the ion gauges, referred to as the beam flux monitor. This ion gauge is used to measure the fluxes of the source material, providing

a beam equivalent pressure (BEP). The second ion gauge in the main chamber is located close to the gate valve separating the main chamber from the buffer chamber.

Pumping on the main chamber is accomplished with three pumps. Two CTI-8 cryo pumps capable of pumping water at 4000 l/s and nitrogen at 1500 l/s are used during growth. To improve the overall background vacuum of the chamber there is a diode ion pump capable of pumping nitrogen at 400 l/s. This pumping provides background pressures in the low 10^{-10} Torr on a nightly basis.

2.1.3.1 Solid Sources

Six of the available source ports on the growth chamber are dedicated to solid elemental sources. Whenever possible, 7N (99.99999%) purity source material is loaded for these sources. The six solid sources are loaded as follows:

- Gallium – Two source ports are dedicated to Ga. One source port contains a Titan dual-filament high capacity cell (E-Science, Hudson, WI). This cell is capable of being loaded with nearly 450 g of Ga and was instrumental in minimizing maintenance during the high growth rate studies. The other source port contains a standard SUMO dual-filament cell (Veeco, St. Paul, MN). This cell is capable of being loaded with approximately 200 g of Ga and serves mainly as a backup in case of issues with the main Titan cell. Also, the second cell can be used for additional fluxes, as in the case of having an alloying flux in addition to the main GaN growth

flux. The crucible used in the Titan cell is a graphite crucible, while a standard pyrolytic boron nitride (pBN) SUMO crucible is used in the SUMO cell.

- Aluminum – One source port is dedicated to Al. This source port contains a standard SUMO dual-filament cell (Veeco, St. Paul, MN) although only the base of the cell is heated. Standard loading of the Al cell is approximately 50 g of Al. The crucible used is a wide-lipped pBN SUMO crucible designed for use in Al SUMO cells. The combination of heating on the base of the cell and the wide-lipped crucible increase the lifetime of the cell by reducing Al creep at the crucible tip.
- Indium – One source port is dedicated to In. This source port contains a standard conical dual-filament cell (Applied Epi, St. Paul, MN), loaded with approximately 150 g of In.
- Silicon – One source port is dedicated to Si which is a n-type dopant in GaN. This port contains a standard single filament high temperature dopant cell. While the standard metals (Ga, Al, In) are all loaded on upward facing source ports due to the molten nature of the material, the Si cell is loaded on a downward facing source port. Therefore the Si source material is melted and fused to the crucible at more than 1600 °C before it is loaded into the chamber. Standard operating temperatures of the cell are below the Si melting point, i.e. the Si doping flux is sublimated from the surface of the source material.

- Magnesium – The final solid source port is dedicated to Mg which is a p-type dopant in GaN. This port contains a dual gas-source and low temperature dopant cell. Unlike Si which is melted into the crucible, the Mg source material remains as a solid ingot. This requires a screen to be put into the pBN crucible to prevent the Mg ingot from falling out due to the downward facing nature of the cell. Similar to Si, the standard operating temperatures of the cell are below the Mg melting point and the material is sublimated from the surface of the ingot.

2.1.3.2 Gas Sources

The final two available downward facing source ports on the growth chamber are used for nitrogen plasma sources. In addition a dual dopant cell is used allowing for gas injection of carbon tetrabromide (CBr_4) on the same source port as the solid Mg cell.

2.1.3.2.1 Riber RFN-50/63Nitrogen Plasma Source

All of the work presented in this thesis was performed using the Riber RFN-50/63 nitrogen plasma source equipped with an auto-tuning attachment. This is a commercially available source which has demonstrated active nitrogen fluxes sufficient for growth rates of 200-500 nm/h [4]. However, the basis of this thesis was on modifying this plasma source to provide active nitrogen fluxes significantly higher than previously used.

Three generations of the Riber nitrogen plasma source will be discussed throughout this work. The purpose of the first two generations was increasing the active nitrogen flux,

while the third generation was focused on reducing detrimental ion fluxes from the plasma source.

2.1.3.2.2 Veeco Unibulb Nitrogen Plasma Source

A second nitrogen plasma source is available on the Nitride Gen II. This source is a standard commercially available Veeco Unibulb source capable of growth rates approaching 200-500 nm/h. While this source has been the primary plasma source here at UCSB, it was not used for the work presented in this thesis.

2.1.3.2.3 CBr_4

Carbon tetrabromide (CBr_4) is used to dope films with carbon, thus providing capability for the growth of semi-insulating material [5]. While injected into the system as a gas source, the actual CBr_4 is a white crystal contained in a stainless steel bubbler within a commercially available source (Applied Epi, St. Paul, MN). It is then sublimated from this crystal, passing through a gas manifold internal to the source and then through a leak valve to drop its effective flux into the 10^{-8}-10^{-9} Torr beam equivalent pressure (BEP).

One of the challenges with the CBr_4 setup on the Nitride Gen II is the fact that the gas injector is co-located with the Mg source. This results in a poisoning effect of the Mg charge, forming a shell around the pure Mg. Thus when p-type doping is necessary, the Mg cell must be heated to a high temperature for an extended period to decompose this shell, allowing the Mg flux to leave the cell.

2.1.4 System Manifold

In addition to each chamber being attached to each other directly, isolated by VAT gate valves, each chamber is also attached to a central system manifold. Each chamber is isolated from the manifold via a metal seal valve. A portion of the manifold assembly is shown in Fig. 5.

Figure 7 -- External portion of the system manifold showing the gas inlets as well as the connection to the main chamber's metal seal valve.

This manifold allows for venting of any of the three chambers independently as well as regeneration of the cryo pumps attached to the main chamber. On the Nitride Gen II's manifold there is a rather large leak, so purging of the manifold and repumping is necessary before any of the isolated chambers (buffer or growth) are exposed.

2.1.5 Electronics Cabinet

The electronics cabinet of the Nitride Gen II was nearly completely upgraded and modernized in 2012. As can be seen in Fig. 6, the right side of the electronics cabinet houses all the systems Eurotherm PID controllers, DC power supplies, MFC controller, switches for opening and closing of VAT gate valves attached to one of the cryo pumps and the growth chamber's ion pump, and the growth chamber's ion gauge controllers.

Figure 8 -- Right side of the Nitride Gen II electronics cabinet.

2.1.6 Growth Software

The brains of the MBE system (beyond hopefully the growers themselves) is a suite of computer software called AMBER (MBE Control, Goleta, CA). In addition to controlling temperature settings and ramp rates of the Eurotherm PID controllers, AMBER has built-in recipe writing functionality. Recipes can be written to control opening and closing of shutters, adjustment of temperature settings, starting and stopping substrate rotation and much more. As an example of the interface for AMBER, the temperature control screen is presented in Fig. 7.

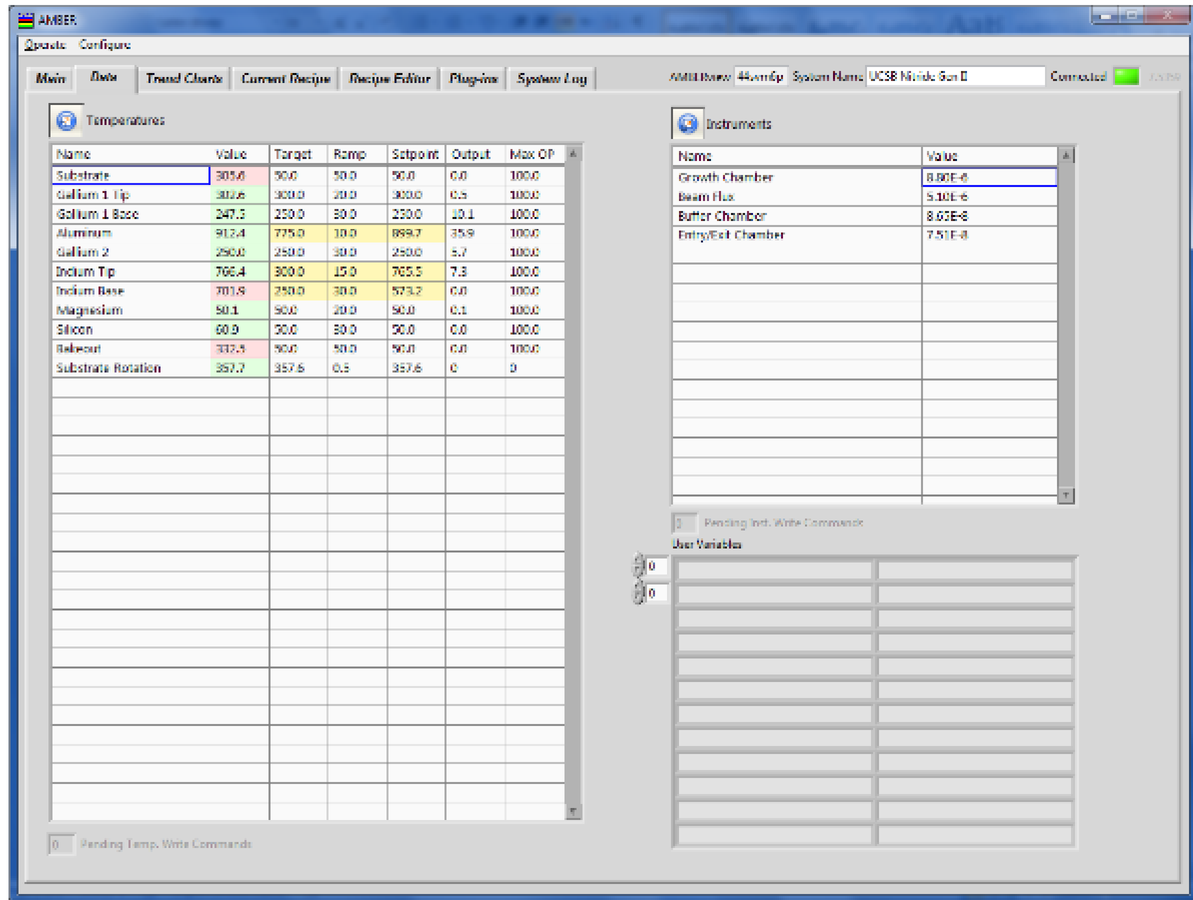

Figure 9 -- Temperature control screen of the Nitride Gen II's operating software, AMBER.

2.2 In-Situ Characterization

The ultra-high vacuum nature of MBE allows for a wealth of in-situ characterization tools.

2.2.1 Reflection High Energy Electron Diffraction (RHEED)

One of the most powerful in-situ characterization tools available on the MBE system is reflection high energy electron diffraction (RHEED). In this technique, a RHEED gun produces high energy electrons which are directed at the sample surface at a grazing angle. These electrons interact with the sample surface and are subsequently reflected and diffracted towards a phosphor coated RHEED screen. The electrons luminescence the phosphors in the RHEED screen, allowing for viewing of the diffraction pattern. On modern systems, a computer connected camera is directed at the RHEED screen which can then take and save images.

The applications of RHEED are vast. Measuring oscillations of the diffraction pattern can provide information of the growth mode of the crystal; if there are oscillations, then the crystal is growing in a 2D layer-by-layer growth mode. No oscillations, but still a strong streaky diffraction pattern suggest that the crystal is growing in a 2D step-flow growth mode. When the streaky pattern becomes spotty, it is likely a transition into a 3D growth mode. Chevrons along the spots indicate faceting of the crystal surface, and rings through the spots tend to indicate a polycrystalline crystal surface.

In PABME growth of GaN, as will be discussed later in this chapter in great detail, RHEED plays an important role in monitoring and maintaining the necessary ~2.4 monolayer (ML) Ga surface coverage during Ga-rich growth. This is accomplished by monitoring the specular spot of the RHEED diffraction pattern along the $[11\bar{2}0]$ azimuth.

2.2.2 Optical Pyrometry

Optical pyrometry allows for measurement of the substrate temperature based upon the blackbody emission from the substrate. Careful calibration of the emissivity of the measured surface is required to ensure accurate temperature measurements. To calibrate the emissivity of our Ti-backed substrates, a 5000 Å thick layer of Al is typically deposited on the surface. Then the calibration sample is slowly heated towards 660 °C, i.e. the melting point of Al. When the Al begins to melt and ball up on the surface, then the pyrometer is aimed at the surface and the emissivity adjusted as we know what the surface temperature is at that point. For all experiments presented in this thesis, an emissivity of 0.63 was used.

2.2.3 Residual Gas Analyzer

A residual gas analyzer (RGA) model RGA 200 (Stanford Research Systems, Stanford, CA) resides on a side port of the growth chamber. The RGA is used to monitor the component gases remaining in the growth chamber. It is effectively a robust quadrupole mass spectrometer, measuring mass to charge ratios from 1 to 100+. This allows early detection of issues in the growth chamber, i.e. leaks, by monitoring the ambient atmosphere for water, oxygen, argon, etc. In addition, the RGA is used to helium leak test after any maintenance is done on the growth chamber.

2.3 Substrates

Three different substrates were used throughout the work presented in this thesis. Two of them are MOCVD grown templates, one being a conductive substrate of ~3 μm GaN:Si on sapphire (STN) with [Si] ~3 x 10^{18} with threading dislocation density of ~5 x 10^8 cm^{-2}. This template was used for the majority of our work, specifically all growth rate and surface morphology characterization. The other template which was used primarily for Hall effect measurement samples was ~3.5 μm of GaN:Fe on sapphire (STINS) with a nominal resistance of 10 MΩ and a threading dislocation density of ~ 8 x 10^8 cm^{-2}.

The third and final substrate used is a free-standing GaN wafer (FS-GaN). These are ~300 μm thick wafers with a threading dislocation density of ~1-2 x 10^7 cm^{-2}, and a resistivity of < 30 mΩ cm. All substrates are purchased from St. Gobain (Lumilog).

To facilitate heating of the transparent substrate, a 5000 Å layer of Ti is deposited on the roughened backside of the single side polished wafers. This layer of Ti also provides the surface to be measured by optical pyrometry as described earlier.

Standard pre-loading cleaning of samples is performed in a solvent hood, and consists of 3 min in acetone, 3 min in methanol, and 3 min in isopropanol; all sonicated in an ultrasonic bath. Loading of the samples is performed in a clean hood.

An example AFM image of the STN substrate is presented in Fig. 8.

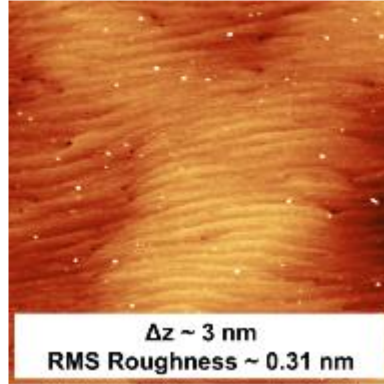

Figure 10 -- AFM of STN substrate.

2.4 Plasma Assisted Molecular Beam Epitaxy of GaN

PAMBE growth of GaN is most commonly performed in a metal rich step flow growth mode with a saturated Ga metal wetting layer on the growth surface. Initial reports on homoepitaxially grown PAMBE GaN demonstrated that growth within a metal rich regime was necessary to achieve smooth surfaces without severe morphological defects. Further, based on reflection high energy electron diffraction (RHEED) patterns Tarsa et al. speculated that there was more than one atomic layer of Ga metal present on the growth surface [6]. The necessity of a saturated Ga metal wetting layer was confirmed through adatom diffusion calculations on the (0001) and $(000\bar{1})$ surfaces of GaN [7]. These calculations demonstrated that there is a significant difference in the Ga adatom diffusion barrier, depending whether the surface is Ga saturated or N saturated. Specifically, the

calculated migration barrier for a Ga adatom increases more than fourfold from 0.4 eV on a Ga metal saturated (0001) surface to 1.8 eV on a N saturated (0001) surface [7]. An initial PAMBE GaN growth diagram was reported demonstrating a transition between an intermediate metal rich regime and a droplet regime, with the best surface morphologies within the intermediate Ga metal rich regime [8].

Additional theory work suggested that the most energetically favorable surface coverage for Ga adatom mobility on the (0001) GaN surface would be a laterally contracted Ga metal bilayer [9]. This was confirmed through the use of line of sight quadrupole mass spectroscopy (LOS-QMS) and reflection high energy electron diffraction (RHEED), the border between this intermediate metal rich regime and droplet regime was shown to be ~2.4 ML of Ga. Further, a specific RHEED intensity trend of the specular spot along the $[11\bar{2}0]$ azimuth was reported which allows for determination of the Ga metal surface coverage during Ga desorption. Namely, Brown et al. showed that when desorbing the Ga adlayer, the RHEED intensity rises during desorption of the top ~1.4 ML of Ga, followed by a short intensity decrease, and finally the RHEED intensity increases during the final desorption of the excess Ga on the GaN surface [10] (the studies of RHEED transients follow earlier work from Adelmann et al. [11]). The duration of the change in RHEED depends on both substrate temperature and excess Ga coverage. Subsequently, Koblmüller et al. studied the RHEED transient during Ga adsorption. Again, an initial decay in the RHEED intensity was observed, followed by a short recovery in intensity and finally a full decay in RHEED

intensity [12]. The initial decay corresponds to the first ~1 ML of Ga adsorbing to the GaN surface with the transient intensity rise corresponding to the completion of the first ML of Ga. The continued RHEED intensity decay corresponds to adsorption of the second ~1.4 ML of Ga, with the decay in the RHEED intensity a result of the complete formation of the Ga bilayer, and thus reducing the intensity of the reflected RHEED beam [8], [12]. Similar to the desorption trends, while the length in time of the RHEED intensity decay is dependent on substrate temperature, the overall trend is dependent only on the actual Ga surface coverage.

PAMBE growth of GaN under metal rich conditions with a saturated Ga wetting layer, but without Ga droplets, has produced amongst the high quality GaN by any technique as shown by Heying et al. [13]. This was demonstrated with a GaN film having a bulk room temperature mobility of 1191 $cm^2/V \cdot s$. However, slight variations in either substrate temperature or Ga/N ratio may result in the formation of Ga droplets. Growth in the droplet growth regime has been demonstrated to affect the surface morphology and electrical properties of GaN, as shown by the room temperature mobility dropping to below 800 $cm^2/V \cdot s$ [13].

Temperature effects can be mitigated through the use of a modulated growth technique [14] in which GaN growth is performed in short periods followed by a prolonged Ga desorption at the growth temperature. The Ga flux used in this technique is fully in the droplet growth regime, however because of the frequent interruptions the time average Ga

flux is below the droplet growth regime border, leaving a smooth surface which is droplet and pit free. The immediate challenge inherent in this modulated growth technique is both the necessity of precise shutter timing to avoid severe droplet formation and the technological challenge of increased wear on the shutter mechanism. Additionally, due to growth in what is effectively the droplet growth regime, there may be morphological remnants leading to possibly inferior material.

High temperature nitrogen rich PAMBE growth of GaN [15] is a viable alternative to the challenges presented with metal rich growth. The necessary adatom mobility for smooth, reduced defect growth is achieved by growing at temperatures above thermal decomposition [16]. Room temperature electron mobilities of more than 1100 $cm^2/V \cdot s$ were reported. In addition, conductive atomic force microscopy demonstrated that material grown in the high temperature, near stoichiometric regime is free of the vertical leakage pathways [17] traditionally associated with metal rich growth. While these results are promising the current generation of RF plasma sources does not provide sufficient active nitrogen to push the growth temperatures much above 780 °C before decomposition dominates growth, thus limiting this growth technique’s full potential.

2.5 Conclusions

In this chapter the growth system used throughout this thesis was described in detail. In addition, a detailed description of the positives and negatives of PAMBE growth of GaN was presented. Throughout this thesis these ideals will be revisited and it will be demonstrated how the high flux nitrogen source modifies and/or improves PAMBE growth of GaN.

2.6 References

[1] Riber, “Riber 7000 Production MBE System.” [Online]. Available: http://www.riber.com/en/products/mbe-systems/production-systems/mbe-7000.html.

[2] VAT, “UHV Gate Valve.” [Online]. Available: http://www.vatvalve.com/products/catalog/A/108_1_V.

[3] Agilant, “TV-301 Navigator Website.” [Online]. Available: http://www.chem.agilent.com/Library/brochures/TV 301 Navigator Brochure.pdf.

[4] K. Klosek, M. Sobanska, G. Tchutchulashvili, Z. R. Zytkiewicz, H. Teisseyre, and L. Klopotowski, “Optimization of nitrogen plasma source parameters by measurements of emitted light intensity for growth of GaN by molecular beam epitaxy,” *Thin Solid Films*, vol. 534, pp. 107–110, 2013.

[5] D. S. Green, U. K. Mishra, and J. S. Speck, “Carbon doping of GaN with CBr 4 in radio-frequency plasma-assisted molecular beam epitaxy,” *J. Appl. Phys.*, vol. 95, no. 12, pp. 8456–8462, 2004.

[6] E. Tarsa, B. Heying, X. Wu, P. Fini, S. DenBaars, and J. Speck, “Homoepitaxial growth of GaN under Ga-stable and N-stable conditions by plasma-assisted molecular beam epitaxy,” *J. Appl. Phys.*, vol. 82, no. June, p. 5472, 1997.

[7] T. Zywietz, J. Neugebauer, and M. Scheffler, “Adatom diffusion at GaN (0001) and $(000\bar{1})$ surfaces,” *Appl. Phys. Lett.*, vol. 73, no. 4, pp. 487–489, 1998.

[8] B. Heying, R. Averbeck, L. F. Chen, E. Haus, H. Riechert, and J. S. Speck, “Control of GaN surface morphologies using plasma-assisted molecular beam epitaxy,” *J. Appl. Phys.*, vol. 88, no. 4, p. 1855, 2000.

[9] J. Northrup, J. Neugebauer, R. Feenstra, and a. Smith, “Structure of GaN(0001): The laterally contracted Ga bilayer model,” *Phys. Rev. B*, vol. 61, no. 15, pp. 9932–9935, 2000.

[10] J. S. Brown, G. Koblmüller, F. Wu, R. Averbeck, H. Riechert, and J. S. Speck, “Ga adsorbate on (0001) GaN: In situ characterization with quadrupole mass spectrometry and reflection high-energy electron diffraction,” *J. Appl. Phys.*, vol. 99, no. 7, pp. 1–8, 2006.

[11] C. Adelmann, J. Brault, E. Martinez-Guerrero, G. Mula, H. Mariette, L. S. Dang, and B. Daudin, “Molecular-Beam Epitaxy of GaN: A Phase Diagram,” *Phys. Status Solidi Appl. Res.*, vol. 188, no. 2, pp. 575–578, 2001.

[12] G. Koblmüller, S. Fernández-Garrido, E. Calleja, and J. S. Speck, “In situ investigation of growth modes during plasma-assisted molecular beam epitaxy of (0001) GaN,” *Appl. Phys. Lett.*, vol. 91, p. 161904, 2007.

[13] B. Heying, I. Smorchkova, C. Poblenz, C. Elsass, P. Fini, S. Den Baars, U. Mishra, and J. S. Speck, “Optimization of the surface morphologies and electron mobilities in GaN grown by plasma-assisted molecular beam epitaxy,” *Appl. Phys. Lett.*, vol. 77, no. 18, p. 2885, 2000.

[14] C. Poblenz, P. Waltereit, and J. S. Speck, “Uniformity and control of surface morphology during growth of GaN by molecular beam epitaxy,” *J. Vac. Sci. Technol. B Microelectron. Nanom. Struct.*, vol. 23, no. 4, p. 1379, 2005.

[15] G. Koblmüller, F. Wu, T. Mates, J. S. Speck, S. Fernández-Garrido, and E. Calleja, “High electron mobility GaN grown under N-rich conditions by plasma-assisted molecular beam epitaxy,” *Appl. Phys. Lett.*, vol. 91, no. 22, pp. 23–25, 2007.

[16] S. Fernández-Garrido, G. Koblmüller, E. Calleja, and J. S. Speck, “In situ GaN decomposition analysis by quadrupole mass spectrometry and reflection high-energy electron diffraction,” *J. Appl. Phys.*, vol. 104, no. 3, pp. 1–6, 2008.

[17] J. J. M. Law, E. T. Yu, G. Koblmüller, F. Wu, and J. S. Speck, “Low defect-mediated reverse-bias leakage in (0001) GaN via higherature molecular beam epitaxy,” *Appl. Phys. Lett.*, vol. 96, no. 10, pp. 7–9, 2010.

Chapter 3: Low Temperature PAMBE Growth of GaN

The main results of low temperature growth experiments are presented in this chapter. As was described in the previous chapter PAMBE GaN growth has been traditionally performed in a metal-rich environment. This is necessary to provide sufficient adatom mobility which then results in smooth surfaces and excellent material quality. Thus all samples discussed throughout this chapter were grown in a metal-rich growth environment.

This chapter is broken up into two main sections, correlating with the first two generations of the high flux plasma source. A growth diagram is proposed with the first generation results facilitating rapid determination of growth conditions regardless of Ga or

N flux. In addition to determining the dependence of growth rates on the source parameters (plasma power and N_2 flow), with the second generation of the high flux plasma source thick buffers were grown, up to 25 μm thick to demonstrate the source's capability and to explore possible dislocation reduction. Finally, motivations for the third generation plasma source are presented based upon inferior electron mobility samples achieved with the second generation of the high flux plasma source.

3.1 First Generation Riber Plasma Source Results

3.1.1 Growth Rate

The RF forward plasma source power and nitrogen flow rate were varied for metal rich growth conditions to determine the highest GaN growth rate. All samples were grown at a substrate temperature of 730 °C with a saturated Ga wetting layer (~2.4 ML Ga) on the sample surface. Based on previous studies of GaN decomposition [1] it was assumed that there would be negligible decomposition at 730 °C. Growth of GaN with a ~2.4 ML saturated Ga wetting layer has previously demonstrated optimal sample surface morphology and material quality for growth in the Ga-rich regime [2]–[5]. The saturated Ga wetting layer thickness was confirmed by RHEED. Samples were grown using N_2 flow rates of 1, 2, 3, 5 and 8 sccm. For each of these N_2 flow rates a sample series varying the RF forward power supplied to the plasma source was grown and characterized, specifically at 200, 300,

400, 500 and 600 Watts. For each active nitrogen flux, i.e. any specific combination of N_2 flow rate and plasma power, the corresponding Ga flux during growth was determined using RHEED to ensure the presence of the 2.4 ML saturated wetting layer. Each growth rate sample consisted of a 45 second $Al_xGa_{1-x}N$ layer was grown followed by a timed 5 minute layer of GaN growth. The AlGaN layer provided a sufficiently different lattice constant such that Pendellösung thickness fringes were readily apparent from HR-XRD scans as can be seen in Fig. 1, and thus the thickness of the GaN layer could be determined from the fringe spacing. In this way the growth rate of GaN, and therefore the active nitrogen flux used in growth at the substrate for any given set of plasma conditions was determined with high accuracy.

According to Lebeau et al. [23], the diffracted x-ray intensity for an epitaxial film can be calculated as a function of the out-of-plane wavevector q_z as $I \propto |E^2|$, where $q_z = 4\pi \sin\theta / \lambda$ and the complex amplitude E is the sum of terms from the film and substrate as:

$$E = F_f \frac{1 - \exp(-iq_z c_f N)}{1 - \exp(-iq_z c_f)} + F_s \frac{1 - \exp\left(-iq_z(c_f N + \delta)\right)}{1 - \exp(-iq_z c_s)}$$

Here c_f and F_f (c_s and F_s) are the (001) lattice parameter and unit cell structure factor for the film (substrate), N is the film thickness in number of unit cells and δ is the offset between the film and substrate. Considering the fact that diffracted x-ray intensity is proportional to $|E^2|$, then the thickness fringing results from a phase mismatch in the above equation.

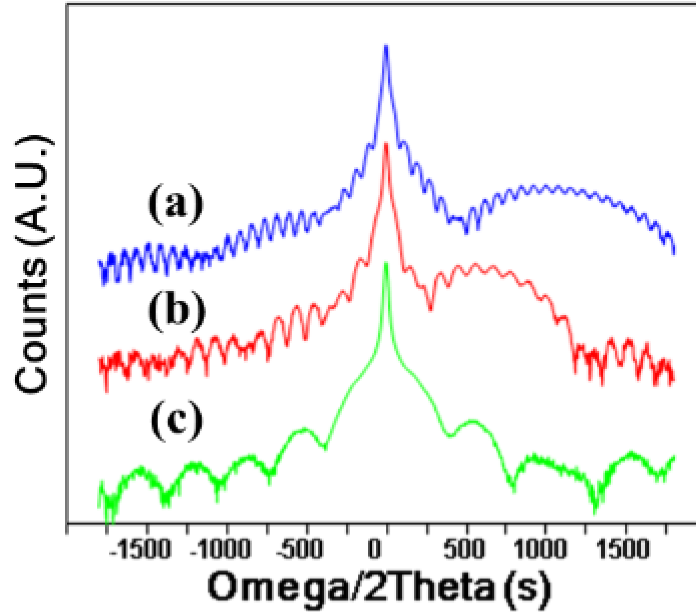

Figure 11 -- HR-XRD ω-2θ scans demonstrating the thickness fringing used to determine growth rate. Plasma source conditions and growth rates for these scans are as follow: (a) 3 sccm/600 W, 2.52 μm/h; (b) 3 sccm/400 W, 1.77 μm/h; (c) 3 sccm/200 W, 0.59 μm/h.

The HR-XRD thickness results were confirmed by high-angle angular dark field scanning transmission electron microscopy (HAADF-STEM) analysis performed on the same sample used for SIMS. Figure 2 shows the dependence of growth rate on the plasma RF forward power and N_2 flow rate. The maximum growth rate was 2.65 μm/h, and this was achieved with 600 W forward RF power on the plasma source and a N_2 flow rate of 8 sccm.

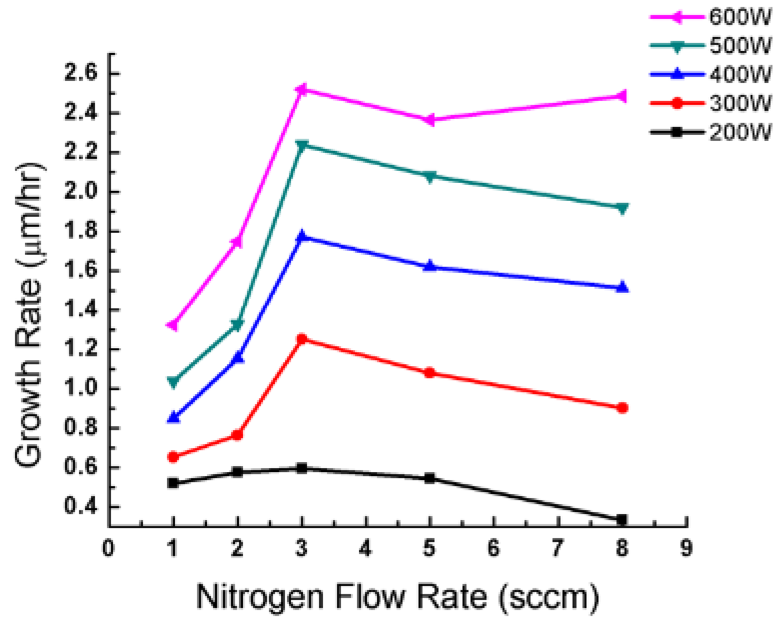

Figure 12 -- Growth rate map demonstrating the growth rate's dependence on plasma source power and N_2 flow rate. The maximum growth rate achieved was 2.65 µm/h. The plasma source operating parameters used to achieve this growth rate were 600 W RF power and a N_2 flow rate of 8 sccm.

The steep increase in growth rate with increasing N_2 flow rate, and subsequent slow decrease in growth rate with increasing N_2 flow rate (3 sccm, 200-500 W, 8 sccm 600 W) is attributed to variations in the active nitrogen species in the growth flux [6]. It is apparent that the flux of whichever species is responsible for the growth of GaN saturates at a nitrogen flow rate of approximate 3 sccm, thus the sharp increase in growth rate when the nitrogen flow rate is increased from 1 sccm to 3 sccm. The slow decrease in growth rate at nitrogen flow rates greater than 3 sccm likely results from a slight diminishment in the

active growth species. However, the determination of the specific atomic N vs. N_2^* active nitrogen species ratio at the substrate growth surface is beyond the scope of this work and therefore the active nitrogen species responsible for the growth rate variations cannot be confirmed at this time.

3.1.2 Surface Morphology

All GaN thin films grown with the Ga bilayer demonstrate a step flow surface morphology across all plasma operating conditions and therefore growth rates. A matrix of AFM images is presented in Fig. 3 that demonstrates this, i.e. regardless of the forward RF power or the N_2 flow rate a step flow surface morphology was present in all samples. The samples shown in Fig.s 3a, 3b and 3c were grown using 200 W of RF power with N_2 flow rates of 1, 3 and 8 sccm respectively. The samples shown in Fig.s 3d, 3e and 3f were grown using 600 W of RF power with N_2 flow rates of 1, 3 and 8 sccm respectively. These samples demonstrate spiral growth hillocks consistent with PAMBE GaN grown on MOCV D template [2]. Individual rms roughness calculations for each of the 3 x 3 μm AFM images (Fig. 3, insets) are reported in the caption for Fig. 3; on average they are all on the order of 1 nm. This is consistent with previously reported PAMBE GaN material [7]. Note that rms roughness of these locally smooth undulating surfaces resulting from step-flow

growth does not guarantee high quality material, just as large rms roughnesses does not necessarily suggest poor quality material.

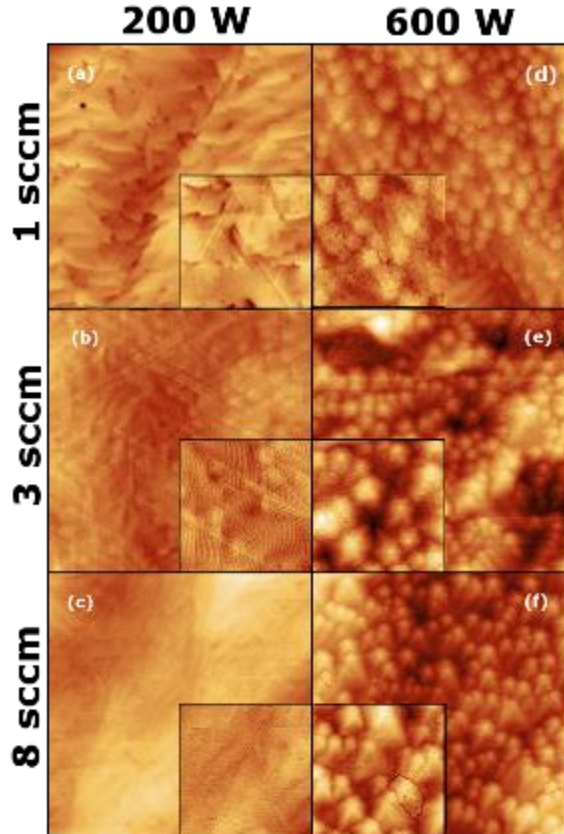

Figure 13 -- 10 x 10 µm and 3 x 3 µm (insets) AFM images of a selection of the growth rate calibration samples. The height scale for all of the 10 x 10 µm images is 15 nm, and the height scale for all of the 3 x 3 µm insets is 7.5 nm. RMS roughness calculations for the 3 µm^2 AFM images are as follow: (a) 0.56 nm; (b) 0.52 nm; (c) 0.44 nm; (d) 0.72 nm; (e) 1.44 nm; (f) 1.03 nm.

Changes of the N_2 flow rate or the RF power of the plasma should have little effect on the resulting surface morphology as the Ga flux was adjusted in accordance with the

plasma source parameters to maintain ~2.4 ML Ga surface coverage. However, while all AFM images demonstrate a surface morphology consistent with step-flow growth as expected from PAMBE metal-rich GaN, there are still some morphological differences evident in the AFM images. One possible explanation is that all samples were grown for a fixed time to allow and facilitate the measurement of the active nitrogen growth flux. Thus the samples grown with plasma RF forward power of 200 W have a significantly thinner AlGaN buffer with a different Al composition and a thinner GaN layer when compared to the samples grown with plasma RF forward power of 600 W. Additionally, the variation in surface morphology may be related to the species contained within the active nitrogen flux. There have been several reports demonstrating that variations of N_2 flow rate into the plasma sources can be directly correlated to film quality and surface morphology [6], [8]–[10]. However, many of these reports rely on optical emission spectroscopy (OES) of the plasma from the back of the plasma source as opposed to sampling the plasma at the growth surface. Further, since OES relies on emissions from molecular and atomic electron transitions, the proportion of atomic N to N_2^* cannot easily be determined. Thus while there is a correlation between the surface morphology and nitrogen plasma source operating conditions, the specific growth species responsible for the morphological variations has not yet been determined. For a more detailed discussion on active nitrogen and N vs N_2^* please see Appendix B.

3.1.3 Unintentional Impurity Incorporation

A GaN SIMS stack was grown at 730 °C and had SIMS analysis performed to quantify the unintentional impurity incorporation. The SIMS stack was grown with 10 minutes of GaN sandwiched between 60 second $Al_xGa_{1-x}N$ marker layers. The GaN layers were grown at 300 W, 400 W and 500 W of RF plasma power at N_2 flow rates of 3, 5 and 8 sccm. This represents a variation in the active nitrogen flux as determined from the growth rate study of more than 300%. The Al cell temperature was fixed at 1120 °C, therefore providing an expected constant flux for each of the marker layers while the Ga flux was varied with the active nitrogen flux to maintain the saturated Ga wetting layer. The sample was analyzed for oxygen, boron and hydrogen. The results of this analysis on oxygen and hydrogen are presented in Fig. 4.

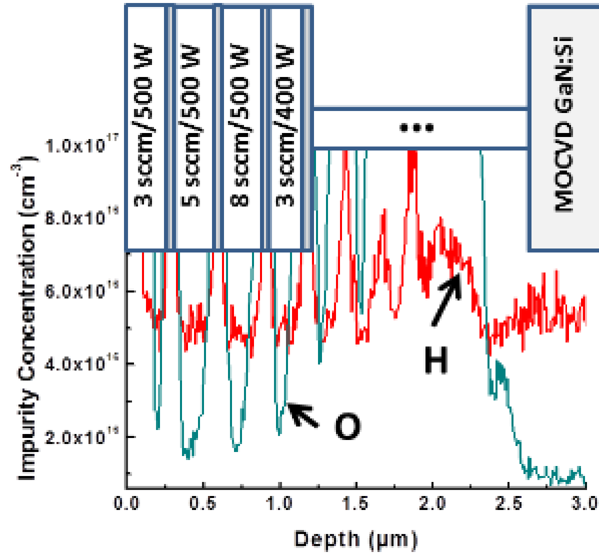

Figure 14 -- Impurity concentration for oxygen and hydrogen as determined by SIMS. Only the layers grown at nitrogen plasma conditions of 5 & 8 sccm, 500W have any scientific validity as interface roughness at the AlGaN marker layers caused smearing of the SIMS data. SIMS analysis performed by Evans Analytical (EAG) Inc, Sunnyvale, CA.

The boron concentration was approximately 7 x 10^{17} cm^{-3} throughout the GaN layers and approximately 3 x 10^{18} cm^{-3} throughout the AlGaN marker layers in the SIMS analysis. The only variations in the boron concentration were during the AlGaN marker layers as expected due to Al reactions with the pBN crucibles used in standard effusion cells [11]. It is believe that the high boron within the GaN layers is a result of etching of the pyrolytic Boron Nitride (pBN) crucible within the plamsa source itself.

Due to interfacial roughness at the AlGaN/GaN interfaces, which was verified by HAADF-STEM (HAADF-STEM results curtesy of Dr. Feng Wu), only the data from two of

the top three layers can be considered to accurately represent the impurity concentration. This corresponds to plasma conditions of 500 W RF forward power and N_2 flow rates of 5 and 8 sccm, with corresponding active nitrogen fluxes of ~34.7 nm/min and ~32.0 nm/min respectively. From the SIMS data in Fig. 4 we can see that the hydrogen concentration is approximately 5 x 10^{16} cm^{-3} and the oxygen concentration is approximately 1 x 10^{16} cm^{-3} in these two layers (5 and 8 sccm, 500W), both of which are nearly the same as the hydrogen and oxygen levels in the MOCVD grown GaN:Si template. The detection limits for hydrogen and oxygen were 5 x 10^{16} cm^{-3} and 9 x 10^{15} cm^{-3} respectively. This demonstrates that the GaN grown using these plasma source operating conditions to achieve the high active nitrogen flux has effectively the same oxygen and hydrogen impurity concentration as commercially available MOCVD material.

The sample that was grown for SIMS analysis suffered from interface roughening at some of the $Al_xGa_{1-x}N$ marker layer heterostructure interfaces. High-angle angular dark field scanning transmission electron microscopy (HAADF-STEM) analysis of the SIMS stack confirmed that the first two $Al_xGa_{1-x}N$ /GaN interfaces from the surface of the sample appear abrupt, albeit with minor thickness variations. The third interface from the surface had severe faceting effects and all other interfaces below that roughened interface appear to be abrupt. Because of this roughening, the SIMS depth profile was compromised due to nonplanar AlGaN interlayers. We believe that this interfacial roughening is a result of unoptimized heterostructure growth and it is not any indication of issues with the nitrogen

plasma source. Further, we believe that the GaN layers between these $Al_xGa_{1-x}N$ marker layers are of high quality with very low unintentional impurity incorporation. Each GaN layer in the SIMS stack was grown with different active nitrogen fluxes. For each different active nitrogen flux, a different Ga flux was necessary to properly develop the saturated Ga wetting layer necessary for high quality growth. The interfacial roughness is a result of prolonged growth interruptions while waiting for the Ga cell temperature to stabilize after growth of the $Al_xGa_{1-x}N$. During this growth interruption for the roughened interface, the Ga bilayer was completely desorbed while the sample was still exposed to the active nitrogen flux which has been previously demonstrated to produce roughened surfaces in our growths. Therefore it should be noted that the interface roughness was an isolated growth issue and is not representative of the high quality material grown using the modified nitrogen plasma source. Further SIMS analysis needs to be performed to properly quantify any improvements in unintentional impurity incorporation from the dramatically increased growth rates.

3.1.4 Electron Mobility

To verify that the material grown using the high active nitrogen flux plasma source had acceptable material quality, an un-optimized n-type sample was grown to measure mobility, electron carrier concentration and sheet resistivity. The sample was grown at a substrate temperature of 730 °C using the previously determined necessary Ga flux

corresponding with active nitrogen conditions of 10 sccm N_2 gas flow and 400 W RF forward power. The sample structure was a 1 µm thick GaN:Si layer grownwith the Si cell temperature of 1135 °C, with an expected Si concentration of approximately 8 x 10^{16} cm^{-3}. To provide an isolation layer, 200 nm of GaN:C was grown using 80 mTorr fore line pressure from a commercially available CBr_4 source (Veeco, Inc.). Carbon doping has been previously demonstrated to provide sufficient electrical isolation from the regrowth interface [12]. Hall measurements resulted in an average bulk carrier concentration of ~3.1 x 10^{16} cm^{-3}, averaged across four measured Van de Pauw patterns. The average sheet resistivity was 3692 Ω/□ and the average mobility measured across the sample was 623 cm^2/V • s, with a peak mobility measured of ~705 cm^2/V • s.

The sample that was grown for mobility measurements had unoptimized growth and doping conditions and as a result the sample had an average bulk carrier concentration of ~3 x 10^{16} cm^{-3}. In addition, the sample did not have an n^+ doped surface layer to facilitate low resistance ohmic contacts. Minor improvements in the carrier concentration, a thin n^+ layer to improve sheet resistivity and further optimized growth conditions would be expected to markedly improve the values reported.

3.1.5 Growth Diagram Modification for High Flux Nitrogen

Currently available PAMBE GaN growth diagrams [2], [4], [5] are constructed based on a fixed active nitrogen flux and thus allow determination of the necessary Ga flux for a specific growth regime. However, any variation in the plasma source's input N_2 flow rate or the RF forward power applied results in a change in the active nitrogen flux. Additionally, the active nitrogen flux tends to vary over time due to deposits that clog the holes in the plasma source's endplate aperture. These changes in active nitrogen flux at the substrate surface result in a change in the Ga/N ratio and the growth regime. Further, the active nitrogen flux used in creation of the currently available growth diagrams is of order 5 nm/min which is significantly lower than the active nitrogen flux available from the modified plasma source.

To improve on the growth diagrams our universal GaN growth diagram is presented in Fig 5. Instead of relying on a fixed nitrogen flux and varying the Ga flux, this growth diagram is constructed based upon the difference between the Ga flux (ϕ_{Ga}) and the active nitrogen flux (ϕ_{N*}), i.e. ϕ_{Ga}- ϕ_{N*}. The fluxes are expressed in GaN growth rate units (nm/min) as measured on Ga-limited and N*-limited films at temperatures of negligible thermal decomposition [2], [4], [13]. In wurtzite GaN, c/2 = 0.259 nm or 1.14 x 10^{15} GaN/cm^2 areal density correspond to 1 ML.

Reflection high energy electron diffraction (RHEED) was used to verify this revised growth diagram. As has been previously reported [4], [14], the specific GaN growth regime

can be determined by measuring the RHEED intensity transients of the specular spot along the $[11\bar{2}0]$ azimuth during GaN growth and subsequent Ga desorption.

The growth diagram has five regions, corresponding to Ga metal surface coverage. Regions (1), (2) and (3) have ϕ_{Ga}- $\phi_{N*} > 1$, and are therefore in the Ga-rich growth regime. Regions (4) and (5) have ϕ_{Ga}- $\phi_{N*} < 1$ and are therefore in the N-rich growth regime.

Region (1) is referred to as the droplet growth regime as there is more than the ~2.4 ML of Ga metal on the growth surface. The excess Ga forms metal droplets on the sample surface. When growth is interrupted to desorb the Ga bilayer the Ga droplets feed the desorbing bilayer, causing a delay in the rise of the RHEED signal after growth, as shown in Fig. 6 (RHEED transient 1). PAMBE growth of GaN in the droplet regime has been found to be step-flow growth and have smooth surfaces. However, growth in the droplet regime has been shown to have detrimental effects on the material quality demonstrated by reduced electron mobility [2].

Region (2) is referred to as the intermediate growth regime, in which the surface coverage of Ga metal is between 1 and ~2.4 ML. The ideal saturated Ga wetting layer of ~2.4 ML is found on the border between regions (1) and (2). The RHEED intensity transient in this region shows desorption of the top ~1.4 ML of Ga followed by the desorption of the final 1 ML of Ga metal as can be seen in Fig. 6 (RHEED transient 2). Growth in the

intermediate regime has been demonstrated to be in the step-flow growth mode and have excellent crystal quality [2].

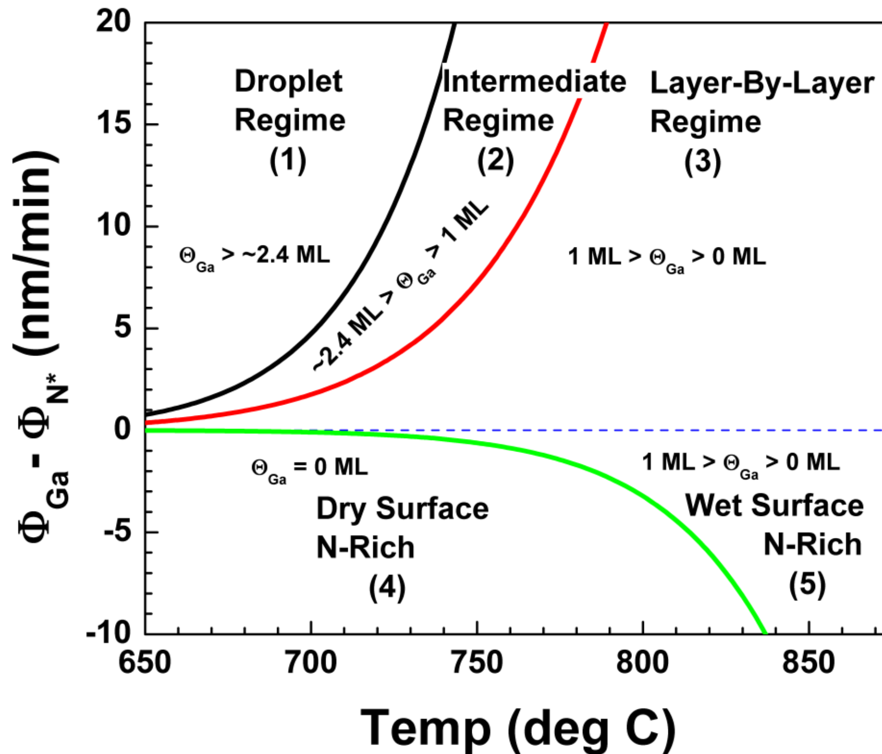

Figure 15 -- Proposed growth diagram with the following regions: (1) Droplet Region; (2) Region with 1ML – 2.4ML Ga surface coverage; (3) Region with 0-1ML Ga Surface coverage above stoichiometric Ga/N fluxes; (4) Region with 0 ML Ga surface coverage, i.e. dry surface with Ga/N flux ratios less than one; (5) Region with some Ga surface coverage below stoichiometric Ga/N fluxes, i.e. wet surface with Ga/N flux ratios less than one. The fluxes are expressed in GaN growth rate units (nm/min) as measured at temperatures of negligible thermal decomposition.

The Ga metal surface coverage in region (3) is between 0 and 1 ML. Growth of GaN in this regime is expected to be a layer-by-layer growth mode, as has been previously shown [4]. While the RHEED transient did not have intensity oscillations which would confirm the layer-by-layer growth mode, the intensity was not reduced as significantly as during growth in either regions (1) or (2) as can be seen in Fig. 6 (RHEED transient 3).

Regions (4) and (5) are both nitrogen rich growth regimes. Region (4) is assumed to have a dry surface, free from liquid Ga metal. Samples grown in region (4) have shown rough surfaces with 3-dimensional growth and very poor crystal quality [2], [4]. The RHEED intensity transient in region (4) shows an immediate degradation of the sample surface as can be seen in Fig. 6 (RHEED transient 4). If growth in this region is continued the RHEED signal will not recover and the overall RHEED pattern will become spotty.

The boundary between regions (4) and (5) is found from the decomposition of GaN in vacuum [1], therefore region (5) is assumed to have some liquid Ga metal on its growth surface even though it is a nitrogen rich growth regime. Growth in region (5) has been shown to have a layer-by-layer growth mode at temperatures up to 780 °C, smooth surfaces and excellent crystal quality as demonstrated through electron mobility measurements [15]. The RHEED intensity transient increases in intensity during growth in this region, as shown in Fig. 6 (RHEED transient 5).

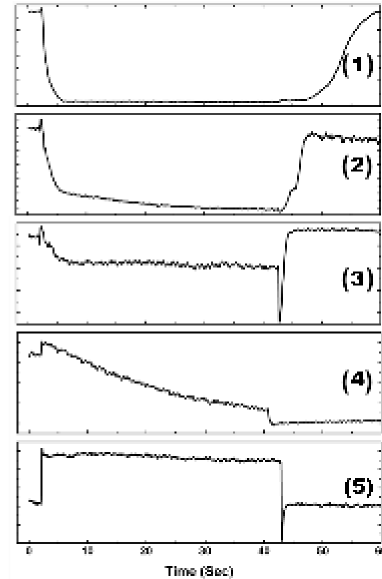

Figure 16 -- RHEED intensity transients measured during 40 sec GaN growth pulses corresponding directly with each of the 5 regions described in the growth diagram (Region 1 in Figure 5 corresponds with RHEED intensity transient (1) and so on). These transients were recorded at a substrate temperature of ~730 °C with an active nitrogen flux of ~2.65 µm/h.

In Fig. 7 we verify the universal growth diagram through the use of RHEED intensity transients for two different active nitrogen fluxes. The active nitrogen fluxes used were ~1.3 µm/h and ~2.65 µm/h. These active nitrogen fluxes correspond to plasma operating conditions of 600 W RF forward power and N_2 flow rates of 1 sccm and 8 sccm respectively. When comparing the RHEED intensity transients during GaN growth with these two fluxes at three different temperatures, we see that the intensity transients correspond well with the growth regimes described above. This demonstrates the applicability of this growth diagram regardless of the active nitrogen flux used.

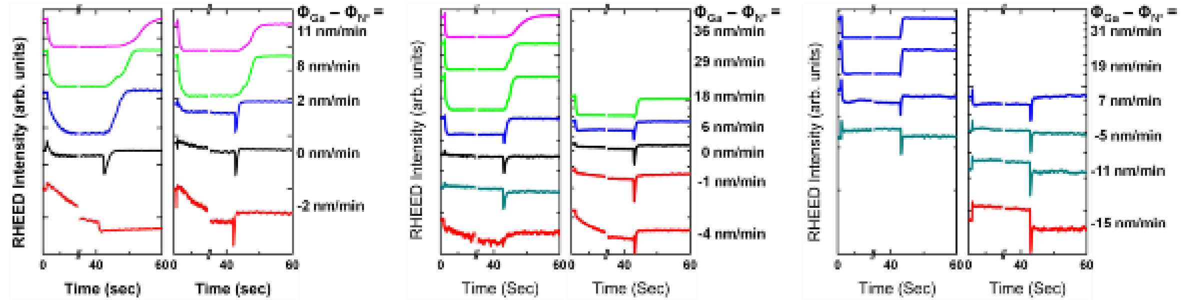

Figure 17 -- Ga flux dependent RHEED intensity transients measured during short 40 sec GaN growth pulses demonstrating the evolution of the regions described within the proposed growth diagram (Fig. 5). Left images are with plasma conditions of 1 sccm/600 W and the right images are with plasma conditions of 8 sccm/600 W, corresponding to active nitrogen fluxes of ~1.3 µm/h (~22.1 nm/min) and ~2.65 µm/h (~44.2 nm/min) respectively. The substrate temperatures used during the growths were (a) 720 °C, (b) 760 °C and (c) 800 °C.

3.2 Second Generation Riber Plasma Source

3.2.1 Growth Rate

RF forward power and nitrogen flow rate were varied for metal rich growth conditions to determine the highest GaN growth rate. All samples were grown at 730 °C in a metal-rich step-flow growth mode verified and controlled through the use of in situ reflection high energy electron diffraction (RHEED). Specifically, the intensity of the RHEED specular spot along the $[11\bar{2}0]$ azimuth was monitored during growth to allow an intensity decay time of approximately 8 seconds and an intensity rise time of 11 seconds. Note that these reported RHEED decay and rise times should only depend on temperature and excess Ga coverage. However, the RF plasma N source with the shutter in the closed

position still has some surviving active nitrogen flux that can reach the substrate and hence affect net growth, desorption and decomposition rates. While the RHEED intensity decay did not consistently show the expected evolution of the ~2.4 ML Ga metal wetting layer, the intensity rise did demonstrate the full desorption of the wetting layer as described previously, thus providing evidence of near optimal growth conditions [2], [3], [13], [16]. Based on previous studies of GaN decomposition [1] it was assumed that there would be negligible decomposition at 730 °C. Growth of GaN with a ~2.4 ML saturated Ga wetting layer has previously demonstrated optimal sample surface morphology and material quality for growth in the Ga-rich regime [2], [3], [13].

Samples were grown using N_2 flow rates of 5, 10, 15, 20 and 25 sccm. For each of these N_2 flow rates a sample series varying the RF forward power supplied to the plasma source was grown and characterized, specifically at 200, 300, 400, 500 and 600 Watts. For each active nitrogen flux, i.e. any specific combination of N_2 flow rate and plasma power, the corresponding Ga flux during growth was determined using RHEED to ensure the presence of the 2.4 ML saturated wetting layer. Each growth rate sample consisted of a thin $Al_xGa_{1-x}N$ layer was grown followed by a timed layer of GaN growth. The AlGaN layer provided an interface layer such that Pendellösung thickness fringes corresponding to the top GaN layer were readily apparent from HR-XRD scans, and thus the thickness of the GaN layer could be determined from the fringe spacing. In this way the growth rate of GaN, and therefore the active nitrogen flux used in growth at the substrate for any given set of

plasma conditions was determined with high accuracy. Figure 8 shows the dependence of growth rate on the plasma RF forward power and N_2 flow rate. The maximum growth rate was ~7.6 µm/h, and this was achieved with 600 W forward RF power on the plasma source and a N_2 flow rate of 25 sccm.

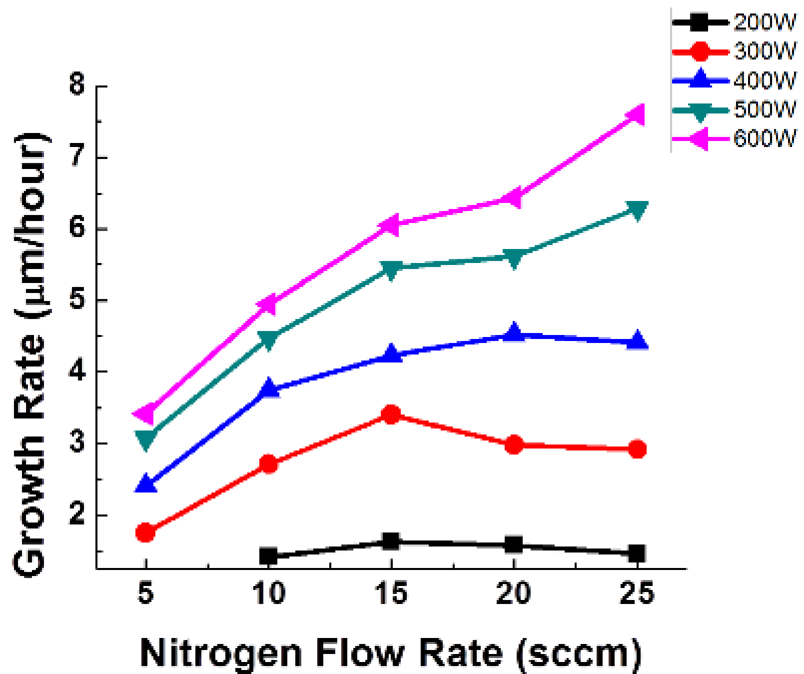

Figure 18 -- Growth rate map demonstrating the growth rate's dependence on plasma source power and N_2 flow rate. The maximum growth rate achieved was ~7.6 µm/h. The plasma source operating parameters used to achieve this growth rate were 600 W RF forward power and a N_2 flow rate of 25 sccm.

The steep increase in growth rate with increasing N_2 flow rate, and subsequent slow decrease in growth rate with increasing N_2 flow rate is attributed to variations in the active

nitrogen species in the growth flux [6]. For 200 W-400 W of RF forward plasma power the peak growth rate can be identified, although it is not at a consistent N_2 flow rate as was found with earlier modifications of the RF plasma source [17]. For 500 W and 600 W of RF forward plasma power this peak growth rate has not yet been reached at a N_2 flow rate of 25 sccm. Higher flow rates were not explored due to pumping limitations of the MBE growth system.

The active nitrogen species from RF plasma sources which are responsible for the growth of GaN remains controversial, with the commonly accepted candidates being atomic nitrogen (N) [9] or a meta-stable excited nitrogen molecule (N_2^*) [8], [18]. While both N and N_2^* have sufficient potential energy to overcome the kinetic barrier of GaN growth [19], there is still no consensus as to which is the dominant growth species. For a detailed discussion on active nitrogen and N vs N_2^* see Appendix B.

It is apparent that the flux of whichever species is responsible for the growth of GaN saturates at a given nitrogen flow rate for each plasma power, representing the maximum active nitrogen species available for a given RF forward plasma power. The slow decrease in growth rate at nitrogen flow rates greater than these maximum likely results from a slight diminishment in the active growth species. However, the determination of the specific atomic N vs. N_2^* active nitrogen species ratio at the substrate growth surface is beyond the scope of this report and therefore the active nitrogen species responsible for the growth rate variations cannot be determined at this time.

3.2.2 Surface Morphology

All GaN thin films grown with the Ga bilayer demonstrate a step flow surface morphology across all plasma operating conditions and therefore growth rates. A matrix of AFM images is presented in Fig. 9 that demonstrates this, i.e. regardless of the forward RF power or the N_2 flow rate, a step flow surface morphology was present in all samples. The samples shown in Fig. 9a, 9b, 9c and 9d were grown using a N_2 flow rate of 5 sccm with RF forward powers of 300 W, 400 W, 500W and 600 W respectively. The samples shown in Fig. 9e, 9f, 9g and 9h were grown using a N_2 flow rate of 20 sccm with RF forward powers of 300 W, 400 W, 500 W and 600 W respectively. This variation in N_2 flow rates and RF forward plasma powers correlate to a change in the GaN growth rate from ~29 nm/min to ~94 nm/min; a variation of the active nitrogen flux of more than 300%. All samples are approximately 75-150 nm in thickness. These samples demonstrate spiral growth hillocks consistent with typical PAMBE GaN grown on MOCVD template [2]. Individual RMS roughness calculations for each of the 3 x 3 µm AFM images (Fig. 9, insets) are all on the order of 1 nm. This is consistent with previously reported PAMBE GaN material [7]. As discussed previously, the rms roughness of these locally smooth undulating surfaces resulting from step-flow growth does not guarantee high quality material, just as large rms roughnesses does not necessarily suggest poor quality material.

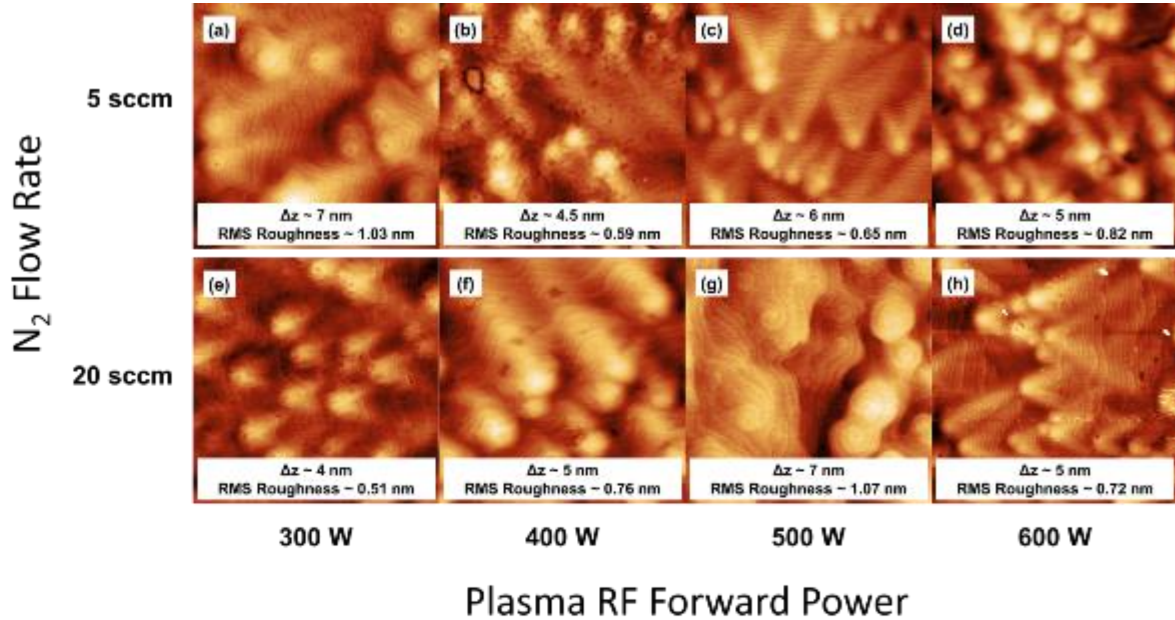

Figure 19 -- 3 µm x 3 µm AFM images of a selection of the Ga-rich high flux growth rate calibration samples. Δz is the height scale from z=0 (black) to z=Δz (white).

Changes of the N_2 flow rate or the RF power of the plasma should have little effect on the resulting surface morphology as the Ga flux was adjusted in accordance with the plasma source parameters to maintain ~2.4 ML Ga surface coverage. However, while all AFM images demonstrate a surface morphology consistent with step-flow growth as expected from PAMBE metal-rich GaN, there are still some morphological differences evident in the AFM images. One possible explanation is that the Ga surface bilayer accumulated sufficient Ga such that the growth strayed slightly into the droplet growth regime away from the optimal Ga-rich growth regime [13]. Typical Ga beam equivalent pressures (BEPs) are of the order 2-6 x 10^{-6} Torr or higher, thus for a fixed growth

temperature the exact ideal growth flux may not have been achievable. This could account for some of the slight pitting and damage on the GaN step edges visible in Figs. 9b and 9h.

A second explanation is that the variation in surface morphology may be related to the species contained within the active nitrogen flux. There have been several reports demonstrating that variations of N_2 flow rate into the plasma sources can be directly correlated to film quality and surface morphology [8], [9], [18], [20]. However, many of these reports rely on optical emission spectroscopy (OES) of the plasma from the back of the plasma source as opposed to sampling the active nitrogen species at the growth surface. Further, since OES relies on emissions from molecular and atomic electron transitions, the proportion of atomic N to N_2^* cannot actually be determined solely by OES. Thus while there is a correlation between the surface morphology and nitrogen plasma source operating conditions, the specific growth species responsible for the morphological variations has not yet been determined. Again, for a detailed discussion on N vs N_2^* see Appendix B.

3.2.3 SIMS Doping/Impurity Analysis

Two SIMS stack were grown at 730 °C and were analyzed to quantify the unintentional impurity incorporation as well as to demonstrate the doping capability of material grown at high growth rate. Each SIMS stack was grown first with 200 W and then with 500 W of RF plasma power, both at a N_2 flow rates of 20 sccm. This represents a variation in the active nitrogen flux as determined from the growth rate study of more than

300%. The Ga flux was varied with the active nitrogen flux to maintain the saturated Ga wetting layer.

The first SIMS stack was grown with ~200 nm layers of GaN:(Si, C) between ~100 nm UID GaN layers. The silicon cell temperature was varied from 1225 °C to 1350 °C in 25 °C increments. The carbon was introduced via a commercially available CBr_4 delivery system operated at foreline pressures of 40 and 80 mTorr. The second SIMS stack was grown with ~200 nm layers of GaN:Mg in between ~100 nm UID GaN layers. The magnesium cell was varied from 2.0-2.6% power in 0.2% increments for the 200 W region, and from 2.1-2.7% power in 0.2% increments for the 500W region. The samples were analyzed for oxygen and hydrogen unintentional impurities.

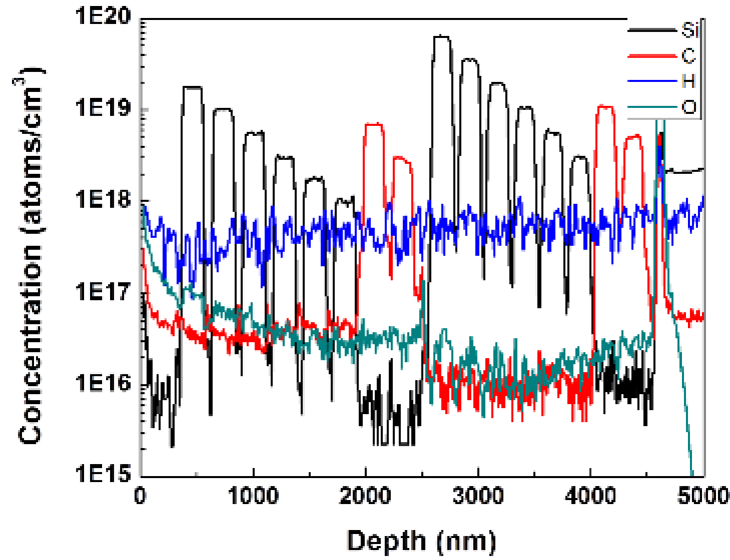

Figure 20 -- SIMS impurity and doping analysis performed demonstrating the doping capabilities of the high growth rate GaN. The dopants used were Si & C. The top portion of the SIMS stack (~2.5 µm) was grown with plasma conditions of 500 W RF forward power and N_2 flow rate of 20 sccm corresponding to a growth rate of ~85 nm/min (~5.1 µm/h). The bottom portion of the SIMS stack was grown with plasma conditions of 200 W RF forward power and N_2 flow rate of 20 sccm corresponding to a growth rate of ~26 nm/min (~1.6 µm/h). SIMS analysis performed by Evans Analytical (EAG) Inc, East Windsor, NJ.

The results of Si/C SIMS sample's analysis are presented in Fig. 10, and the results of the Mg SIMS sample's analysis are presented in Fig. 11.

From the SIMS data in Fig. 10 we can see that the silicon and carbon intentional dopants demonstrate a top hat profile. The average turn on/turn off for Si within the 500 W region was 12.1 and 11.4 nm/decade respectively. The average turn on/turn off

for Si within the 200 W region was 18.3 and 20.3 nm/decade respectively. The relatively slow turn on/turn off for the 200 W region may be a result of the depth of the SIMS crater and other crater effects. The hydrogen concentration was at detection limit throughout the sample, approximately 5 x 10^{17} cm^{-3}. The oxygen concentration was approximately 3 x 10^{16} cm^{-3} in the 500 W region, and 1 x 10^{16} cm^{-3} in the 200 W region.

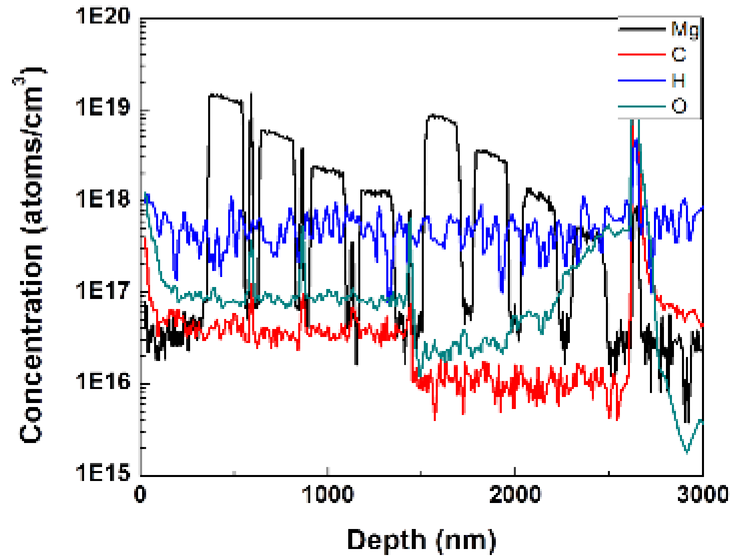

Figure 21 -- SIMS impurity and doping analysis performed demonstrating the doping capabilities of the high growth rate GaN. The dopant used was Mg. The top portion of the SIMS stack (~1.5 µm) was grown with plasma conditions of 500 W RF forward power and N_2 flow rate of 20 sccm corresponding to a growth rate of ~85 nm/min (~5.1 µm/h). The bottom portion of the SIMS stack was grown with plasma conditions of 200 W RF forward power and N_2 flow rate of 20 sccm corresponding to a growth rate of ~26 nm/min (~1.6 µm/h). SIMS analysis performed by Evans Analytical (EAG) Inc, East Windsor, NJ.

While all of the doping profiles for magnesium in Fig. 11 are not sharp top hat profiles, the initial doping profile for each power does demonstrate a clear top hat. The other profiles' lack of clear top hats is a result of operating the Mg cell at constant power and not allowing sufficient time for the flux to stabilize. The average turn on/turn off for Mg within the 500 W region was 9.8 and 10.7 nm/decade respectively. The average turn on/turn off for Mg within the 200 W region was 17.3 and 16.3 nm/decade respectively. The relatively slow turn on/turn off for the 200 W region may be a result of the depth of the SIMS crater and other crater effects. Further, note that while MOCVD has sharp turn on of Mg dopants, there is a significant memory effect within the reactor which causes a very slow turn off [24], [25]. The hydrogen concentration was at detection limit throughout the sample, approximately 6 x 10^{17} cm^{-3}. The oxygen concentration in the 500 W region was approximately 9 x 10^{16} cm^{-3} and 2 x 10^{16} cm^{-3} in the 200 W region.

The detection limits for hydrogen and oxygen were 4-7 x 10^{17} cm^{-3} and 5-6 x 10^{15} cm^{-3} respectively.

3.2.4 Thick Buffer Growth

To provide an initial demonstration of the growth capabilities of the modified plasma source, 5 µm thick UID, conductive, and resistive buffers layers were grown. These samples were grown with a plasma source forward RF power of 500 W and a N_2 flow rate of 15 sccm corresponding to a growth rate of ~5.5 µm/h. AFM images of the UID GaN, GaN:Si

and GaN:C are presented in Fig. 12a, 12b and 12c respectively. The conductive buffer was grown with a [Si] concentration of ~3 x 10^{18} cm^{-3} and the resistive buffer was grown with a [C] concentration of ~4 x 10^{18} cm^{-3} as determined from the previous SIMS analysis. From Hall Effect measurements, the UID buffer had a carrier concentration of ~2.6 x 10^{16} cm^{-3} and a mobility of 112.8 cm^2/V•s corresponding to an electrical resistivity of 2.13 Ω•cm. The conductive buffer had a carrier concentration of ~2.95 x 10^{18} cm^{-3} and a mobility of 234.5 cm^2/V•s corresponding to an electrical resistivity of 9.04 x 10^{-3} Ω•cm. The carbon doped buffer was too resistive to be measured.

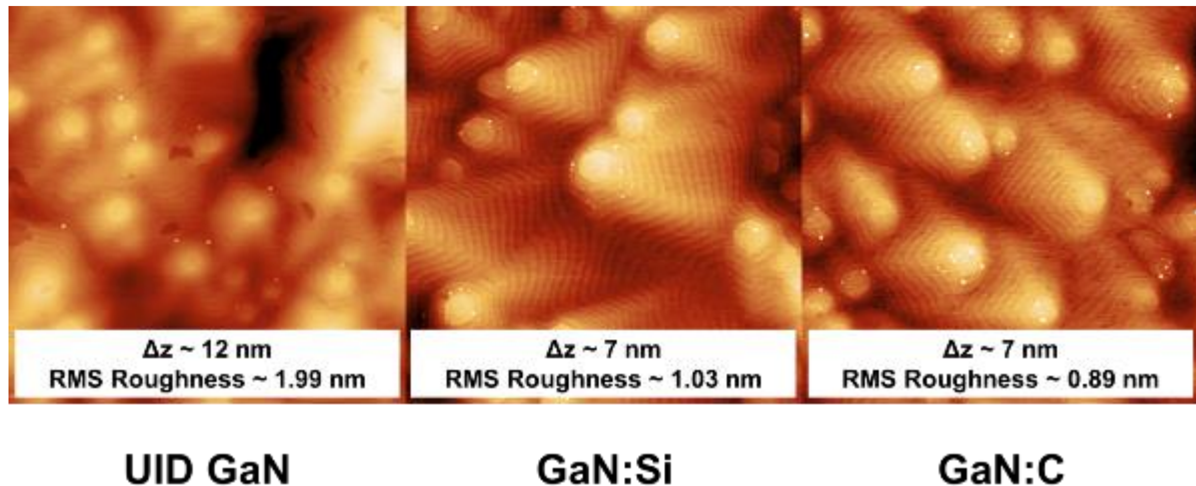

Figure 22 -- 3 µm x 3 µm AFM images of the 5 µm thick UID, conductive and resistive buffer layers from left to right. Δz is the height scale from z=0 (black) to z=Δz (white).

Finally, a very thick 25 µm sample was grown to demonstrate the possibility of dislocation reduction in thick buffers grown by PAMBE. X-ray diffraction rocking curves

were used as the FWHM of the $(20\bar{2}1)$ peak as measured in a skew-symmetric geometry has been previously demonstrated to correlate with the edge dislocation density [21]. Before growth, the FWHM of the $(20\bar{2}1)$ peak was found to be 401.8 arcsec, and after growth it was 344.5 arcsec. From rough estimates, this corresponds to a reduction in edge dislocation density from ~5 x 10^8 cm^{-2} to ~3 x 10^8 cm^{-2}. These estimates were based on calibration curves developed from plan-view transmission electron microscopy (PV-TEM) data [18], [22].

3.2.5 Electron Mobility

To verify that the material grown using the second generation high active nitrogen flux plasma source had acceptable material quality, un-optimized n-type samples were grown at selected growth conditions to measure mobility and carrier concentration. Samples was grown at a substrate temperature of 730 °C using the previously determined necessary Ga flux corresponding with active nitrogen conditions of 15 sccm N_2 gas flow and 200, 400 and 500 W RF forward power. These plasma operating conditions correspond to growth rates of 1.58 µm/h, 4.86 µm/h, and 5.51 µm/h respectively. The sample structure used was 2 µm GaN:Si, with an expected Si concentration of approximately 8 x 10^{16} cm^{-3}. To provide an electrical isolation layer, ~1 µm of GaN:C was grown using 80 mTorr fore line pressure from a commercially available CBr_4 source (Veeco, Inc.). Carbon doping has been previously demonstrated to provide sufficient electrical isolation from the regrowth interface

[12]. From these samples, Greek cross Van der Pauw patterns were photolithographically defined and mesa isolated to accurately measure the carrier concentration and Hall electron mobility. Prior to processing all samples demonstrated smooth surfaces with step-flow spiral growth around dislocations as is expected from PAMBE growth on MOCVD templates.

The results from the Hall effect measurements are presented in Fig 13. While the carrier concentration for these samples do not align well, nor are they all ideal for optimum electron mobility there appears to be a definitive trend. As the plasma power increases, the carrier mobility decreases. This could be an effect of increasing growth rate, however another possible explanation is provided in the next section.

Sample	T_Pryo	Plasma (sccm/W)	GR (μm/hr)	Avg [e-]	Avg (Max) μ (cm^2/V s)
A	720 °C	15/200	1.58	1.6E16	550 (558)
B	720 °C	15/400	4.86	3.0E15	308 (324)
C	720 °C	15/500	5.51	5.7E16	249 (278)

Figure 23 -- Mobility and carrier concentration results from selected samples.

3.2.6 Detrimental Ion Flux

One possible explanation for the poor mobilities despite acceptable carrier concentrations described in the previous section could be a large energetic ion flux impinging on the sample surface. Energetic ions have been previously suggested to cause knock-on damage resulting in point defects [9]. This was one of the benefits resulting from the transition of ECR plasma sources to RF plasma sources, namely a strong reduction in the concentration of energetic ions. The details of the ion measurement process is presented in Appendix C.

As a result of the uncertainty in the ionic species involved in producing the measured ion current (N^+ or N_2^+) and the uncertainty in the exact dimensions of the probe, it is not possible to report the exact energetic ion flux resulting from the Riber high flux nitrogen plasma source. In addition, the energetic electron flux could not be determined as the voltage source used was limited to 200 V, and the electron current never reached full saturation.

3.3 Conclusions

In conclusion, using the first generation Riber nitrogen plasma source we have demonstrated growth rates for PAMBE GaN in excess of 2.6 µm/h. AFM images verify that the films were grown in a metal-rich regime near the Ga droplet border, as the films

demonstrate a step-flow growth surface morphology. SIMS analysis demonstrates the low unintentional impurity concentration within the grown GaN, specifically a hydrogen concentration below the SIMS baseline and an oxygen concentration of 1 x 10^{16} cm^{-3}. A revised universal growth diagram is proposed allowing the rapid determination of the metal flux needed to grow in a specific growth regime for any and all active nitrogen fluxes available. In addition, an emphasis was placed on the high temperature growth regime within the growth diagram taking into consideration growth of material deep into the GaN decomposition region.

Using the second generation of the Riber nitrogen plasma source we have demonstrated growth rates for PAMBE GaN in excess of 7.6 μm/h. AFM images verify that the films were grown in a metal-rich regime near the Ga droplet border, as the films demonstrate a step-flow growth surface morphology. SIMS analysis demonstrates the low unintentional impurity concentration within the grown GaN, specifically a hydrogen concentration below the SIMS baseline and an oxygen concentration of 1 x 10^{16} cm^{-3}. The SIMS analysis also demonstrates the doping capability of the high growth rate material, with top hat doping profiles and sharp dopant turn-on/turn-off even at growth rates of several μm/h. Finally, electron mobility measurements were performed which demonstrated a decrease in mobility as plasma power increased and an energetic ion flux was suggested as one possible reason for this mobility degradation.

3.4 References

[1] S. Fernández-Garrido, G. Koblmüller, E. Calleja, and J. S. Speck, "In situ GaN decomposition analysis by quadrupole mass spectrometry and reflection high-energy electron diffraction," *J. Appl. Phys.*, vol. 104, no. 3, pp. 1–6, 2008.

[2] B. Heying, R. Averbeck, L. F. Chen, E. Haus, H. Riechert, and J. S. Speck, "Control of GaN surface morphologies using plasma-assisted molecular beam epitaxy," *J. Appl. Phys.*, vol. 88, no. 4, p. 1855, 2000.

[3] J. S. Brown, G. Koblmüller, F. Wu, R. Averbeck, H. Riechert, and J. S. Speck, "Ga adsorbate on (0001) GaN: In situ characterization with quadrupole mass spectrometry and reflection high-energy electron diffraction," *J. Appl. Phys.*, vol. 99, no. 7, pp. 1–8, 2006.

[4] G. Koblmüller, S. Fernández-Garrido, E. Calleja, and J. S. Speck, "In situ investigation of growth modes during plasma-assisted molecular beam epitaxy of (0001) GaN," *Appl. Phys. Lett.*, vol. 91, p. 161904, 2007.

[5] C. Poblenz, P. Waltereit, and J. S. Speck, "Uniformity and control of surface morphology during growth of GaN by molecular beam epitaxy," *J. Vac. Sci. Technol. B Microelectron. Nanom. Struct.*, vol. 23, no. 4, p. 1379, 2005.

[6] E. Iliopoulos, a. Adikimenakis, E. Dimakis, K. Tsagaraki, G. Konstantinidis, and a. Georgakilas, "Active nitrogen species dependence on radiofrequency plasma source operating parameters and their role in GaN growth," *J. Cryst. Growth*, vol. 278, no. 1–4, pp. 426–430, 2005.

[7] F. Natali, Y. Cordier, C. Chaix, and P. Bouchaib, "Advances in quality and uniformity of (Al,Ga)N/GaN quantum wells grown by molecular beam epitaxy with plasma source," *J. Cryst. Growth*, vol. 311, no. 7, pp. 2029–2032, 2009.

[8] T. H. Myers, M. R. Millecchia, a J. Ptak, K. S. Ziemer, and C. D. Stinespring, "Influence of active nitrogen species on high temperature limitations for (0001) GaN growth by rf plasma-assisted molecular beam epitaxy," *J. Vac. Sci. Technol. B Microelectron. Nanom. Struct.*, vol. 17, no. 4, p. 1654, 1999.

[9] A. V. Blant, O. H. Hughes, T. S. Cheng, S. V. Novikov, and C. T. Foxon, "Nitrogen species from radio frequency plasma sources used for molecular beam epitaxy growth of GaN," *Plasma Sources Sci. Technol.*, vol. 9, no. 1, pp. 12–17, 2000.

[10] K. Klosek, M. Sobanska, G. Tchutchulashvili, Z. R. Zytkiewicz, H. Teisseyre, and L. Klopotowski, "Optimization of nitrogen plasma source parameters by measurements of emitted light intensity for growth of GaN by molecular beam epitaxy," *Thin Solid Films*, vol. 534, pp. 107–110, 2013.

[11] A. J. SpringThorpe, A. Majeed, S. J. Ingrey, G. M. Smith, I. C. Bassignana, D. Macquistan, and J. T. Szymanski, "Reactions between molten aluminum and pyrolytic boron nitride crucibles," *Journal of Vacuum Science & Technology B: Microelectronics and Nanometer Structures*, vol. 11, no. 3. p. 1032, 1993.

[12] D. S. Green, U. K. Mishra, and J. S. Speck, "Carbon doping of GaN with CBr 4 in radio-frequency plasma-assisted molecular beam epitaxy," *J. Appl. Phys.*, vol. 95, no. 12, pp. 8456–8462, 2004.

[13] B. Heying, I. Smorchkova, C. Poblenz, C. Elsass, P. Fini, S. Den Baars, U. Mishra, and J. S. Speck, "Optimization of the surface morphologies and electron mobilities in GaN grown by plasma-assisted molecular beam epitaxy," *Appl. Phys. Lett.*, vol. 77, no. 18, p. 2885, 2000.

[14] C. Adelmann, J. Brault, E. Martinez-Guerrero, G. Mula, H. Mariette, L. S. Dang, and B. Daudin, "Molecular-Beam Epitaxy of GaN: A Phase Diagram," *Phys. Status Solidi Appl. Res.*, vol. 188, no. 2, pp. 575–578, 2001.

[15] G. Koblmüller, F. Wu, T. Mates, J. S. Speck, S. Fernández-Garrido, and E. Calleja, "High electron mobility GaN grown under N-rich conditions by plasma-assisted molecular beam epitaxy," *Appl. Phys. Lett.*, vol. 91, no. 22, pp. 23–25, 2007.

[16] T. Zywietz, J. Neugebauer, and M. Scheffler, "Adatom diffusion at GaN (0001) and (000$\bar{1}$) surfaces," *Appl. Phys. Lett.*, vol. 73, no. 4, pp. 487–489, 1998.

[17] B. M. McSkimming, F. Wu, T. Huault, C. Chaix, and J. S. Speck, "Plasma assisted molecular beam epitaxy of GaN with growth rates >2.6μm/h," *J. Cryst. Growth*, vol. 386, pp. 168–174, 2014.

[18] P. Waltereit, S.-H. Lim, M. McLaurin, and J. S. Speck, "Heteroepitaxial Growth of GaN on 6H-SiC(0001) by Plasma-Assisted Molecular Beam Epitaxy," *Phys. Status Solidi*, vol. 194, no. 2, pp. 524–527, 2002.

[19] N. Newman, "The energetics of the GaN MBE reaction: a case study of meta-stable growth," *J. Cryst. Growth*, vol. 178, no. 1–2, pp. 102–112, 1997.

[20] V. Kirchner, H. Heinke, U. Birkle, S. Einfeldt, D. Hommel, H. Selke, and P. L. Ryder, "Ion-induced crystal damage during plasma-assisted MBE growth of GaN layers," *Phys. Rev. BCondensed Matter*, vol. 58, no. 23, pp. 15749–15755, 1998.

[21] B. Heying, X. H. Wu, S. Keller, Y. Li, D. Kapolnek, B. P. Keller, S. P. Denbaars, and J. S. Speck, "Role of threading dislocation structure on the x-ray diffraction peak widths in epitaxial GaN films," *Appl. Phys. Lett.*, vol. 643, no. 1996, p. 643, 1995.

[22] S. W. Kaun, P. G. Burke, M. Hoi Wong, E. C. H. Kyle, U. K. Mishra, and J. S. Speck, "Effect of dislocations on electron mobility in AlGaN/GaN and AlGaN/AlN/GaN heterostructures," *Appl. Phys. Lett.*, vol. 101, no. 26, pp. 19–23, 2012.

[23] S.J. Lebeau, R. Engel-Herbert, B. Jalan, J. Cagnon, P. Moetakef, S. Stemmer, and G. B. Stephenson, "Stoichiometry optimization of homoepitaxial oxide thin films using x-ray diffraction," *Appl. Phys. Lett.,* vol. 95, 142905, 2009

[24] Y. Ohba and A. Hatano, "A study on strong memory effects for Mg doping in GaN metalorganic chemical vapor deposition," *J. Cryst. Growth,* vol. 145, pp. 214-218, 1994.

[25] H. Xing, D. S. Green, H. Yu, T. Mates, P. Kozodoy, S. Keller, S. P. Denbaars, and U. K. Mishra, "Memory Effect and Redistribution of Mg into Sequentially Regrown GaN Layer by Metalorganic Chemical Vapor Deposition," *Jpn J. Appl. Phys..* vol. 42, 50, 2003.

Chapter 4: High Temperature PAMBE Growth of GaN

Low temperature PAMBE growth of GaN presents many challenges to the grower. The necessity of tight control over both the Ga-flux and the substrate temperature to ensure the sample remains at the border between the droplet regime and the intermediate regime is perhaps the largest of these challenges.

High temperature PAMBE growth of GaN lifts this tight control on flux and temperature by growing at temperatures above GaN decomposition. Early demonstrations [1], [2] of high temperature nitrogen-rich PAMBE growth were most promising. Record electron mobilities were achieved [1] and this high temperature growth environment demonstrated low vertical leakage through the sample [3]. However, these early attempts at

high temperature growth were in fact limited to temperatures of ~770 °C due to the low active nitrogen flux available at the substrate.

In this chapter we explore this high temperature regime. With the high active nitrogen flux plasma source we are able to achieve growth at temperatures ~150 °C above our standard Ga-rich growth conditions, and ~100 °C greater than was previously attainable. In addition, a growth diagram is proposed demonstrating the large growth window available at these growth temperatures.

4.1 Decomposition Analysis

Substrate temperature and Ga/N ratio were varied to determine the relative growth rates for samples grown at high temperature within the GaN decomposition regime. All samples were grown with plasma conditions of 400 W RF forward power and a N_2 flow rate of 20 sccm. To prevent unwanted decomposition and surface roughening, samples were heated to the growth temperature and quenched after growth under a N_2 flow rate of 20 sccm and the plasma was only on during the growth itself. Based on our study of Ga-rich GaN growth rate these plasma conditions correlate to an active nitrogen flux of ~70 nm/min. The Ga-rich GaN growth rate study was performed at low temperature with no evidence of decomposition, thus this provides a good estimate of the active nitrogen flux.

Each sample consisted of a thin $Al_xGa_{1-x}N$ layer followed by a timed layer of GaN growth. Pendellösung thickness fringes were readily apparent from HR-XRD scans, and thus the thickness of the GaN layer could be determined from the fringe spacing. In this way the growth rate of GaN was determined with high accuracy. Subtracting the expected growth rate from the measured growth rate provides an accurate decomposition rate for each set of growth conditions. Figure 1 shows the dependence of decomposition rate on growth conditions as compared with GaN decomposition in vacuum [4]. For samples with a Ga/N ratio of ~1 and greater, we see an increase in the decomposition rate due to catalytic decomposition from the excess Ga. Conversely, for samples with a Ga/N ratio of <1 we see a suppression in decomposition due to recapture of Ga adatoms by the excess active nitrogen impinging on the substrate. These trends in decomposition rate are consistent with those reported by Fernández-Garrido et al.[4].

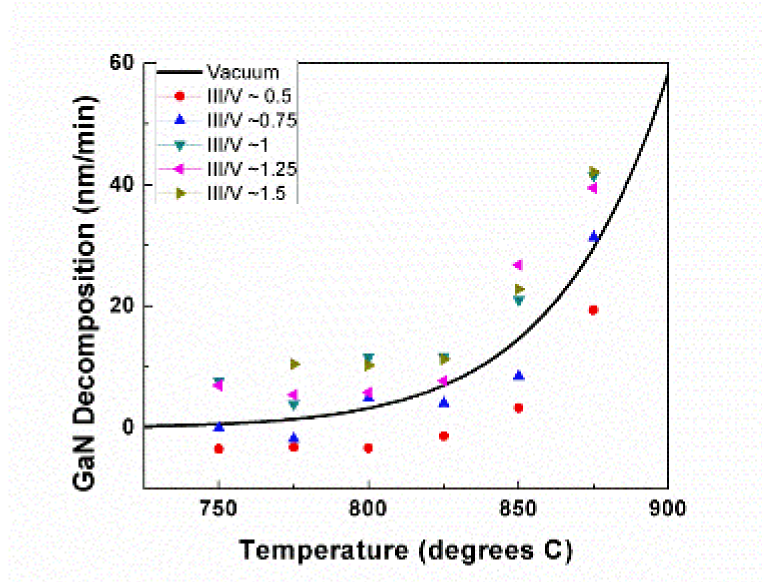

Figure 24 -- Decomposition rates of various Ga/N ratios versus temperature. For Ga/N ratios ≥ 1, the decomposition rates are greater than that of GaN in vacuum. For Ga/N ratios < 1, the decomposition rates are less than that of GaN in vacuum. The solid line is the decomposition rate of GaN in vacuum after [4]**.**

Decomposition of GaN in vacuum has been reported to have Arrhenius behavior with an apparent 3.1 eV activation energy [4]. An Arrhenius plot of select decomposition trends is presented in Fig 2. From this analysis it was found that samples grown with a Ga/N ratio ≥ 1 have a smaller decomposition activation energy than Ga/N in vacuum, specifically ~2.8 eV. The activation energy for decomposition of GaN from samples with Ga/N < 1 is ~7.9 eV which is much larger than that of Ga/N in vacuum. Thus the change in decomposition rate is not simply a prefactor effect in the Arrhenius equation but rather an actual variation in the apparent decomposition activation energy.

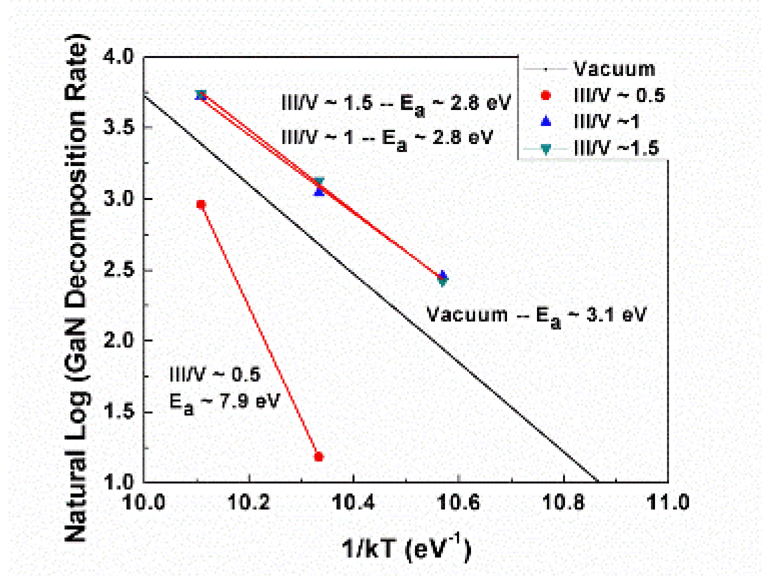

Figure 25 -- Arrhenius analysis of the natural log of decomposition rates of various Ga/N ratios versus 1/kT. The activation energies for decomposition of samples with Ga/N ratios ≥ 1 are less than that of Ga/N in vacuum. The activation energy for decomposition of GaN from samples with Ga/N < 1 is much greater than that of Ga/N in vacuum. The GaN in vacuum decomposition curve is after [4]**.**

Fernández-Garrido et al.[4] provide a detailed description of the mechanisms involved in decomposition of GaN both in vacuum and when growth fluxes are involved. Specifically they explain the decreased decomposition under nitrogen-rich growth conditions as a result of excess active nitrogen on the growth surface capturing and reincorporating Ga adatoms resulting from decomposition. Under Ga-rich growth conditions there is no excess active nitrogen available to recapture decomposing Ga adatoms

as they are all expected to be incorporated and used by the incoming Ga flux. Additionally it has been reported that the excess Ga on the sample surface in Ga-rich growth conditions may catalytically aid decomposition [5]. This model thus explains the trend we see in decomposition, with samples grown under Ga/N ratios ≥ 1having increased decomposition with respect to GaN in vacuum and samples grown with Ga/N ratios < 1 having reduced decomposition.

4.2 Surface Morphology

The surface morphology of samples grown at high temperatures was also studied as a function of temperature and Ga/N ratio. Initially we investigated Ga/N ratios of ~0.5, ~1, and ~1.5 and temperatures of 825 °C, 850 °C and 875 °C. The resulting AFM image matrix of 3 μm x 3 μm scans is shown in Fig. 3.

For samples grown with a Ga/N ratio of ~0.5, there was no temperature at which a smooth surface could be achieved. These samples showed surface morphologies consistent with earlier reports of lower temperature growth of GaN in a N-rich environment [6].

Samples grown with a Ga/N ratio of ~1 demonstrate three distinct regions of varying surface morphologies. First, at 825 °C while the surface had some smooth areas, there were

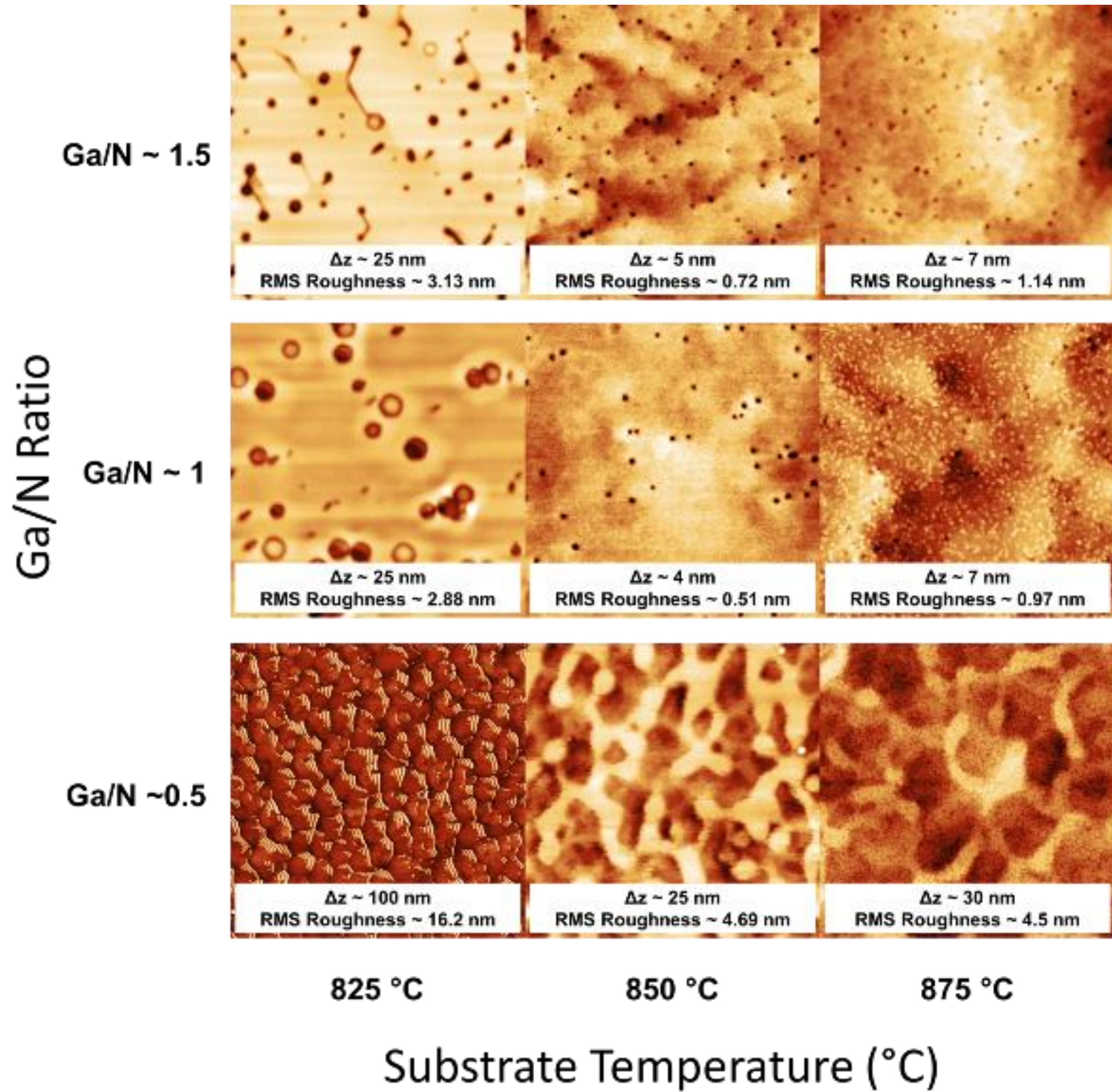

Figure 26 -- 3 µm x 3 µm AFM images of a selection of the high temperature growth rate calibration samples. Δz is the height scale from z=0 (black) to z=Δz (white).

large pits across the sample. This appears to be a result of insufficient Ga adatom mobility necessary to have smooth growth across the sample when combating decomposition resulting from the lower substrate temperature. At 850 °C the sample surface was smooth with shallow pits resulting from increased decomposition around dislocations. This smoothness was reflected in the 0.51 nm RMS roughness of the AFM image. At 875 °C the sample began to roughen as small GaN clusters start to appear on the surface, suggesting a transition into a decomposition related roughening growth mode.

Samples grown with a Ga/N flux ratio of ~1.5 similarly had different surface morphologies across the three growth temperatures. At 825 °C the sample had a distinctive intermediate regime surface morphology [8]. This suggests that the Ga surface coverage at this temperature and Ga/N ratio is approaching a full monolayer. At 875 °C we saw a similar smooth surface morphology as was found for samples grown with a Ga/N ratio of ~1 at 850 °C. The increased number of shallow pits is likely a result of the increased temperature and higher Ga surface coverage. The sample grown at 850 °C and a Ga/N ratio of ~1.5 appears to be a mixture of the intermediate growth found at 825 °C, and the smooth growth found at 875 °C.

Figure 4 explores in finer detail the growth regime around a Ga/N ratio of ~1, and temperatures between 830 °C and 860 °C. As before, the optimum growth regime was found at a Ga/N ratio of ~1 at temperatures of approximately 840-850 °C. Samples grown at a Ga/N ratio of ~1.25 showed increasing decomposition pitting as the temperature increases.

These shallow pits are likely due to catalyzed decomposition resulting from the excess Ga on the surface. Samples grown at a Ga/N ratio of ~0.75 demonstrate significant surface roughness except for the sample grown at 850 °C. This sample shows a smooth surface without the shallow pitting found in the samples with Ga/N ratios ≥ 1.

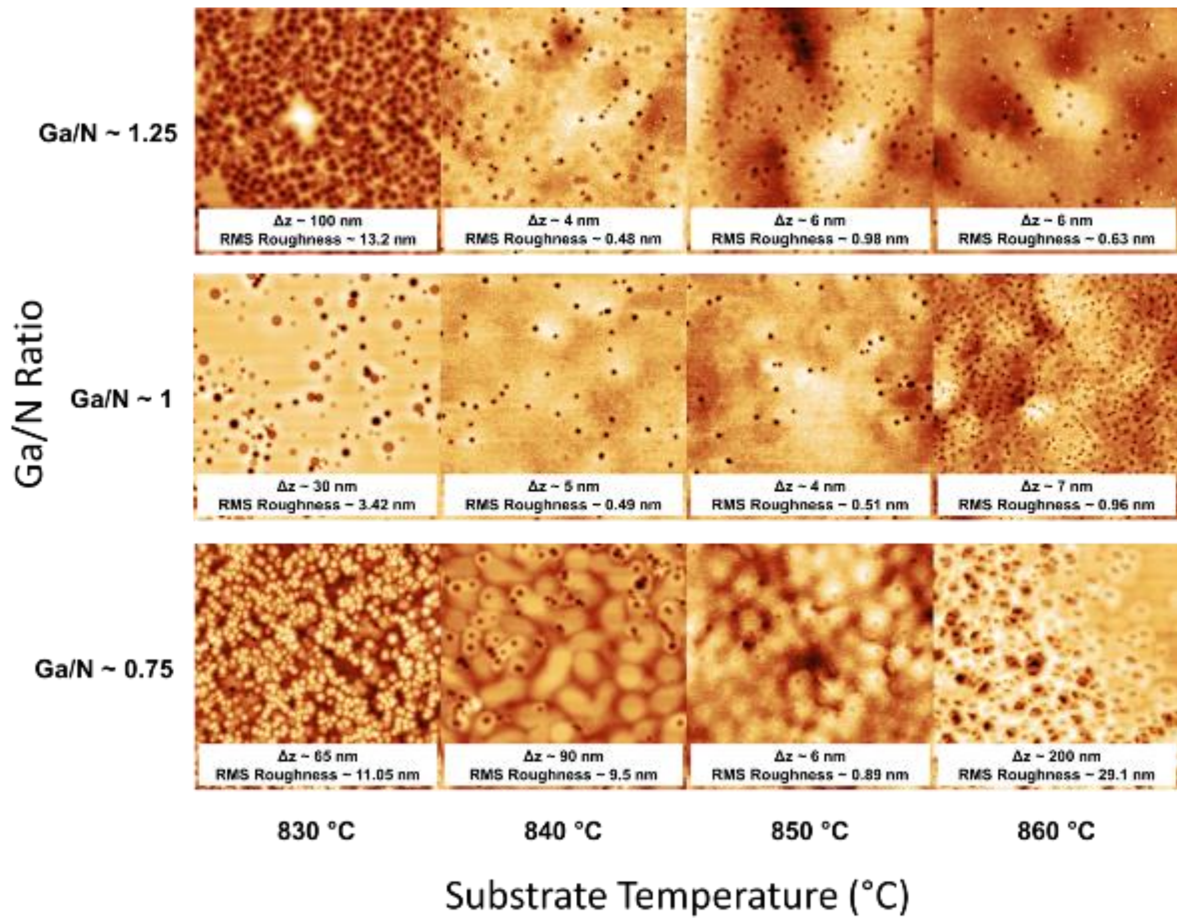

Figure 27 -- 3 µm x 3 µm AFM images of a selection of the high temperature growth rate calibration samples. Δz is the height scale from z=0 (black) to z=Δz (white).

The trends observed in the surface morphologies of high temperature growth of PAMBE GaN can be understood if we consider three different growth regimes. First at lower temperatures (≤ 830 °C) the morphology is dominated by the high potential barrier for adatom diffusion. This explains the intermediate growth regime seen for a Ga/N ratio of ~1.5 at 825 °C and the rough surface morphology for all other samples at 825-830 °C. Second, at intermediate temperatures (840-850 °C) we see a transition to a 2D nucleation/layer by layer growth mode. For samples with a Ga/N ratio of ~1, these surfaces are smooth with a number of shallow decomposition pits. As the Ga/N ratio was increased, these surfaces showed an increasing amount of shallow decomposition pits. Samples with a Ga/N ratio of > 1 did not show decomposition pitting, although the growth window appears to be much smaller, with the best surface morphology only for the sample with a Ga/N ratio of ~0.75 grown at 850 °C. Finally, the third regime appeared initially for a Ga/N ratio of ~1 at 860°C. Starting with this temperature the growth appeared to change into a decomposition related roughening regime. This roughening regime is readily apparent in Fig. 3 for a Ga/N ratio of ~1. Samples with lower Ga/N ratios enter into this roughening regime at lower temperatures due to their lower growth rate and reduced Ga surface coverage. Samples with higher Ga/N ratios enter the roughening regime at higher temperature due to increased Ga adatom surface diffusion corresponding with increased Ga surface coverage.

4.3 Growth Diagram

From the decomposition analysis and surface morphology analysis a growth diagram depicting the large growth window at high temperatures was produced. This growth diagram is presented in Fig. 5. Initially this diagram was developed by taking the universal growth diagram which was previously developed in chapter 3, which is closely based on previously reported growth diagrams [2], [7], and extrapolating the intermediate growth regime and N-rich regimes for the significantly higher temperatures and Ga fluxes. The closed circles on the growth diagram represent a selection of the samples grown in the high flux regime.

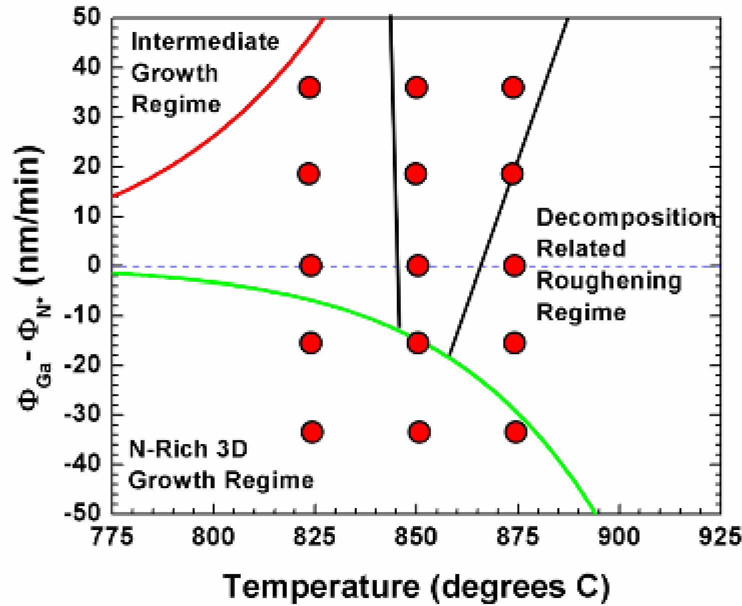

Figure 28 -- Growth diagram with the intermediate and N-Rich 3D growth regimes labeled. The closed circles represent a selection of the samples referenced throughout this report. The apparent "window" fork high quality growth is between the two solid black lines.

4.4 Electron Mobility

To verify that the material grown using the second generation high active nitrogen flux plasma source had acceptable material quality, an un-optimized n-type sample was grown to measure mobility and carrier concentration. The sample was grown with substrate temperature of 840 °C, Ga/N ratio of ~ 1.2, rf forward plasma power of 600 W and N_2 flow rate of 13 sccm correlating to an active nitrogen flux of approximately 2.4 μm/h. Due to

decomposition effects, the actual growth rate of the sample was calibrated and determined to be ~1.44 µm/h. The sample structure used was 2 µm GaN:Si, with an expected Si concentration of approximately 6 x 10^{16} cm^{-3}. To provide an electrical isolation layer, ~1 µm of GaN:C was grown using 80 mTorr fore line pressure from a commercially available CBr_4 source (Veeco, Inc.). Carbon doping has been previously demonstrated to provide sufficient electrical isolation from the regrowth interface [8]. From these samples, Greek cross Van der Pauw patterns were fabricated using a photolithographically defined and mesa isolated process to accurately measure the carrier concentration and Hall electron mobility.

The unoptimized mobility sample was grown at a Ga/N ratio of ~1.2, at a substrate temperature of 840 °C. The expected active nitrogen flux was ~2.4 µm/h, and the calibrated growth rate for these conditions was ~1.44 µm/h. A 3 µm x 3 µm AFM image of the sample surface before processing is presented in Fig. 6.

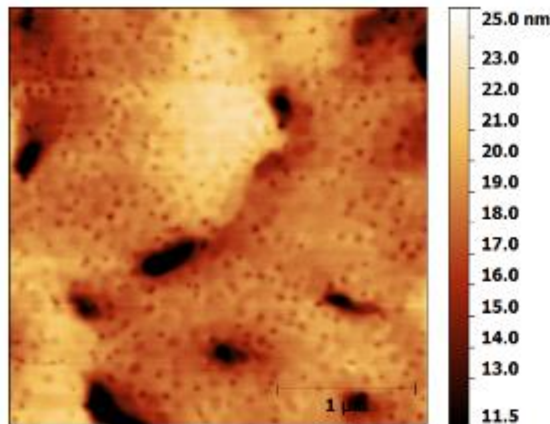

Figure 29 -- AFM image of the high temperature mobility sample.

From an average of five Hall effect measurements across the sample, the average electron concentration was found to be ~1.82 x 10^{16} cm^{-3}. The average electron mobility across the sample was 718.05 cm^2/V s, with a maximum mobility found to be 733.15 cm^2/V s.

4.5 Conclusions

In conclusion, the high temperature growth regime enabled by this high active nitrogen flux was explored. GaN thin films were grown at various Ga/N ratios and substrate temperatures, enabling us to outline a PAMBE high temperature growth window. AFM images verify that optimum growth conditions exist near a Ga/N ratio of ~1, however there exists a large window in which samples with smooth surfaces and < 1 nm RMS roughness can be grown. Finally, samples were grown, processed and tested to measure the electron mobility achievable within this high temperature growth regime, and a maximum mobility of more than 730 cm^2/V s was found.

4.6 References

[1] G. Koblmüller, F. Wu, T. Mates, J. S. Speck, S. Fernández-Garrido, and E. Calleja, "High electron mobility GaN grown under N-rich conditions by plasma-assisted molecular beam epitaxy," *Appl. Phys. Lett.*, vol. 91, no. 22, pp. 23–25, 2007.

[2] G. Koblmüller, S. Fernández-Garrido, E. Calleja, and J. S. Speck, "In situ investigation of growth modes during plasma-assisted molecular beam epitaxy of (0001) GaN," *Appl. Phys. Lett.*, vol. 91, p. 161904, 2007.

[3] J. J. M. Law, E. T. Yu, G. Koblmüller, F. Wu, and J. S. Speck, "Low defect-mediated reverse-bias leakage in (0001) GaN via higherature molecular beam epitaxy," *Appl. Phys. Lett.*, vol. 96, no. 10, pp. 7–9, 2010.

[4] S. Fernández-Garrido, G. Koblmüller, E. Calleja, and J. S. Speck, "In situ GaN decomposition analysis by quadrupole mass spectrometry and reflection high-energy electron diffraction," *J. Appl. Phys.*, vol. 104, no. 3, pp. 1–6, 2008.

[5] A. Pisch and R. Schmid-Fetzer, "In situ decomposition study of GaN thin films," *J. Cryst. Growth*, vol. 187, no. 3–4, pp. 329–332, 1998.

[6] E. Tarsa, B. Heying, X. Wu, P. Fini, S. DenBaars, and J. Speck, "Homoepitaxial growth of GaN under Ga-stable and N-stable conditions by plasma-assisted molecular beam epitaxy," *J. Appl. Phys.*, vol. 82, no. June, p. 5472, 1997.

[7] B. Heying, I. Smorchkova, C. Poblenz, C. Elsass, P. Fini, S. Den Baars, U. Mishra, and J. S. Speck, "Optimization of the surface morphologies and electron mobilities in GaN grown by plasma-assisted molecular beam epitaxy," *Appl. Phys. Lett.*, vol. 77, no. 18, p. 2885, 2000.

[8] D. S. Green, U. K. Mishra, and J. S. Speck, "Carbon doping of GaN with CBr 4 in radio-frequency plasma-assisted molecular beam epitaxy," *J. Appl. Phys.*, vol. 95, no. 12, pp. 8456–8462, 2004.

Chapter 5: High Nitrogen Flux Growth of InGaN

In industry, InGaN growth is dominated by the MOCVD growth technique. In general, for low indium concentrations, MOCVD growth tends to produce superior optoelectronic material. However when MOCVD attempts to grow at the low temperature necessary for higher indium concentration, structural "V-defects" begin to form when the material is grown on c-plane [1].

Over the past 10 years, PAMBE growth of InGaN has been a focus of numerous researchers around the world. In 2006, Iliopoulos et al. demonstrated the capabilities of PAMBE to grow virtually any composition of InGaN [2]. Building on this work, Skierbiszewski and his group have demonstrated lasers which emit light from blue through

green [3], as well as demonstrating the industrial capability of this technology [4]. In 2013, Gačević et al. proposed a growth diagram for PAMBE growth of InGaN [5]. This growth diagram demonstrated that ideal growth of InGaN would be with > 1 monolayer (ML) of indium on the surface. Having < 1 ML of indium on the surface resulted in incomplete coalescence of the layers and severe pitting. Further, Turski et al. performed significant work on the material science aspect of PAMBE InGaN growth [6], among which was demonstrating the advantages of PAMBE growth with high active nitrogen fluxes. Most notably among these advantages is the ability to grow InGaN at higher substrate temperatures while maintaining high indium composition [6].

In this chapter we explore the implications of high active nitrogen flux on the growth of Indium Gallium Nitride (InGaN).

5.1 Initial InGaN Growth

Four series of samples were grown to determine the temperature dependence on indium incorporation when growing under the influence of high active nitrogen flux. All samples were grown with rf plasma conditions of 400 W forward rf power and N_2 flow rate of 20 sccm. This corresponds to ~70 nm/min of active nitrogen as determined from the growth rate study presented in chapter 3. Of the four series grown, two series were slightly nitrogen-rich with III/V flux ratios of ~0.9, and the other two series were slightly metal-rich

with III/V flux ratios of 1.1. For both the nitrogen-rich and metal-rich series, one set of samples was grown with an In/Ga ratio of ~1 and the other set of samples was grown with an In/Ga ratio of ~5. All samples were grown for five minutes.

The AFM results from the first sample series are presented in Fig. 1. The corresponding XRD results are presented in Fig. 2. This first series was grown slightly nitrogen-rich, with a III/V ratio of ~0.9 and an In/Ga ratio of ~1.

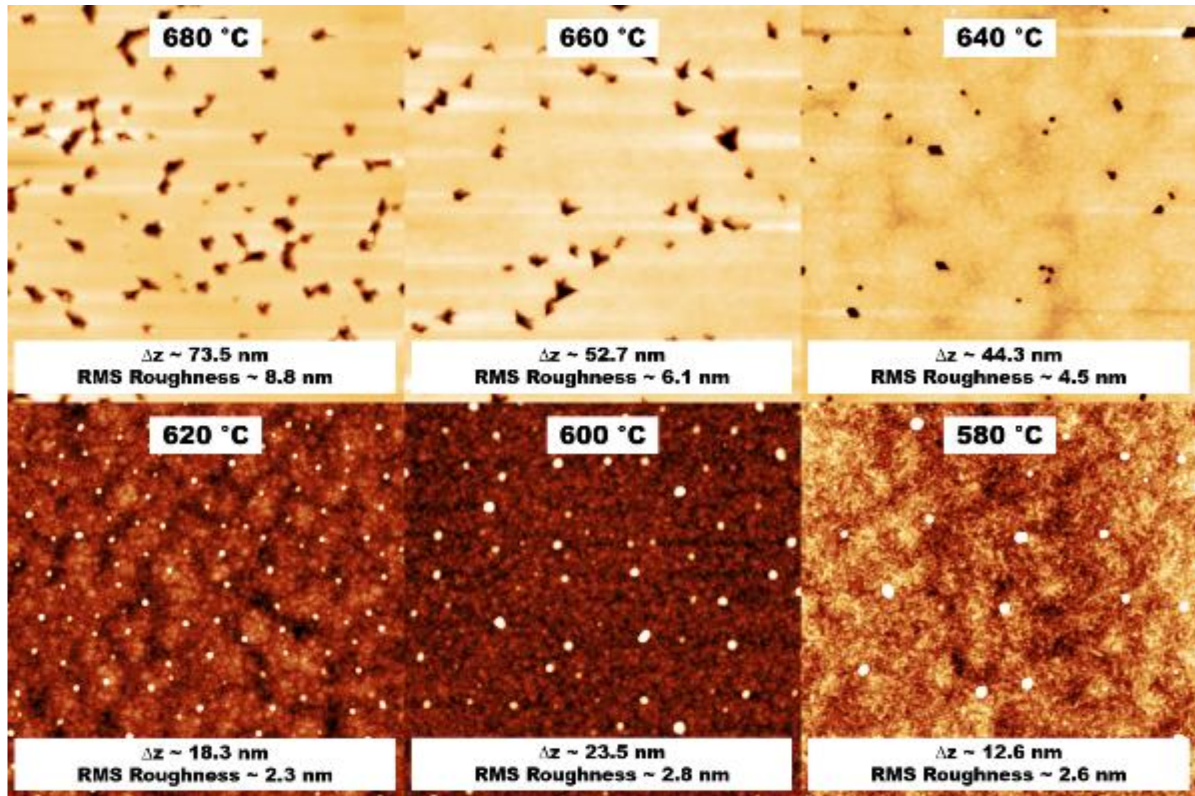

Figure 30-- AFM results from the first InGaN sample series with III/V ratio of ~0.9 and an In/Ga ratio of ~1.

From the 3 µm x 3 µm AFM images presented in Fig. 1 we see that for a In/Ga ratio of ~1 there is incomplete coalescence of the layer for samples grown at 680 °C, 660 °C and 640 °C. This is consistent with the growth diagram proposed by Gačević et al. for growth in the intermediate metal-rich regime with < 1 monolayer (ML) of indium on the surface [5]. For samples grown colder than 640 °C we see 3D growth and surface roughening suggesting relaxation of the films.

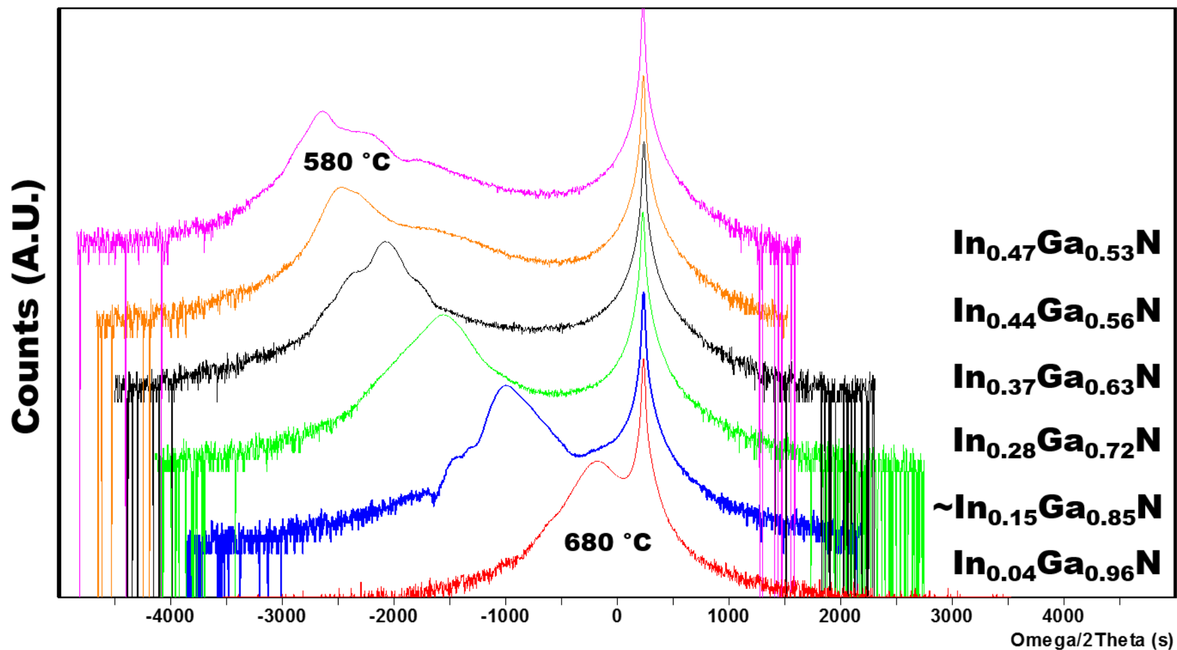

Figure 31-- XRD Omega/2Theta scans of the first InGaN sample series with III/V ratio of ~0.9 and In/Ga ratio of ~1.

As can be seen from the HR-XRD scans in Fig. 2, the indium composition of the InGaN layers varies from 4% at 680 °C to 47% at 580 °C. Paired off-axis open detector rocking curve measurements were performed on the sample grown at 640 °C, which was found to be ~93% relaxed.

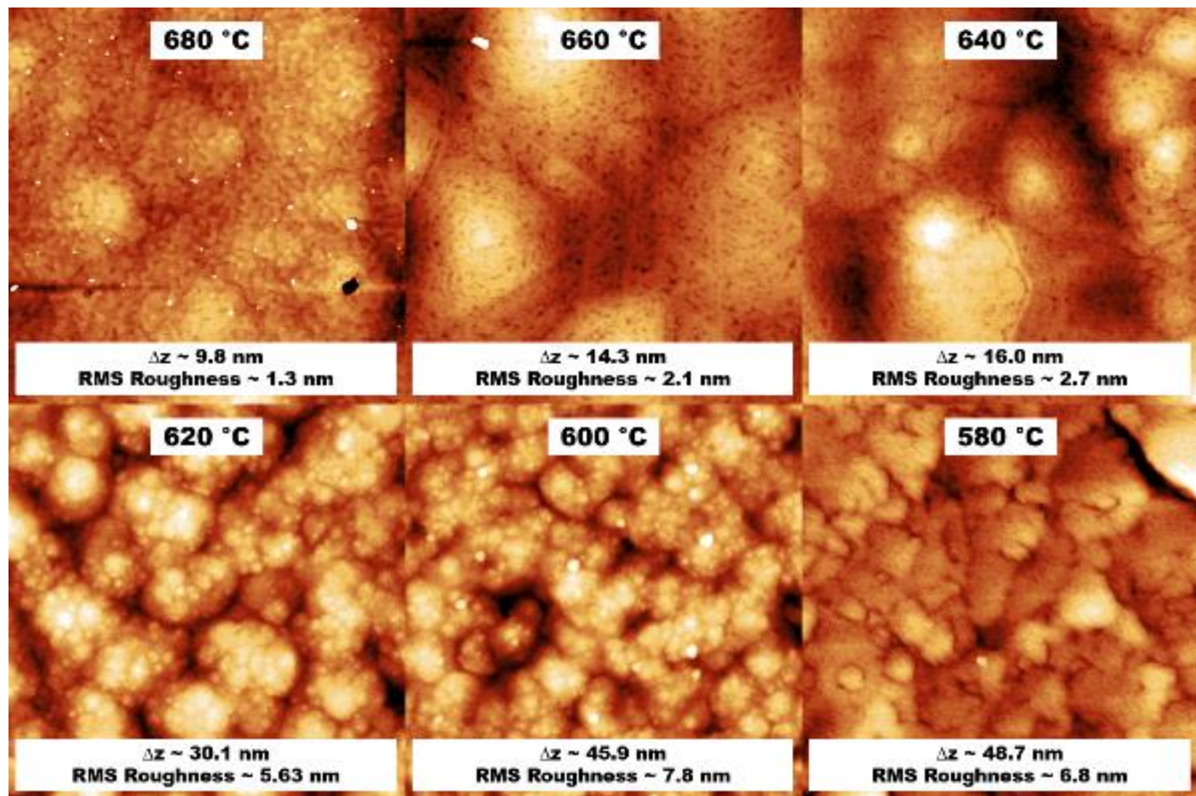

Figure 32 -- AFM results from the second InGaN sample series with III/V ratio of ~0.9 and an In/Ga ratio of ~5.

From the 3 µm x 3 µm AFM images presented in Fig. 3 we see that for a In/Ga ratio of ~5 there is complete coalescence of the layer for samples grown at 680 °C, 660 °C and 640 °C. This is consistent with the growth diagram proposed by Gačević et al. for growth in the intermediate metal-rich regime with > 1 monolayer (ML) of indium on the surface [5]. For samples grown colder than 640 °C we see 3D growth and significant surface roughening suggesting relaxation of the films.

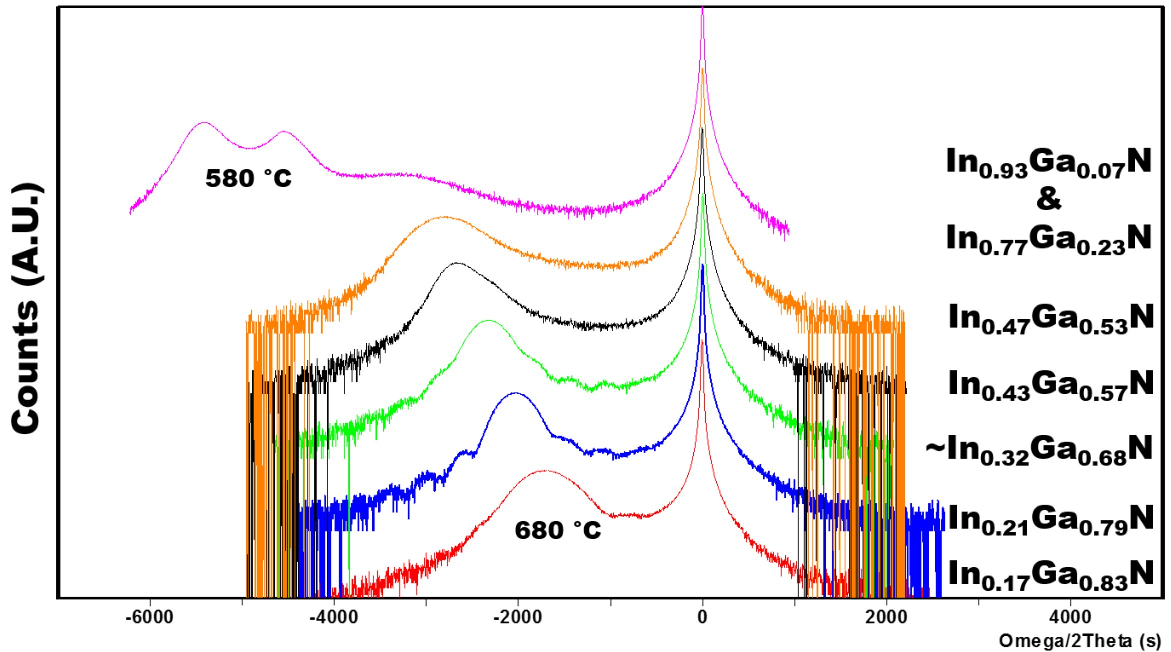

Figure 33 -- XRD Omega/2Theta scans of the second InGaN sample series with III/V ratio of ~0.9 and In/Ga ratio of ~5.

As can be seen from the HR-XRD scans in Fig. 4, the indium composition of the InGaN layers varies from 17% at 680 °C to 47% at 600 °C. For the sample grown at 580 °C there appears to be some phase separation with two peaks in the XRD scan corresponding to indium compositions of 93% and 77%. Paired off-axis open detector rocking curve measurements were performed on the sample grown at 660 °C, which was found to be ~4% relaxed.

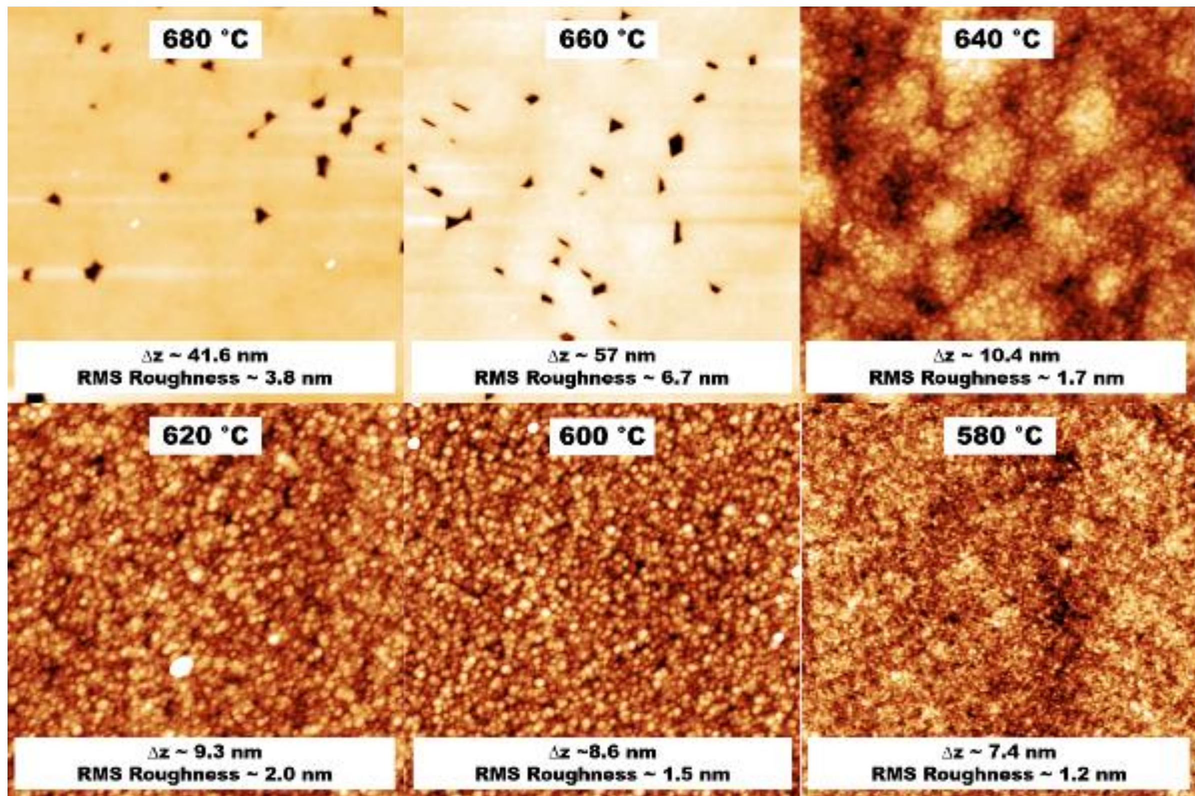

Figure 34 -- AFM results from the third InGaN sample series with III/V ratio of ~1.1 and an In/Ga ratio of ~1.

From the 3 µm x 3 µm AFM images presented in Fig. 5 we see that for a In/Ga ratio of ~1 there is incomplete coalescence of the layer for samples grown at 680 °C and 660 °C. This is consistent with the growth diagram proposed by Gačević et al. for growth in the intermediate metal-rich regime with < 1 monolayer (ML) of indium on the surface [5]. For samples grown colder than 660 °C we see 3D growth and surface roughening suggesting relaxation of the films.

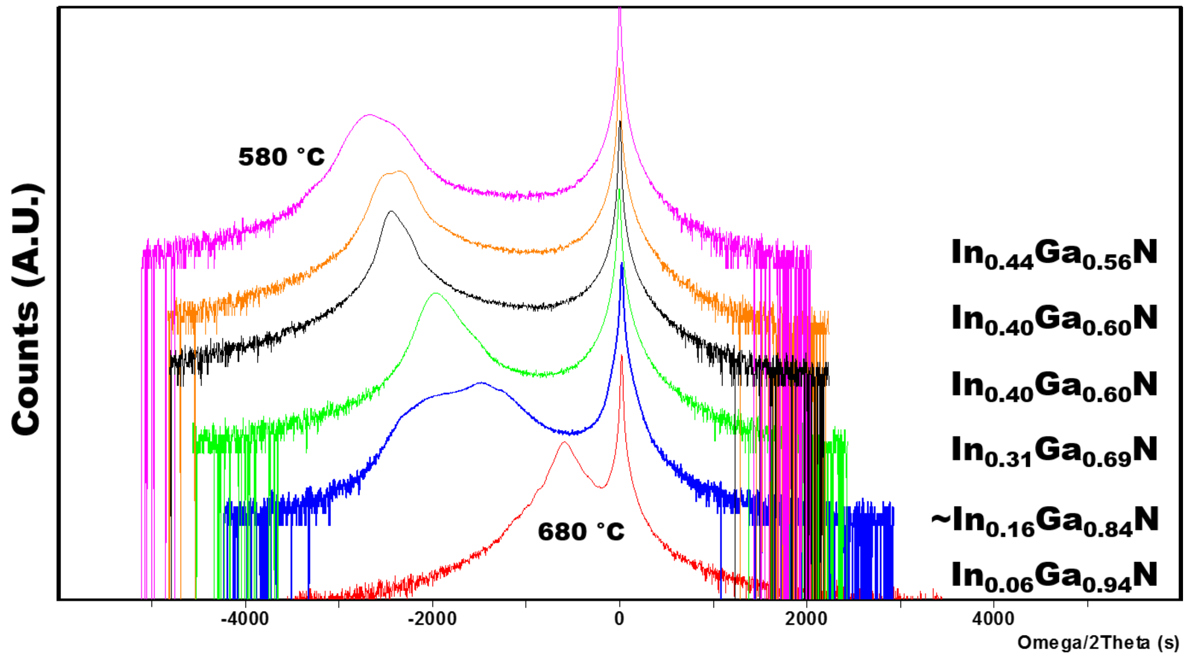

Figure 35 -- XRD Omega/2Theta scans of the third InGaN sample series with III/V ratio of ~1.1 and In/Ga ratio of ~1.

As can be seen from the HR-XRD scans in Fig. 6, the indium composition of the InGaN layers varies from 6% at 680 °C to 44% at 580 °C. Paired off-axis open detector rocking curve measurements were performed on the sample grown at 640 °C, which was found to be ~96% relaxed.

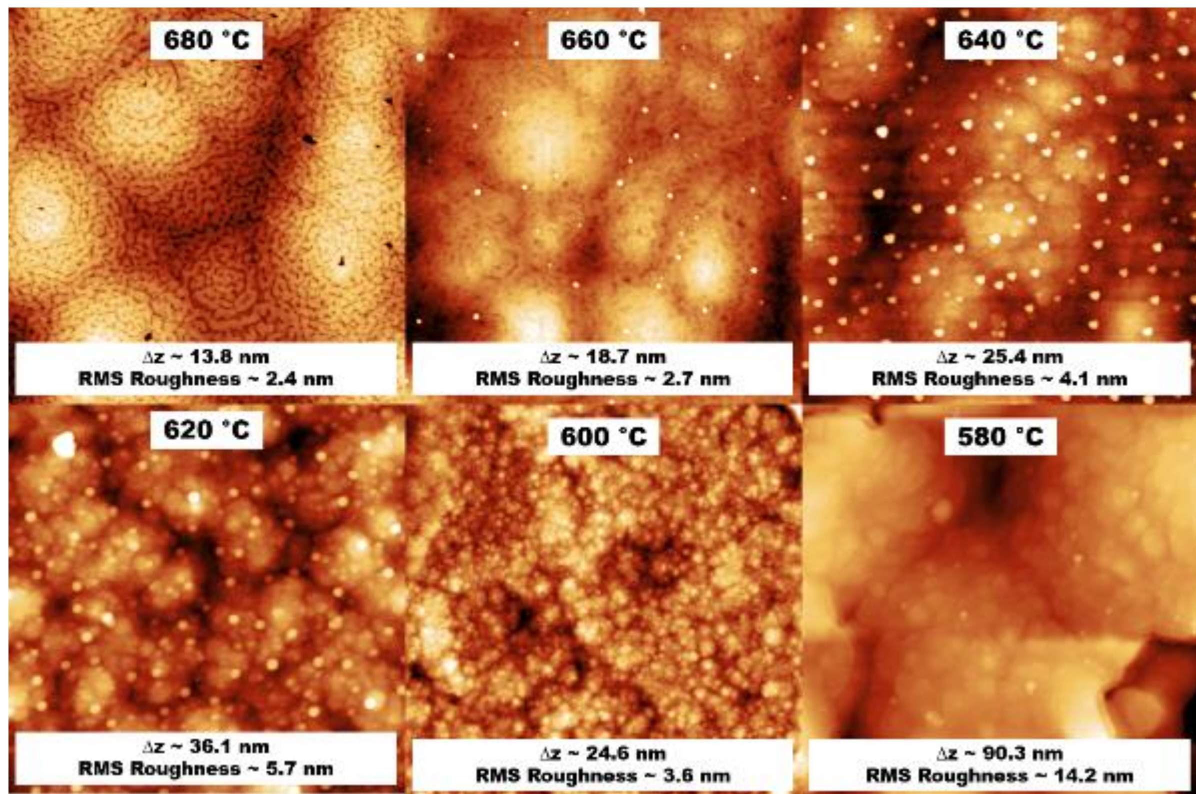

Figure 36 -- AFM results from the fourth InGaN sample series with III/V ratio of ~1.1 and an In/Ga ratio of ~5.

From the 3 μm x 3 μm AFM images presented in Fig. 7 we see that for a In/Ga ratio of ~5 there is complete coalescence of the layer for samples grown at 680 °C, 660 °C and 640 °C. This is consistent with the growth diagram proposed by Gačević et al. for growth in the intermediate metal-rich regime with > 1 monolayer (ML) of indium on the surface [5]. Indium droplets are observed for the samplse grown at 640 °C and colder suggesting a transition into a droplet growth regime. For samples grown colder than 640 °C we see 3D growth and significant surface roughening suggesting relaxation of the films.

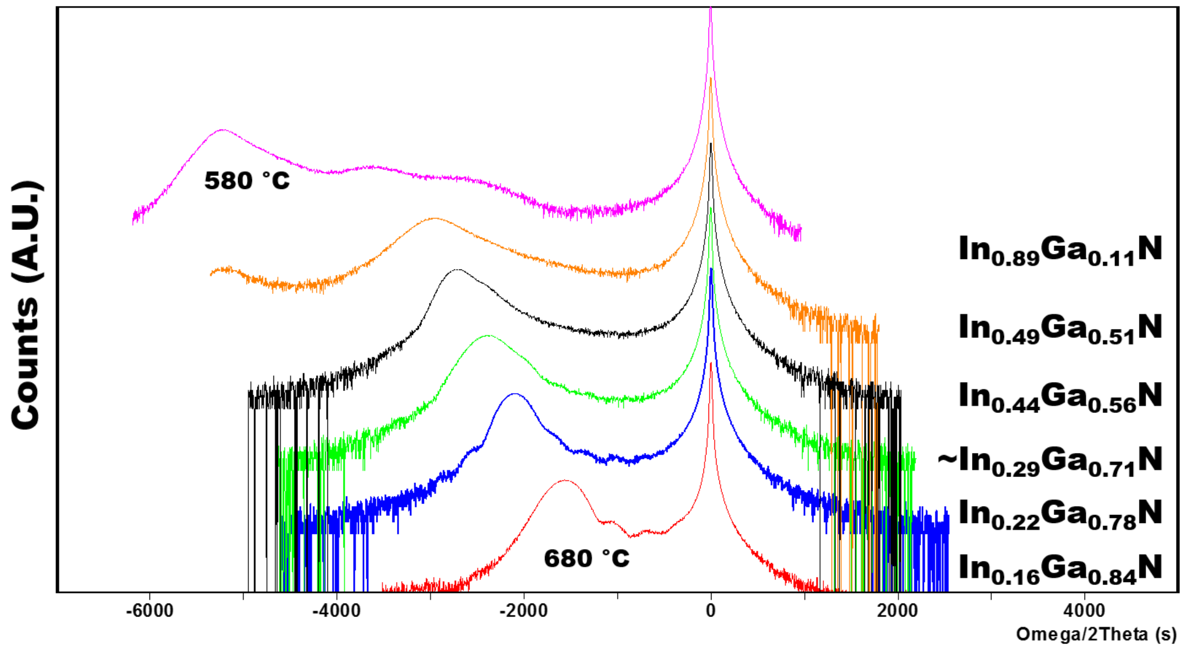

Figure 37 -- XRD Omega/2Theta scans of the fourth InGaN sample series with III/V ratio of ~1.1 and In/Ga ratio of ~5.

As can be seen from the HR-XRD scans in Fig. 8, the indium composition of the InGaN layers varies from 16% at 680 °C to 49% at 600 °C. For the sample grown at 580 °C there appears to be some phase separation with multiple peaks in the XRD scan with the largest peak providing an indium composition of 89%. Paired off-axis open detector rocking curve measurements were performed on the sample grown at 660 °C, which was found to be ~4% relaxed.

5.2 Growth of a PAMBE LED

Using the information gained from the InGaN growth calibrations performed, two LED samples were grown. Both samples were grown with In/Ga ratios of ~5, one sample having the InGaN grown slightly nitrogen-rich (III/V ~0.9) and the other sample having the InGaN active region grown slightly metal-rich (III/V ~1.1). A schematic of the LED structure is presented in Fig. 9.

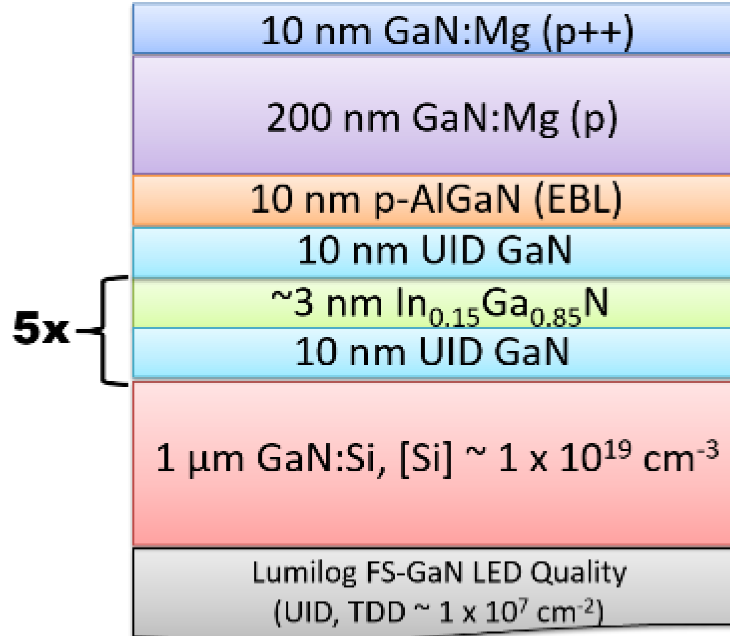

Figure 38-- Schematic of LED structure grown.

The entire sample was grown at a substrate temperature of 660 °C, so there was no growth interrupt at the active region to decrease temperature for the InGaN growth. The only growth interrupt in the sample was for adjustment of the Mg cell, allowing for the p++ layer to be grown.

A 3 µm x 3 µm AFM image of the sample surface after growth is presented in Fig. 10. Note that while there appears to be some areas of incomplete coalescence of the sample surface, overall the surface appears to be smooth and of high quality.

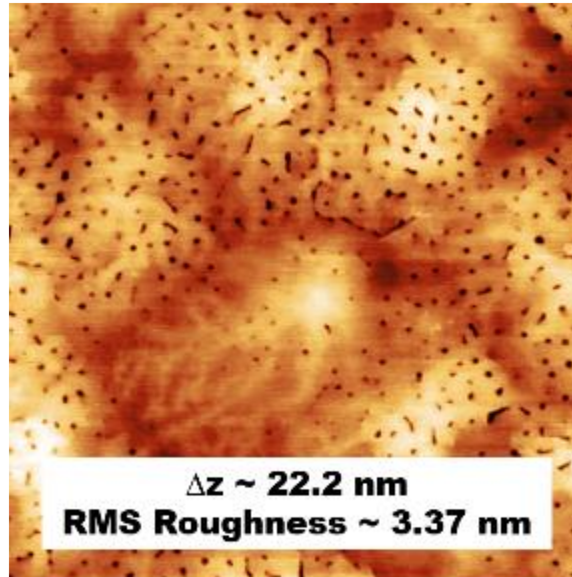

Figure 39 -- 3 µm x 3 µm AFM image of the LED sample surface.

While the growth of the LED samples appeared to be performed will and with ample calibrations, under indium-dot contacts to the p- and n-type regions neither sample produced any electroluminescence (EL). Both samples were biased up to 20 V, and while there appeared to be turn on of the pn-junctions within the sample, they emitted no light. Further, the active regions emitted no photoluminescence (PL) when excited either with a 405 nm laser or a 325 nm HeCd laser.

However, when the sample was excited in using cathodoluminescence (CL), there does appear to be a weak emission centered at ~430 nm. The CL spectrum is presented in Fig 11.

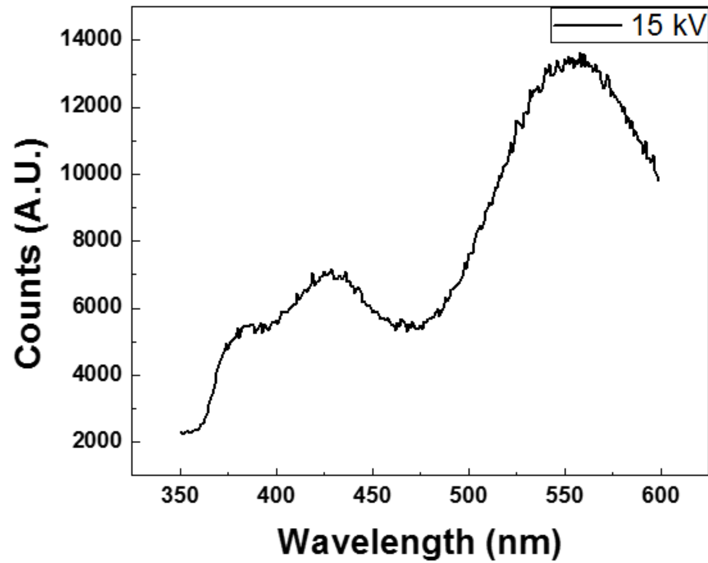

Figure 40 -- Cathodoluminescence spectrum of the LED structure.

From the CL spectrum we see not only the weak InGaN emission centered at ~430 nm, but also a strong yellow band emission suggesting that there may be a significant concentration of point defects in the material.

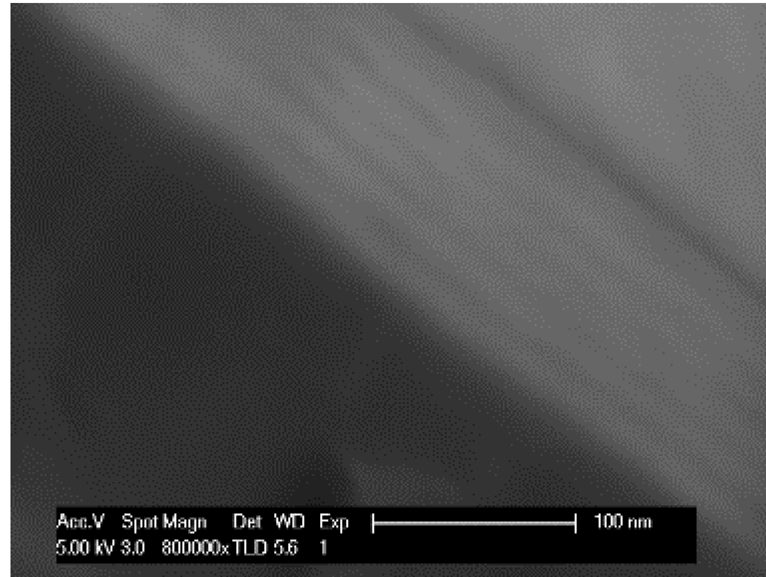

Figure 41 -- SEM image of the active region of the LED sample.

Finally, in an attempt to determine the cause of the lack of EL or PL emission of the LED the sample was cleaved and the active region was imaged using scanning electron microscopy (SEM). The resulting SEM image is presented in Fig. 12. While the quantum wells (QWs) are visible in the SEM image, note that the thickness of the active region appears to be > 100 nm. The n- and p-type regions when imaged had thicknesses as expected from growth rate calibrations, however the InGaN active region was nearly twice the expected thickness. Thus instead of ~3 nm InGaN QWs, it is believed that the QWs are nearly 10 nm, providing one possible explanation for the lack of EL and PL emission.

5.3 Conclusions

In conclusion, InGaN samples were grown using the Riber high active nitrogen flux plasma source. While the samples were grown to a thickness such that high indium composition material entered a 3D growth regime and had rough surfaces, samples with indium compositions from ~4% through more than 80%. It is important to note that the growth temperatures used throughout the composition study are more than 100 °C above standard InGaN growth temperatures. The high indium incorporation at greatly increased temperatures is a result of the ~70 nm/min active nitrogen flux.

Finally, LED structures were grown and tested. While there was no EL or PL and only weak CL emission, the samples appeared to be of high quality. Inaccuracies in the InGaN growth rates resulted in much thicker than expected QWs, thus providing a viable reason for the lack of light emission.

5.4 References

[1] X. H. Wu, C. R. Elsass, A. Abare, M. Mack, S. Keller, P. M. Petroff, S. P. DenBaars, J. S. Speck, and S. J. Rosner, “Structural origin of V-defects and correlation with localized excitonic centers in InGaN/GaN multiple quantum wells,” *Appl. Phys. Lett.*, vol. 72, no. 6, p. 692, 1998.

[2] E. Iliopoulos, a. Georgakilas, E. Dimakis, a. Adikimenakis, K. Tsagaraki, M. Androulidaki, and N. T. Pelekanos, “InGaN(0001) alloys grown in the entire composition range by plasma assisted molecular beam epitaxy,” *Phys. Status Solidi Appl. Mater. Sci.*, vol. 203, no. 1, pp. 102–105, 2006.

[3] C. Skierbiszewski, Z. R. Wasilewski, I. Grzegory, and S. Porowski, “Nitride-based laser diodes by plasma-assisted MBE—From violet to green emission,” *J. Cryst. Growth*, vol. 311, no. 7, pp. 1632–1639, Mar. 2009.

[4] C. Skierbiszewski, M. Siekacz, H. Turski, G. Muziol, M. Sawicka, P. Perlin, Z. R. Wasilewski, and S. Porowski, “MBE fabrication of III-N-based laser diodes and its development to industrial system,” *J. Cryst. Growth*, vol. 378, pp. 278–282, 2013.

[5] Ž. Gačević, V. J. Gómez, N. G. Lepetit, P. E. D. Soto Rodríguez, A. Bengoechea, S. Fernández-Garrido, R. Nötzel, and E. Calleja, “A comprehensive diagram to grow (0001)InGaN alloys by molecular beam epitaxy,” *J. Cryst. Growth*, vol. 364, pp. 123–127, 2013.

[6] H. Turski, M. Siekacz, Z. R. Wasilewski, M. Sawicka, S. Porowski, and C. Skierbiszewski, “Nonequivalent atomic step edges - Role of gallium and nitrogen atoms in the growth of InGaN layers,” *J. Cryst. Growth*, vol. 367, pp. 115–121, 2013.

Chapter 6: Conclusions and Future Work

In this thesis, we explored the capabilities of a high flux nitrogen plasma source, and the implications of a high active nitrogen flux on the growth of GaN and InGaN. Specifically, the work presented in this thesis should serve as a guideline towards making PAMBE an industrially relevant growth technique. While MBE may never surpass MOCVD's optoelectronic capabilities and market saturation, there does exist a vast amount of opportunities within electronic devices.

The detailed mapping of growth rates possible with the high flux nitrogen plasma source was presented in chapter 3. Here we demonstrated capabilities of more than 2.6 μm/h with the first generation Riber plasma source, and growth rates of more than 7.5 μm/h with the second generation of the Riber plasma source. Both generations of plasma sources bring PAMBE metal-rich growth rates in line with traditional MOCVD growth rates of GaN, and demonstrate the capability of growth rate scaling for active regions as necessary. A revised universal growth

diagram was proposed allowing for rapid determination of growth conditions regardless of the available active nitrogen flux.

In chapter 4 high temperature growth of GaN was explored using the full capabilities of the high active nitrogen flux source. Not only was it shown that high quality surfaces could be achieved, but in addition a growth map was proposed suggesting a high temperature growth window. It is here that the true power of the high flux source was demonstrated, and it is in this high temperature growth regime that the most potential for PAMBE lies.

In chapter 5 an alloy, InGaN, was explored using the high active nitrogen flux source. Here, growth temperatures far exceeded what was previously achievable for any appreciable indium composition. Both nitrogen-rich and metal-rich growth conditions were explored, with neither one necessarily being better than the other at this time.

This thesis lays the groundwork for a vast amount of future work. Truly the possibilities are only limited by the imagination of the reader. However, some immediate suggestions include:

- High-temperature p-GaN – In this work we only scratched the surface on possible high temperature PAMBE growth of GaN. We presented some results on high temperature electron mobility, but if both n-GaN and p-GaN could be achieved at high temperature then truly there is no limit to the devices which could be achieved in this exciting growth regime.

- AlGaN/AlN – Pure AlN is an area in which MBE has a capability which MOCVD does not possess. It has been shown (and discussed in the introduction) that through proper control of surface adlayers pure AlN is achievable in MBE. This is in stark contrast to MOCVD where even attempts to grown pure AlN are met with an AlGaN alloy. However, these capabilities were not able to be explored in this thesis and deserve attention.
- InGaN – While some preliminary work was performed on InGaN growth using high active nitrogen fluxes, there remains significant room for improvement. A universal InGaN growth diagram independent of absolute active nitrogen flux is one example. Also work could be performed on understanding the lack of photoluminescence (PL) from PAMBE InGaN, for example a quantum well series. Looking at the PL spectrum from this material could also provide information on the randomness of the alloy, and would be a good companion to atom probe tomography work.
- Devices – While we attempted to grow an LED, there are vast numbers of devices which could prove to be only able to be grown with the high active nitrogen flux source. A good example of this would be the quantum well HET in which the AlN layer is grown directly on top of the InGaN layer. The high growth temperatures demonstrated for high composition InGaN would allow for growth without interrupt before the AlN layer, and no fear of InGaN decomposition.

Chapter 6: Conclusions and Future Work

In conclusion, this thesis has presented results on the growth of GaN and InGaN by PAMBE utilizing the Riber high active nitrogen flux plasma source. The capabilities of the source have only begun to be realized. High growth rates bring PAMBE in line with MOCVD; high active nitrogen fluxes however provide amazing growth opportunities not previously accessible and growth regimes previously unattainable.

Appendix A: Processing Methods

In this appendix the basic processing methods used throughout the thesis on samples are described. The acronyms ACE, ISO and DI refer to acetone, isopropanol and di-ionized water respectively.

A.1 n-type Hall Effect Samples

- $HF:HNO_3$ dip to remove the Ti backside metal.
- 3 min ACE, 3 min ISO and 3 min DI sample cleaning in the ultrasonic bath.
- Dehydrate bake at 115 °C for 5 min.
- Spin negative photoresist AZnLOF 2020 for 30 sec at 3 krpm.
- Soft bake at 110 °C for 90 sec.
- Expose resist for 10 seconds with an i-Line filter. An image of one die on the mask is presented in Fig. 1.
- Post exposure bake at 110 °C for 60 sec.

- Develop the exposed resist pattern for 60 seconds in AZ300MIF developer.

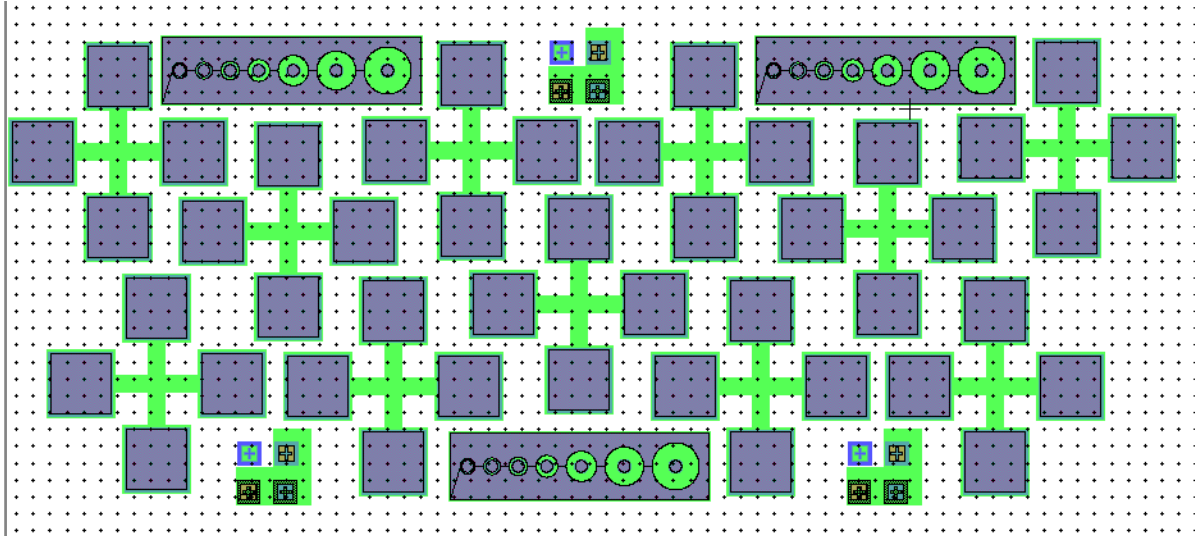

Figure 42 -- A single die showing the Van der Pauw patterns used for Hall Effect measurements.

- 30 sec O_2 plasma descum at 300 mTorr O_2 flow rate, 100 W plasma power.
- 30 sec HCl dip followed by DI rinse
- Metal deposition using standard electron beam evaporation
    - Metal stack: 50 ÅTi/500 Å Al/50 Å Ni/2000 Å Au
- Lift-off of metal in 1165 on a hotplate at 80 °C for 3-4 hours.
- Anneal contact stack in Rapid Thermal Annealer, N_2 ambient at 730 °C for 30 sec.

- 3 min ACE, 3 min ISO and 3 min DI sample cleaning in the ultrasonic bath.
- Dehydrate bake at 115 °C for 5 min.
- Spin positive photoresist SPR-220 7.0 for 45 sec at 3.5 krpm.
- Soft bake at 115 °C for 120 sec.
- Expose resist for 60 seconds without a filter (7.5 mW/cm2 using 405-nm detector). An image of one die on the mask is presented in Fig. 1.
- Wait for 5 minutes to let the resist finish the reaction.
- Develop the exposed resist pattern for 70 seconds in AZ300MIF developer.
- Mesa etch using Reactive Ion Etcher
  - 30 sec BCl_3 oxide removal, 100 W plasma power, 10 sccm BCl_3
  - Cl_2 GaN etch, 150 W plasma power, 10 sccm Cl_2
    - Etch rate ~ 1-2 nm/sec

Appendix B: Active Nitrogen – N vs. N_2^*

The true nature of the components of active nitrogen emitted from a nitrogen plasma source is still a point of debate in the GaN growth community. This appendix is devoted to providing a concise review of the topic from the available literature. It is not intended to provide a definitive answer as to what are the specific growth species as that is beyond the scope of this thesis. Rather this appendix is intended to be a reference for future users of nitrogen plasma sources so that they can appreciate and ponder the influences of active nitrogen on the growth of their thin films.

B.1 Active Nitrogen

"Active nitrogen" is a term used to refer to any excited form of nitrogen, molecular or atomic, or a combination of these, of sufficient lifetime that it may be removed from the region in which it is formed" [1]. This is the basic definition provided by Wright and

Appendix B: Active Nitrogen – N vs. N_2^*

Winkler in the preface to their seminal tome *Active Nitrogen* from 1968. From the perspective of the PAMBE growth scientist, we consider not all excited forms of nitrogen such that it can be removed, but a much smaller subset of these forms. Specifically, we are only concerned with the excited forms of nitrogen which have sufficient lifetimes such that they can impinge on the substrate and participate in the growth of GaN. An attempt to completely classify and understand all species generated by the plasma is outside the scope of this thesis.

First, it is useful to determine what species within the activated nitrogen could be responsible for the growth of GaN. Figure 1 compares the potential energy of a variety of species contained within active nitrogen with the Gibbs free energy necessary for the reaction:

$$2\ Ga\ (l) + N_2\ (g) \rightarrow 2\ GaN\ (s) \qquad (1)$$

Growth of GaN is an example of meta-stable growth [2] in which the reverse reaction has a large kinetic barrier to decomposition, thus allowing positive net growth. From Fig. 1 it is apparent that there are a wide variety of species which have sufficient potential energy to drive the reaction to form GaN, including the excited neutral metastable states of molecular nitrogen ($A^3\Sigma_u^+$, $B^3\Pi_g$, $a^1\Pi_g$ and $C^3\Pi_u$), the ionized molecular nitrogen ($X^2\Sigma_g^+$) and atomic nitrogen (^4S, ^2P and ^2D).

As summarized by Newman [2] these reactions are:

Appendix B: Active Nitrogen – N vs. N_2^*

$$Ga\ (l) + \tfrac{1}{2}\ N_2^*\ (g) \rightarrow GaN\ (s) \qquad (2)$$

where $N_2^* = A^3\Sigma_u^+$, $B^3\Pi_g$, $a^1\Pi_g$ or $C^3\Pi_u$

$$Ga\ (l) + \tfrac{1}{2}\ N_2^+\ (g) \rightarrow GaN\ (s) \qquad (3)$$

where $N_2^+ = X^2\Sigma_g^+$

$$Ga\ (l) + N\ (g) \rightarrow GaN\ (s) \qquad (4)$$

where $N = {}^4S$

$$Ga\ (l) + N\ (g) \rightarrow GaN\ (s) \qquad (5)$$

where $N = {}^2P$ or ${}^2D$

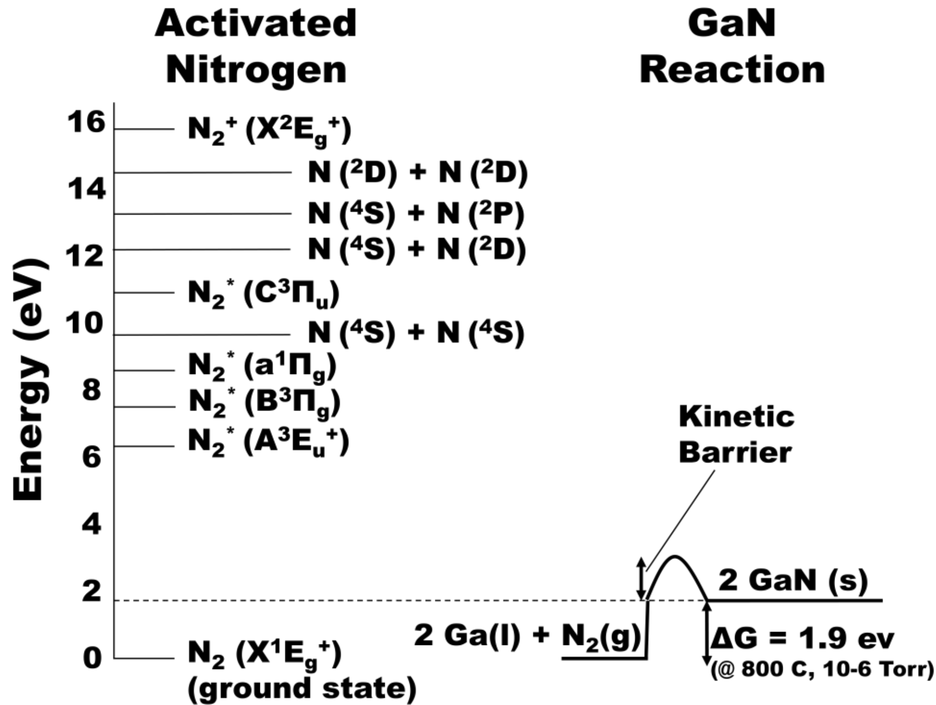

Figure 43 -- A comparison of the potential energy of activated nitrogen with the Gibbs free energy for the forward reaction of GaN growth. After Newman [2].

While all these species have sufficient potential energy to drive the forward growth reaction, not all species have sufficient lifetime to traverse the necessary 20 cm from the plasma source to the substrate. Assuming that the temperature of the gas in the plasma source is approximately 720 °C [3] with an average thermal velocity of 8.66×10^4 cm/s [3], then the length of time necessary for the active nitrogen to travel from the source to the substrate is approximately 230 μs.

Appendix B: Active Nitrogen – N vs. N_2^*

Considering first the metastable molecular nitrogen species, only the $A^3\Sigma_u^+$ specie with its lifetime of 2-3 s [4] can survive long enough before a radiative transition to reach the sample surface. The lifetime of the $B^3\Pi_g$ state is approximately 4-13 μs [5] before it decays into $A^3\Sigma_u^+$. The lifetime of the $C^3\Pi_u$ state is a mere 36-39 ns [5] before it relaxes to the $B^3\Pi_g$ state. Thus we can consider only the $A^3\Sigma_u^+$ state of excited molecular nitrogen to be of any possible relevance to the growth of GaN.

The formation mechanisms for the $A^3\Sigma_u^+$ metastable state and the $B^3\Pi_g$ state are as follow:

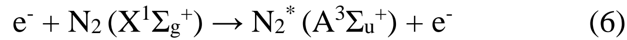

$$e^- + N_2\,(X^1\Sigma_g^+) \rightarrow N_2^*\,(A^3\Sigma_u^+) + e^- \qquad (6)$$

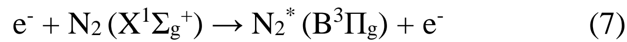

$$e^- + N_2\,(X^1\Sigma_g^+) \rightarrow N_2^*\,(B^3\Pi_g) + e^- \qquad (7)$$

The energy necessary to excite a ground state nitrogen molecule to the $A^3\Sigma_u^+$ metastable state is ~6.2 eV, and the energy necessary to excite a ground state nitrogen molecule to the $B^3\Pi_g$ state is ~7.4 eV [1]. The $B^3\Pi_g$ metastable state is listed above as it rapidly decays to the $A^3\Sigma_u^+$ metastable state which was previously demonstrated has having sufficient lifetime to participate in the growth of GaN.

Relaxation of atomic nitrogen is a 3 body problem, often involving two nitrogen atoms and the wall of the plasma source. Thus the radiative recombination efficiency is

very low, and the radiative lifetime of the nitrogen atom can be greater than 2 s [6]. Therefore atomic nitrogen has sufficient lifetime to participate in the growth of GaN.

Note that the potential energy diagram in Fig. 1 suggests that metastable states of N_2 may also dissociate into atomic N without having to undergo dissociative ionization, for example:

$$e^- + N_2\,(X^1\Sigma_g^+) \rightarrow N(^4S) + N(^4S) + e^- \qquad (8)$$

$$e^- + N_2\,(A^3\Sigma_u^+) \rightarrow N(^4S) + N(^4S) + e^- \qquad (9)$$

$$e^- + N_2\,(B^3\Pi_g) \rightarrow N(^4S) + N(^4S) + e^- \qquad (10)$$

These reactions occur at 9.76 eV (eq. 8), 3.6 eV (eq. 9) and 2.4 eV (eq. 10) as determined from the potential energy diagram.

Therefore, from the perspective of the PAMBE growth scientist we can safely assume that the predominant growth species from the nitrogen plasma source are either atomic nitrogen or excited molecular nitrogen in the $A^3\Sigma_u^+$ metastable state.

B.2 Measurement Techniques

There exist multiple techniques for determining the composition of a plasma. Three of the more frequently used techniques are described below.

B.2.1 Optical Emission Spectroscopy (OES)

Optical emission spectroscopy (OES) is a technique which measures the relaxation emission spectrum of the excited species within the plasma. This is most commonly performed through a quartz window on the back of the plasma source itself. An optical fiber is attached to the quartz window and the emission spectrum of the plasma is measured using a spectrometer. An example of the emission spectrum of the second generation Riber high flux plasma source is presented in Fig. 2.

There are several important regions labelled in Fig. 2. From ~500 nm- ~750 nm is the first positive system of N_2. This corresponds to the relaxation from the $B^3\Pi_g$ metastable state of molecular nitrogen to the $A^3\Sigma_u^+$ metastable state. It is this emission which is most frequently referred to and used to quantify N_2^* (recall that only the $A^3\Sigma_u^+$ metastable state has sufficient lifetime to reach the substrate surface from the plasma source). Next there are three peaks labelled atomic nitrogen, however if the spectrometer measuring the emission spectrum is sensitive enough it would detect a triplet centered at ~744 nm, a 7-plet centered at ~821 nm, and a 12-plet centered at ~865 nm. These correspond to the (^4P-$^4S^0$) relaxation, the (^4P-$^4P^0$) relaxation and the (^4P-$^4D^0$) relaxation respectively. Finally the second positive system of N_2 corresponds to the relaxation from the $C^3\Pi_u$ metastable state of molecular nitrogen to the $B^3\Pi_g$ metastable state [1].

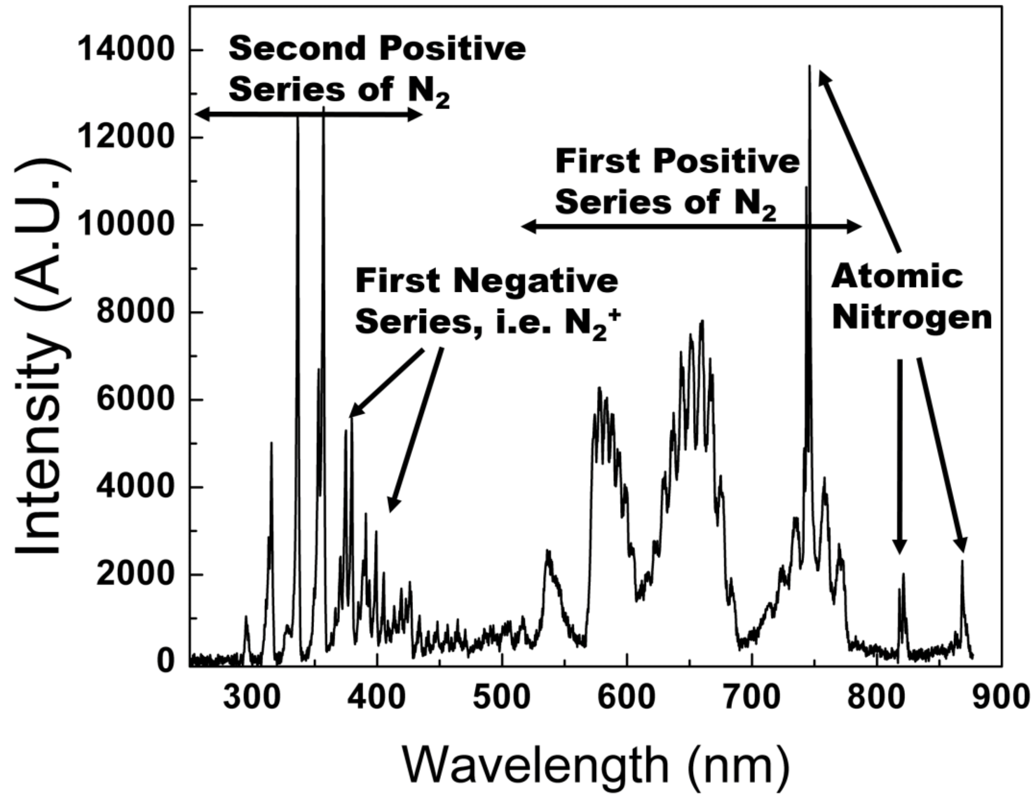

Figure 44 -- OES Spectrum of the second generation Riber high flux nitrogen plasma source. Source operating conditions were 600 W rf forward power and N_2 flow rate of 25 sccm.

While being a very simple way of attempting to understand the components of the plasma, there are several issues with OES. First, it relies on the relaxation emission of the plasma constituents. Therefore certain plasma species with exceptionally long lifetimes, for example atomic N which requires a three-body interaction to relax, can be underrepresented

in the emission spectrum. Thus the intensity of the peaks representing various species within the plasma do not necessarily provide information about the concentration of those species within the plasma. Second, from a growth perspective, the distance between the optical viewport on the back of the plasma source is not necessarily the same distance as the source to the substrate. Thus short lived species may have be present in the optical emission spectrum which do not have sufficient lifetimes to reach the substrate and participate in the growth of GaN.

B.2.2 Line of Sight Quadrupole Mass Spectroscopy (LOS-QMS)

Line of sight quadrupole mass spectroscopy (LOS-QMS) is a technique where a QMS is placed at some distance from the vacuum end of the plasma source, directly facing the output. Then a measurement is made, and this is where the technique varies from group to group. Most often the measurement is one in which the ionizer energy of the QMS is set to some point high enough to ionize both molecular and atomic nitrogen (> 15 eV) but below the dissociation threshold of molecular nitrogen (< 28 eV). Then m/e = 14 and m/e = 28 are measured, and from this information is gathered about the density of atomic nitrogen and metastable nitrogen molecules respectively. A second measurement in which the ionization energy is set to ~13-14 eV (slightly below the 15.6 eV direct ionization energy of the nitrogen molecule) should be able to better detect the metastable $A^3\Sigma_u^+$ state of molecular nitrogen.

B.2.3 Line of Sight Threshold Ionization Mass Spectroscopy (LOS-TIMS)

Line of sight threshold ionization mass spectroscopy (LOS-TIMS) is a variation of LOS-QMS where the ionization energy is swept and then measurements made at each varying ionization energy. This allows for the distinction between direct and dissociative ionization of atomic N (direct ionization occurs at ~14.5 eV, while dissociative ionization occurs at ~24.3 eV). Further this technique allows for the distinction between ionization of a metastable excited nitrogen molecule, N_2^*, from the ground state N_2 as the threshold ionization energies for these two species are different.

The challenge in this technique (and LOS-QMS as well) results from the need for an independent calibration of the ion flux beams in order to obtain absolute densities. Specifically, the absolute density of the experimental gas needs to be calibrated with the signal from a known ionization of a reference gas with known partial pressure and with a m/e value close to the species of interest [7].

B.3 Literature Results from OES

In 1994, Vaudo et al. reported on the atomic nitrogen production from an ASTeX compact ECR plasma source [8]. Based upon their OES results they concluded that their ECR plasma source produces an appreciable flux of neutral nitrogen atoms. Further, they noted that as the input power to the plasma increases the emission lines in the OES spectrum

grew more quickly than the molecular bands corresponding to N_2^*. Thus they surmised that a larger input power results in a larger fraction of nitrogen molecules dissociating, and therefore a greater atomic nitrogen flux. Further, by decreasing the N_2 gas flow and therefore the pressure within the plasma bulb the overall intensity of the emission is reduced. However the atomic lines decreased at a slower rate than the molecular bands. Therefore Vaudo et al. concluded that atomic nitrogen is the dominant species from their ECR plasma source [8].

Contrary to this result, in late 1994 Molnar et al. [9] performed both OES on the plasma and a Langmuir-like probe analysis to determine the effect of charged species on the growth of GaN. They were unable to discern the active nitrogen species resulting in growth of GaN, however the authors note that there were no atomic nitrogen lines able to be measured in their OES spectrum [9].

By 1995 we begin to see reports in the literature of radio frequency (RF) plasma sources and their characterization. Van Hove et al. [10] characterized a SVTA Model RF 4.5 plasma source and demonstrated, as had been previously shown for ECR plasma sources, that low plasma power results in low levels of atomic nitrogen while higher plasma powers result in much higher levels of atomic nitrogen. However unlike the ECR results, Van Hove et al. show that the highest levels of atomic nitrogen are for low N_2 flow rates (and high plasma power) while higher N_2 flow rates resulted in reduced atomic nitrogen signals. So while both atomic nitrogen and molecular nitrogen are present in the OES

emission spectrum, Van Hove et al. compared the different growth regimes to GaN material quality via Schottky diodes and ultra-violet photo-response. Based upon these studies they propose that the optimum GaN is grown under high atomic nitrogen flux [10].

Later in 1995 Hughes et al. [11] directly compared an ASTeX compact ECR plasma source and an Oxford MPD21 RF plasma source. They found that the RF plasma source emitted a much larger fraction of atomic nitrogen and the 1st-positive series of excited molecular nitrogen in contrast to the ECR source which produced mainly 2nd-positive series of excited molecular nitrogen and nitrogen ions when operated under the same conditions. Hughes et al. determined that the RF plasma source produced much better material, however they were unwilling to specify which specie from the nitrogen plasma they felt was the result of this. Only that the "active" nitrogen from the source is most likely a mixture of the 1st-positive series of excited molecular nitrogen and atomic nitrogen. However it was noted that as plasma forward rf power was increased the atomic nitrogen signature increased more rapidly than that of excited molecular nitrogen, and that this increase in power led to increased growth rate [11].

In 1997 Johnson et al. [12] compared the OES spectrum of three different rf plasma sources, specifically the SVTA rf source, an Oxford MPD21 rf source, and an EPI rf plasma source. When operated at the same plasma conditions of 400 W rf forward power and 5×10^{-5} Torr of N_2 pressure the three OES spectrums were very different. Most notable is the strong 2nd-positive series of excited molecular nitrogen emitted by the SVTA source, and the

complete absence of the 2nd-positive series of excited molecular nitrogen from the EPI sourced. While the authors compare these sources based upon the material grown, all that they are willing to say with regard to the "active" nitrogen from the source is that both atomic nitrogen and the 1st-positive series of excited molecular nitrogen are responsible for growth of high quality GaN [12].

Blant et al. [13] in 2000 compared two commercially available Oxford RF plasma sources, the CARS25 and a newer HD25 source. For both sources they found strong emissions corresponding to atomic nitrogen, and only weak emission from the 1st-positive series of excited molecular nitrogen. Further with the newer HD25 source these emissions from atomic nitrogen were much stronger when compared to the CARS25 source, with no increase in the 1st-positive series of excited molecular nitrogen. In addition they report that regardless of plasma operating conditions there was no increase in the emission from the 1st-positive series of excited molecular nitrogen. Thus Blant et al. report that RF plasmas are rich in atomic nitrogen and therefore are suitable for high quality growth of GaN [13].

Between 2005 and 2007 there was a flurry of work on determining the optimum plasma operating conditions with regard to both dilute nitride growth and standard III-nitride growth. Wistey et al. [14] performed OES analysis of their SVTA rf nitrogen plasma source and reported emissions from both the 1st-positive series of excited molecular nitrogen and from atomic nitrogen, however they neglect to suggest a preference for one specie or the other. Iliopoulos et al. [15] performed OES on their Oxford HD25 RF plasma source, and

as opposed to trying to simply look at the variation in the OES in different growth regimes they compared the relative intensities of the atomic nitrogen emission and the 1st-positive metastable molecular nitrogen ($A^3\Sigma_u^+$) emission. They found that any increase in the growth rate at higher plasma powers/N_2 flow rate is a result of increase in the $A^3\Sigma_u^+$ metastable molecular nitrogen emission spectrum as opposed to the atomic nitrogen spectrum. Specifically, they say that the concentration of excited molecular nitrogen increases with monotonically with RF power and nitrogen flow, while the atomic nitrogen concentration appears to be insensitive to the gas flow and only depends on the RF power. Thus the plasma source can be tuned to emit either a significant amount of atomic nitrogen or mainly excited nitrogen molecules, and that the excited metastable nitrogen molecules were predominantly responsible for the growth of the III-Nitrides [15].

Performing OES on an Arios IRFS RF plasma source, Kikuchi et al. [16]suggest that N_2^* ($A^3\Sigma_u^+$) contributes to the growth mechanism in PAMBE of III-Nitrides. Specifically, they propose a method to look at the integrated OES intensity (IOI) from the OES spectrum as a way of quantifying the relative components of the nitrogen plasma from the OES spectrum. Considering this IOI, they determined that the production of atomic N reaches a maximum as opposed to N_2^*. Thus while both may contribute to growth, as the plasma pressure and rf forward power increase, there is an increase in the N_2^* component as opposed to the atomic nitrogen component of the OES spectrum [16].

Appendix B: Active Nitrogen – N vs. N_2^*

In 2006, two reports from Anderson et al. [17], [18] suggest that through their OES spectrum measurements that the Oxford HD25 nitrogen plasma source supplied both atomic nitrogen and N_2*. As has been previously demonstrated, when the RF power is increased the relative amount of atomic nitrogen produced increases approximately linearly, while operating the plasma source at lower flow rates (i.e. lower internal plasma pressures) the amount of N_2^* increased. While Anderson et al. in these reports are unwilling to claim one specie over the other as being responsible for growth, they do note that growth in a regime dominated by N_2^* produced improved InN when grown on GaN/sapphire templates, resulting in improved electrical properties [17], [18].

Once again considering the impact of N vs N_2^* on dilute nitrides, Oye et al. [19] considered three different growth regimes, one where atomic nitrogen appeared to dominate, one where the relative integrated OES intensity for atomic nitrogen and N_2^* appeared to be the same, and one where the metastable N_2^* dominated. These measurements were performed for an Applied-Epi Unibulb rf plasma source, and they found that they had optimum results for their dilute nitride material when it was grown in a regime that the atomic nitrogen was dominant. These results were based upon the global maximum in there photoluminescence peak intensity after annealing of the material [19].

Finally, in 2013 Klosek et al. [20] performed an OES analysis of an Addon (Riber) nitrogen RF plasma source and compared it with the growth rate of GaN material. They found that while the growth rate of GaN was well correlated with the integrated intensity of

the 1st-positive metastable molecular nitrogen emission, there was no dependence on the integrated intensity of the atomic nitrogen related lines observed. Thus Klosek et al. conclude that metastable excited nitrogen molecules, i.e. N_2^*, are responsible for the growth of GaN as opposed to atomic nitrogen [20].

B.4 Literature Results from LOS-QMS & LOS-TIMS

In 1998/1999, Voulot et al. [21], [22] reported on LOS-QMS characterization of the SVTA RF 4.5 nitrogen plasma source. Specifically they focused on the dissociation fraction of N_2, thus providing evidence for a large concentration of atomic nitrogen emitted from the plasma source. Similar trends to many of the OES studies were found, as the dissociation fraction increased with increasing plasma source rf forward power. However they found that the dissociation fraction decreased with increasing plasma source pressure, i.e. increasing N_2 flow rate. Regardless of the plasma conditions, there was still evidence of the 1st-positive molecular nitrogen series, i.e. N_2^*. Even still they found that at optimum operating conditions, up to 40% of the N_2 which was flowed into the plasma source was dissociated. Unfortunately, there was no correlation to growth in their studies [21], [22].

From 1999-2004, five reports were published from T.H. Myers' group at West Virginia University which compared the "active" nitrogen output from two rf nitrogen plasma sources, the Oxford CARS-25 source and the Applied-EPI Unibulb source [23]–[27].

Appendix B: Active Nitrogen – N vs. N_2^*

It was reported that these were basic LOS-QMS measurements in which the ionizer energy was set high enough to ionize both molecular and atomic nitrogen (typically > 15 eV), but below the dissociation threshold of molecular nitrogen (< 28 eV). During the characterization of the Applied-EPI source, considerable molecular nitrogen ions were produced with ionization energies ~ 6 eV below that normally required to ionize molecular nitrogen, and thus these were considered to be the $A^3\Sigma_u^+$ metastable state of molecular nitrogen. Further the measured atomic nitrogen flux was less than the measured growth rate, so for this source it was reported that the "active" nitrogen species responsible for growth is the $A^3\Sigma_u^+$ metastable state of molecular nitrogen. However, the Oxford source under their operating conditions produced primarily atomic nitrogen, specifically at a rate of nearly 10x their measured growth rates [23]–[27].

Cho et al. [28] compared an ECR nitrogen plasma source and a RF nitrogen plasma source from Irie and Eiko Co. respectively. They found that for the ECR plasma source the intensity of molecular nitrogen was stronger than that of atomic nitrogen, and that both intensities increased with increasing plasma power. However, for the RF nitrogen plasma source they found the opposite, in that the signal from atomic nitrogen was always stronger than that of molecular nitrogen. In addition, the signal for atomic nitrogen increased significantly with increasing plasma power, while the signal for molecular nitrogen only showed modest increase with increasing plasma power. From these measurements, they

conclude that atomic nitrogen is the species responsible for growth of GaN from the RF nitrogen plasma source [28].

In 2007 Osaka et al. [29] reported on the atomic nitrogen role during the growth of GaN using a SVTA rf nitrogen plasma source. As with previous reports, they set the LOS-QMS to detect atomic nitrogen by keeping the ionization energy of the QMS at 21 eV, above the ionization threshold of atomic nitrogen but below the dissociation threshold of N_2 molecules. They attempted to measure the metastable N_2^* ($A^3\Sigma_u^+$) by setting the ionization energy of the QMS to 13-14 eV, however there was no detectible signal at the QMS even though the OES spectrum demonstrated the 1st-positive series of molecular nitrogen. Thus from this measurement and the correlating growth study they deduced that the growth species responsible for GaN growth is atomic nitrogen [29].

Finally, in 2003 Argawal et al. [7], [30] performed proper LOS-TIMS on an inductively coupled plasma (ICP) used for semiconductor processing. The plasma was operated at 750 W forward rf power and 50 sccm flow rate while the internal plasma pressure was varied from 10-200 mTorr. By varying the ionization energy while measuring m/e = 14 for N^+ and m/e = 28 for N_2^+, and then comparing the counts with a reference gas they were able to perform absolute measurements of the respective atomic nitrogen and metastable nitrogen molecular densities. They found that at low plasma pressures, specifically ~50 mTorr that the N_2^* and atomic nitrogen densities were equal. However for higher plasma pressures atomic nitrogen increases linearly while N_2^* decreases rapidly [7],

[30].

B.5 Conclusions

In conclusion, this appendix has provided a concise review of the available literature which attempts to correlate the growth of GaN with the "active" nitrogen species involved. Unfortunately, there is little consensus across the literature as to which species within "active" nitrogen are responsible for growth, be it N_2^* ($A^3\Sigma_u^+$) or atomic nitrogen. It appears that the relative concentrations of atomic nitrogen and N_2^* vary depending on which manufacturer's plasma source is being used. However, regardless of which plasma source is being used there are some similarities. First, with increasing plasma power and/or plasma pressure there is an increase in atomic nitrogen available from the source. Second, OES analysis of nitrogen plasma sources is insufficient to give qualitative data as to which is the dominant growth species.

In order to answer the question of what "active" nitrogen species is optimal for the growth of GaN detailed LOS-TIMS analysis of modern rf nitrogen plasma sources is necessary. This analysis needs to be performed at the proper source to substrate distance, across all possible rf forward plasma powers and N_2 flow rates, and correlated with the growth of GaN.

B.6 References

[1] A. N. Wright and C. A. Winkler, *Active Nitrogen*. New York, NY: Academic Press, Inc., 1968.

[2] N. Newman, "The energetics of the GaN MBE reaction: a case study of meta-stable growth," *J. Cryst. Growth*, vol. 178, no. 1–2, pp. 102–112, 1997.

[3] R. Beresford, K. S. Stevens, Q. Cui, A. Schwartzman, and H. Cheng, "Material and Device Characteristics of MBE-Grown GaN Using a New rf Plasma Source," *MRS Proc.*, vol. 449, p. 361, Jan. 1996.

[4] L. G. Piper, "Reevaluation of the transition-moment function and Einstein coefficients for the N2(A 3Σ+u–X 1Σ+g) transition," *J. Chem. Phys.*, vol. 99, no. 5, p. 3174, 1993.

[5] H.-J. Werner, J. Kalcher, and E.-A. Reinsch, "Accurate ab initio calculations of radiative transition probabilities between the A 3Σ+u, B 3Πg, W 3Δu, B′ 3Σ−u, and C 3Πu states of N2," *J. Chem. Phys.*, vol. 81, no. 5, p. 2420, 1984.

[6] K. M. Evenson, "Atomic-Nitrogen Recombination," *J. Chem. Phys.*, vol. 45, no. 7, p. 2450, 1966.

[7] S. Argawal, "Studying Plasma-Surface Interactions," University of California, Santa Barbara, 2004.

[8] R. P. Vaudo, J. W. Cook Jr., and J. F. Schetzina, "Atomic nitrogen production in a molecular-beam epitaxy compatible electron cyclotron resonance plasma source," *J. Vac. Sci. Technol. B Microelectron. Nanom. Struct.*, vol. 12, no. 2, p. 1232, Mar. 1994.

[9] R. J. Molnar and T. D. Moustakas, "Growth of gallium nitride by electron-cyclotron

resonance plasma-assisted molecular-beam epitaxy: The role of charged species," *J. Appl. Phys.*, vol. 76, no. 8, p. 4587, 1994.

[10] J. M. Van Hove, G. J. Cosimini, E. Nelson, A. M. Wowchak, and P. P. Chow, "GaN growth by a controllable RF-excited nitrogen source," *J. Cryst. Growth*, vol. 150, pp. 908–911, May 1995.

[11] W. C. Hughes, W. H. Rowland Jr., M. A. L. Johnson, S. Fujita, J. W. Cook Jr., J. Ren, and J. A. Edmond, "Molecular beam epitaxy growth and properties of GaN films on GaN/SiC substrates," *J. Vac. Sci. Technol. B Microelectron. Nanom. Struct.*, vol. 13, no. 4, p. 1571, Jul. 1995.

[12] M. A. L. Johnson, Z. Yu, C. Boney, W. C. Hughes, J. W. Cook, J. F. Schetzina, H. Zhao, B. J. Skromme, and J. A. Edmond, "Reactive MBE Growth of GaN and GaN:H on GaN/SiC Substrates," *MRS Proc.*, vol. 449, p. 215, Jan. 1996.

[13] A. V Blant, O. H. Hughes, T. S. Cheng, S. V Novikov, and C. T. Foxon, "Nitrogen species from radio frequency plasma sources used for molecular beam epitaxy growth of GaN," *Plasma Sources Sci. Technol.*, vol. 9, no. 1, pp. 12–17, Feb. 2000.

[14] M. A. Wistey, S. R. Bank, H. B. Yuen, H. Bae, and J. S. Harris, "Nitrogen plasma optimization for high-quality dilute nitrides," *J. Cryst. Growth*, vol. 278, no. 1–4, pp. 229–233, May 2005.

[15] E. Iliopoulos, A. Adikimenakis, E. Dimakis, K. Tsagaraki, G. Konstantinidis, and A. Georgakilas, "Active nitrogen species dependence on radiofrequency plasma source operating parameters and their role in GaN growth," *J. Cryst. Growth*, vol. 278, no. 1–4, pp. 426–430, May 2005.

[16] T. Kikuchi, A. S. Somintac, O. Ariyada, M. Wada, and T. Ohachi, "Role of excited nitrogen species in the growth of GaN by RF–MBE," *J. Cryst. Growth*, vol. 292, no. 2, pp. 221–226, Jul. 2006.

[17] P. A. Anderson, R. J. Kinsey, C. E. Kendrick, I. Farrel, D. Carder, R. J. Reeves, and

S. M. Durbin, “Influence of Nitrogen Species on InN Grown by PAMBE,” *MRS Proc.*, vol. 892, pp. 0892–FF06–04, Jan. 2005.

[18] P. A. Anderson, R. J. Reeves, and S. M. Durbin, “RF plasma sources for III-nitrides growth: influence of operating conditions and device geometry on active species production and InN film properties,” *Phys. status solidi*, vol. 203, no. 1, pp. 106–111, Jan. 2006.

[19] M. M. Oye, T. J. Mattord, G. A. Hallock, S. R. Bank, M. A. Wistey, J. M. Reifsnider, A. J. Ptak, H. B. Yuen, J. S. Harris, and A. L. Holmes, “Effects of different plasma species (atomic N, metastable N[sub 2][sup,” *Appl. Phys. Lett.*, vol. 91, no. 19, p. 191903, 2007.

[20] K. Klosek, M. Sobanska, G. Tchutchulashvili, Z. R. Zytkiewicz, H. Teisseyre, and L. Klopotowski, “Optimization of nitrogen plasma source parameters by measurements of emitted light intensity for growth of GaN by molecular beam epitaxy,” *Thin Solid Films*, vol. 534, pp. 107–110, May 2013.

[21] D. Voulot, R. . McCullough, W. . Thompson, D. Burns, J. Geddes, G. . Cosimini, E. Nelson, P. . Chow, and J. Klaassen, “Characterisation of an RF atomic nitrogen plasma source,” *J. Cryst. Growth*, vol. 201–202, pp. 399–401, May 1999.

[22] D. Voulot, R. W. McCullough, W. R. Thompson, D. Burns, and J. Geddes, “Determination of the atomic nitrogen flux from a radio frequency plasma nitride source for molecular beam epitaxy systems,” *J. Vac. Sci. Technol. A Vacuum, Surfaces, Film.*, vol. 16, no. 6, p. 3434, Nov. 1998.

[23] A. J. Ptak, M. R. Millecchia, T. H. Myers, K. S. Ziemer, and C. D. Stinespring, “The relation of active nitrogen species to high-temperature limitations for $(000\bar{1})$ GaN growth by radio-frequency-plasma-assisted molecular beam epitaxy,” *Appl. Phys. Lett.*, vol. 74, no. 25, p. 3836, 1999.

[24] A. J. Ptak, K. S. Ziemer, M. R. Millecchia, C. D. Stinespring, and T. H. Myers, “Influence of Active Nitrogen Species on the Nitridation Rate of Sapphire,” *MRS Proc.*, vol. 537, p. G3.10, Jan. 1998.

[25] T. H. Myers, M. R. Millecchia, A. J. Ptak, K. S. Ziemer, and C. D. Stinespring, "Influence of active nitrogen species on high temperature limitations for (0001̲) GaN growth by rf plasma-assisted molecular beam epitaxy," *J. Vac. Sci. Technol. B Microelectron. Nanom. Struct.*, vol. 17, no. 4, p. 1654, 1999.

[26] B. L. VanMil, H. Guo, L. J. Holbert, K. Lee, T. H. Myers, T. Liu, and D. Korakakis, "High temperature limitations for GaN growth by rf-plasma assisted molecular beam epitaxy: Effects of active nitrogen species, surface polarity, hydrogen, and excess Ga-overpressure," *J. Vac. Sci. Technol. B Microelectron. Nanom. Struct.*, vol. 22, no. 4, p. 2149, 2004.

[27] B. L. VanMil, H. Guo, L. J. Holbert, K. Lee, C. H. Swartz, T. Liu, D. Korakakis, and T. H. Myers, "High temperature limitations for GaN growth by RF-plasma assisted molecular beam epitaxy: Effects of active nitrogen species, surface polarity, and excess Ga-overpressure," *Phys. status solidi*, vol. 2, no. 7, pp. 2174–2177, May 2005.

[28] S.-H. Cho, H. Okumura, and K. Akimoto, "Comparison of excited nitrogen sources for molecular-beam-epitaxy GaN growth: Radio frequency and electron cyclotron resonance plasma sources," *Appl. Phys. Lett.*, vol. 76, no. 26, p. 3861, 2000.

[29] J. Osaka, M. Senthil Kumar, H. Toyoda, T. Ishijima, H. Sugai, and T. Mizutani, "Role of atomic nitrogen during GaN growth by plasma-assisted molecular beam epitaxy revealed by appearance mass spectrometry," *Appl. Phys. Lett.*, vol. 90, no. 17, p. 172114, 2007.

[30] S. Agarwal, B. Hoex, M. C. M. van de Sanden, D. Maroudas, and E. S. Aydil, "Absolute densities of N and excited N[sub 2] in a N[sub 2] plasma," *Appl. Phys. Lett.*, vol. 83, no. 24, p. 4918, 2003.

Appendix C: Ion Measurement Technique

Nearly 100 years ago Mott-Smith and Langmuir [1] developed the theory of collectors in gaseous discharges. Today, Langmuir probes are considered to be one of the easiest ways to measure some basic properties of a plasma [2] including ion density and electron temperature (i.e. kinetic energy). The traditional Langmuir probe is a wire inserted into the plasma, however the geometries of the MBE growth system prevent us from utilizing this traditional probe. In 1995, Molnar et al. [3] described a method for using the nude Bayard-Alpert ion gauge on the back of the substrate heater as an effective Langmuir probe for analysis of the ion flux emitted by an ECR plasma source. This technique was later used by Wistey et al. [4] to analyze a rf nitrogen plasma source.

C.1 Ion Measurement Technique – Langmuir-like Probe

As described by Molnar et al. [3] and Wistey et al. [4], the experimental setup is rather simple. A schematic of this setup is shown in Fig. 1. The nude Bayard-Alpert ionization gauge, in Fig. 1 referred to as the BFM, is rotated such that it is in line of sight of the emission from the plasma source. Then a voltage source and ammeter are connected to the grid of the ion gauge. Note that Molnar et al. [3] used the collector filament of the ion gauge while Wistey et al. [4] compared all three parts of the ion gauge, i.e. collector, grid and filament and demonstrated that they all provided equivalent data.

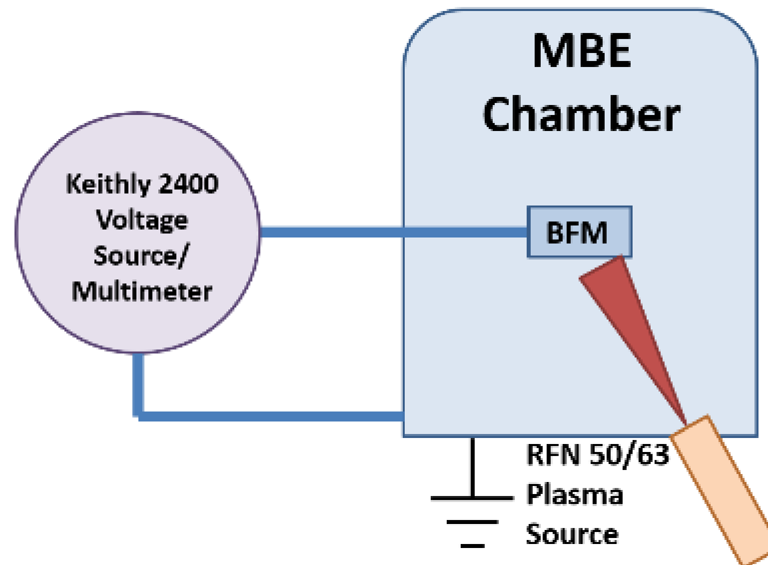

Figure 45 -- Experimental setup of Langmuir-like probe measurement technique.

Once attached, the plasma source is ignited with the desired plasma parameters (rf forward power, N_2 flow rate) and voltage is swept across the grid while measuring the

associated current. Figure 2 shows representative curves acquired using the Riber high flux plasma source.

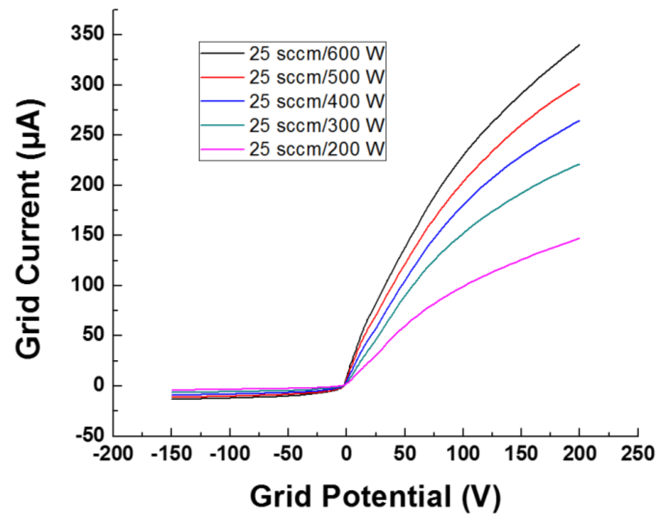

Figure 46 -- Representative Langmuir-like probe I-V curves acquired using the Riber high nitrogen flux plasma source.

Langmuir-like probe I-V curves may be characterized by three distinct regimes. First, when the bias applied to the grid (V_p) is greater than the space potential (V_s), then electrons from the plasma are attracted to the probe and collected, and ions are repelled. This is described as the electron saturation current regime. The space potential is an important parameter in that ions are accelerated across a potential equal to the difference between the space potential and the electrical potential of the impact surface prior to

collision, thus their kinetic energy is directly related to the space potential [5]. When a large negative bias is placed across the grid then electrons from the plasma are repelled and only ions are attracted to the probe and collected. This is the ion saturation current regime. Finally, there is an intermediate regime where the grid potential V_p is less that V_s so both ions and electrons reach the probe.

C.2 References

[1] H. M. Mott-Smith and I. Langmuir, “The Theory of Collectors in Gaseous Discharges,” *Phys. Rev.*, vol. 28, no. 4, pp. 727–763, Oct. 1926.

[2] F. F. Chen, “Lecture Notes on Langmuir Probes.” [Online]. Available: http://www.seas.ucla.edu/~ffchen/Publs/Chen210R.pdf.

[3] R. J. Molnar, R. Singh, and T. D. Moustakas, “Operation of a compact electron cyclotron resonance source for the growth of gallium nitride by molecular beam epitaxy (ECR-MBE),” *J. Electron. Mater.*, vol. 24, no. 4, pp. 275–281, Apr. 1995.

[4] M. A. Wistey, S. R. Bank, H. B. Yuen, J. S. Harris, M. M. Oye, and A. L. Holmes, “Using beam flux monitor as Langmuir probe for plasma-assisted molecular beam epitaxy,” *J. Vac. Sci. Technol. A Vacuum, Surfaces, Film.*, vol. 23, no. 3, p. 460, 2005.

[5] J. E. Heidenreich, J. R. Paraszczak, M. Moisan, and G. Sauve, “Electrostatic probe analysis of microwave plasmas used for polymer etching,” *J. Vac. Sci. Technol. B Microelectron. Nanom. Struct.*, vol. 5, no. 1, p. 347, Jan. 1987.